Analytical Methods in Environmental Chemistry Journal Vol 2 (2019) 5-14

AMECJ

Research Article, Issue 4

Analytical Methods in Environmental Chemistry Journal

Journal home page: www.amecj.com/ir

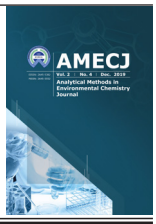

Synthesis of bismuth oxide: Removal of benzene from waters by bismuth oxide nanostructures

Negar Motakef Kazemi[a],* and Masoumeh Yaqoubi[b]

[a] *Department of Medical Nanotechnology, Faculty of Advanced Sciences and Technology, Tehran Medical Sciences, Islamic Azad University, Tehran, Iran.*

[b] *Department of Nanochemistry, Faculty of Pharmaceutical Chemistry, Tehran Medical Sciences, Islamic Azad University, Tehran, Iran.*

ARTICLE INFO:

Received 15 Sep 2019

Revised form 11 Nov 2019

Accepted 30 Nov 2019

Available online 26 Dec 2019

Keywords:

Bismuth oxide nanostructures,
Synthesis,
Benzene removal,
Waters,
Liquid-micro solid phase extraction

ABSTRACT

In this research, the bismuth oxide (Bi_2O_3) nanostructures were prepared via chemical method at 90 °C for 3 h. the results samples were characterized by Fourier transform infrared (FTIR) for determination of functional groups, X-ray diffraction (XRD) for evaluation of crystal structure, dynamic light scattering (DLS), scanning electron microscope (SEM) for presentation of morphology and size, energy-dispersive X-ray spectroscopy (EDS) for determination of chemical composition, and diffuse reflection spectroscopy (DRS) for ultraviolet (UV) blocking. Also, the Bi_2O_3 nanostructures were used for benzene extraction from waters in pH=5-7. By procedure, 30 mg of Bi_2O_3 mixed with hydrophobic ionic liquid ([HMIM][PF6]) and injected to water samples. After shaking and centrifuging, benzene removed from water by ionic liquid-micro solid phase extraction (IL-µSPE) and determined by gas chromatography with flame ionization detector (GC-FID). The absorption capacity and recovery was obtained 167.8 mg per gram of Bi_2O_3 and more than 96%, respectively. Based on the results, the bismuth oxide nanostructures were observed with rod morphology and the diameter of nanometer. The antibacterial activities of the samples were determined against Salmonella using inhibition zone diameter. Based on the study, bismuth oxide nanostructures have good potential for removal of benzene from waters. By IL-µSPE method, the results validated by spiking of samples

1. Introduction

Nanotechnology has attracted a great attention in very interesting applications in various fields [1, 2]. Today, the nanostructured metal oxides have much attention of researchers actively engaged in various scientific due to their interesting properties and potential applications [3, 4]. One of applied materials is the nanostructures with nanometer-scale rod morphology [5]. Bismuth oxide nanostructure is one of a good candidate of metal oxide for different applications such as immunosensor [6], gas sensor [7], photocatalyst [8], catalyst [9], preparation of nanostructures [10], photovoltaic [11], biomedical [12, 13], antibacterial effect [14], X-ray shielding [15], optical properties [16], white-light LEDs [17], and magnetic properties [18]. The common methods of bismuth nanostructures synthesis include solution [19], solution combustion [20], solvothermal [21], hydrothermal [22], laser ablation [23], green synthesis [24], sol–gel [25], flame spray pyrolysis [26], thermal decomposition [27], vapor phase deposition [28], and sputtering

*Corresponding Author: Negar Motakef Kazemi
Email: motakef@iaups.ac.ir
https://doi.org/10.24200/amecj.v2.i04.79

deposition [29]. There are different polymorphs of bismuth oxide including α-Bi_2O_3, β-Bi_2O_3, γ-Bi_2O_3, δ-Bi_2O_3, ε-Bi_2O_3, and ω-Bi_2O_3 which related to the temperature of their formation. The stable polymorph is monoclinic α-Bi_2O_3 in low temperature and cubic δ-Bi_2O_3 in high temperature [30]. The increase of temperature was caused the decrease of tetragonal β-Bi_2O_3 structure and the show monoclinic α-Bi_2O_3 in XRD patterns [31]. The ultraviolet light can be caused the increase of risk for skin cancer and ocular damage. The UV radiation included three regions UV-A (320–400 nm), UV-B (280-320 nm), and UV-C (180-280 nm). The earth's atmosphere shields the more harmful UV-C and greater than 99% of UV-B radiation. The UV-A blocking is very important to prevention from hazardous effects of exposure to direct sunlight [32]. Recently, the bismuth oxide was reported as UV-absorber application [33]. Antibacterial activity is another application of bismuth oxide nanoparticles against some pathogenic Gram-negative bacteria [14]. Also, bismuth oxide was used for removal VOCs, BTEX from waters by analytical chemistry. In the present study, bismuth oxide nanostructures were synthesized by chemical method for application of UV blocking and antibacterial activity. In addition, the bismuth oxide (Bi_2O_3) nanostructures were used for benzene extraction from waters by IL-μSPE. Ionic liquid caused to collected solid phase which was extracted by Bi_2O_3 in optimized pH.

2. Experimental

2.1. Materials

All chemicals used were analytical grade. Materials including bismuth nitrate ($Bi(NO_3)_3$), nitric acid (HNO_3), and sodium hydroxide (NaOH) were purchased from Merck (Darmshtadt Germany). All aqueous solutions were prepared in deionized water (DW, Millipore). The bismuth oxide (Bi_2O_3) nanostructures syntheses by Azad University. Benzene (CAS N: 71-43-2; C_6H_6) and ionic liquid of 1-Hexyl-3-methylimidazolium hexafluorophosphate ([HMIM][PF6]; CAS N:304680-35-1) purchased from Sigma Aldrich.

Five calibration solutions of benzene were prepared and the approximate concentrations of benzene were 0.5, 1.0, 5.0, 10 and 50 mg L^{-1}. The other chemicals with high purity (99%) were purchased from Sigma (Germany).

For analysis of benzene, gas chromatography based on flame ionization detector (GC-FID) and air sample loop injection (ASL) was used (Netherland). The Agilent 7890A GC can accommodate up to three detectors identified as front detector, back detector, and auxiliary detector. The FID detector chosen was selected for benzene analysis in gas/liquid. Before injection, Slide the plunger carrier down until it is completely over the syringe plunger, and tighten the plunger thumb screw until finger-tight. The injector temperature was adjusted to 200°C and the detector temperature at 250°C. The GC oven temperature was programmed from 30°C to 220°C which was held for 10 min. Hydrogen as the carrier gas was used at a flow rate of 1.0 mL min^{-1} with split ratio of 1:100.

2.2. Characterization

The bismuth oxide nanostructures were characterized by Fourier transform infrared spectroscopy, X-ray diffraction, dynamic light scattering, scanning electron microscope, energy-dispersive X-ray spectroscopy, and diffuse reflection spectroscopy. FTIR spectra were recorded on a Shimadzuir 460 spectrometer in a KBr matrix in the range of 400–4000 cm^{-1}. XRD pattern was performed for evaluation of crystalline structure using a Philips Company X'pert diffractometer utilizing Cu-Ka radiation (ASENWARE, AW-XBN300, China). DLS was reported the size and size distribution of nanoparticles (ZEN314, England). SEM was investigated the morphology (KYKY, EM3200, China). EDS was evaluated the elemental and chemical analysis (ASK SEM-CL View VIS, Oxford instruments, UK). DRS was investigated for light absorption and UV blocking properties of nanocomposite (UV2550, Shimadzu).

The antibacterial activity was evaluated using disk diffusion method against Salmonella Gram-negative bacteria, strains ATCC 1231, procured from Islamic Azad University.

2.3. Synthesis of bismuth oxide nanostructures

Bismuth oxide nanostructures were prepared via chemical method based on schematic reaction as follows (Formula):

$$2BiNO_3 + 6NaOH \xrightarrow[3h]{90°c} Bi_2O_3 + 6\,NaNO_3 + 3$$

In a typical reaction, 0.97 g (0.2 mmol) bismuth nitrate was solved in 1 ml nitric acid, and 9 ml deionized water. Then, 100 ml sodium hydroxide (0.1 mol/L^{-1}) was added to the resulting solution [8]. The reactants were sealed under reflux and stirred at 90 °C for 3 h. Then, the reaction mixture was cooled to room temperature, and separated by centrifugation. The crystals were washed with deionized water to remove residual salt, and dried in a vacuum oven at 80 °C for 5 h.

2.4. Procedure

The bismuth oxide nanostructures based on IL-µSPE method was used for extraction of benzene from waters. By procedure, 30 mg of bismuth oxide (Bi_2O_3) nanostructures mixed with o,2 g of 1-Hexyl-3-methylimidazolium hexafluorophosphate ([HMIM][PF6] and diluted with 0.2 mL of pure acetone. Then the mixture was injected into 10 mL of water sample or benzene standard samples with different concentration (1-100 mg L-1). The cloudy solution shacked for 5 min and after centrifuging for 3 min (3500rpm), the upper solution (water or standard solution) was determined by GC-FID. After benzene extraction by IL-µSPE procedure, the recoveries of proposed method were measured with the ratio of initial/final concentration of benzene (signal peak area) before determined with GC-FID (Equation EQ1). In addition, adsorption capacity and removal efficiency (RE) was calculated by equation EQ2 and EQ3. A is the initial concentration of benzene in solution and B is final concentration of benzene which determinate by GC-FID in waters. The adsorption capacity of benzene (mg g^{-1}) and, the removal efficiency of benzene (%) was shown in EQ2 and EQ3. The C_i (mg L^{-1}) and C_f (mg L^{-1}) are the concentration of benzene before and after extraction procedure, Vs (L) is the sample volume, and M(g) is the amount of Bi_2O_3.

$$\text{–} \qquad \text{(EQ1)}$$

$$\frac{(c \quad _f)\times}{} \qquad \text{(EQ2)}$$

$$(\%) \quad \text{——} \qquad \text{(EQ3)}$$

3. Results and Discussion

3.1. Fourier transforms infrared

FTIR spectra of bismuth oxide nanostructures were recorded in the range of 400–4000 cm^{-1} with KBr pellets (Fig. 1). The O–H stretching vibrations appear at 3421 cm^{-1}. The peak at 1400 cm^{-1} is related to C-O vibrations due to organic solvent. The peak at 435~505 cm^{-1} is originated from the metal-oxygen (Bi-O) bond. Fourier transform infrared result is

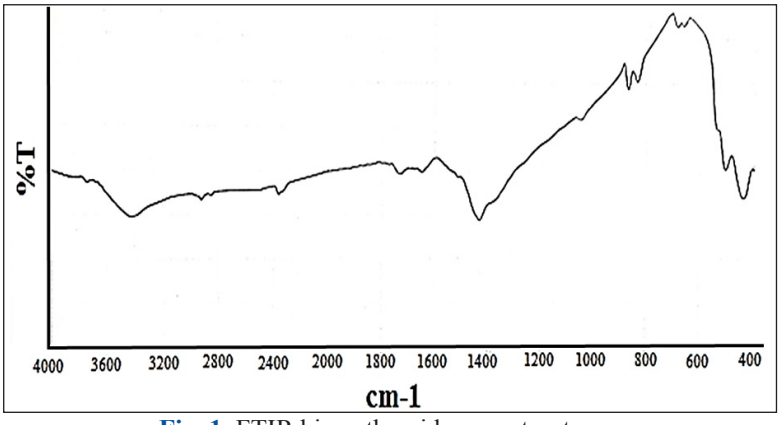

Fig. 1. FTIR bismuth oxide nanostructures.

similar to a previously reported pattern [25].

3.2. X-ray diffraction

XRD measurement was used to determine the crystalline structure of bismuth oxide nanostructures in 2θ range 5 to 80° (Fig. 2). The sharp peak observed at 2θ around 28°, and all diffraction peaks can be indexed the monoclinic α-Bi_2O_3 (JCPDS card No. 41-1449). XRD result is similar to a previously reported pattern [8].

3.3. Dynamic light scattering

The dynamic light scattering was used to find out the size and distribution diagram of nanoparticles (Fig. 3). DLS results presented two peaks at 900 nm and 17 μm with narrow distribution at room temperature. The observation of two peaks confirms that the nanostructure is rod shaped.

3.4. Scanning electron microscope

The size and morphology structures of samples were studied using SEM that shown rod-shaped with an average diameter of 500 nm, and the length of 11 μm (Fig. 4). SEM result confirmed the DLS result.

3.5. Energy-dispersive X-ray spectroscopy

EDS was used to evaluate the chemical composition of bismuth oxide nanostructures. This analysis was clearly showed the identification strong peaks of bismuth (Bi) and oxygen (O) elements. Based on the result the absorption peaks were exhibited at 2.4, 3.2, 10.8, and 11.8 keV, which illustrated a typical absorption of the metallic bismuth. The energy-dispersive X-ray spectroscopy and mapping of bismuth oxide nanostructures were carried out for elemental analysis (Fig. 5).

3.6. Diffuse reflection spectroscopy

DRS absorption spectra of bismuth oxide nanostructures showed UV blocking in three Ultraviolet: UV-A, UV-B, and UV-C (Fig 6). Based on DRS result, the absorption peak was observed 90% ultraviolet in range of 200-400 nm. Based on teh result, bismuth oxide nanostructures are good candidates as UV blocking for research development.

3.7. Antibacterial activity

The antibacterial activity was measured against *Salmonella* as Gram-negative bacteria by disk diffusion method for bismuth oxide nanostructures with concentration 0.01 $g(mL)^{-1}$. The zone inhibition was examined approximately 8.6 mm. The cell wall of Gram-negative bacterium is composed a thin layer of peptidoglycan surrounded by a membranous structure called the outer membrane. The presence of carboxylic groups causes to the negative charge of bacterial cells at biological pH. The main mechanisms of antibacterial activity are

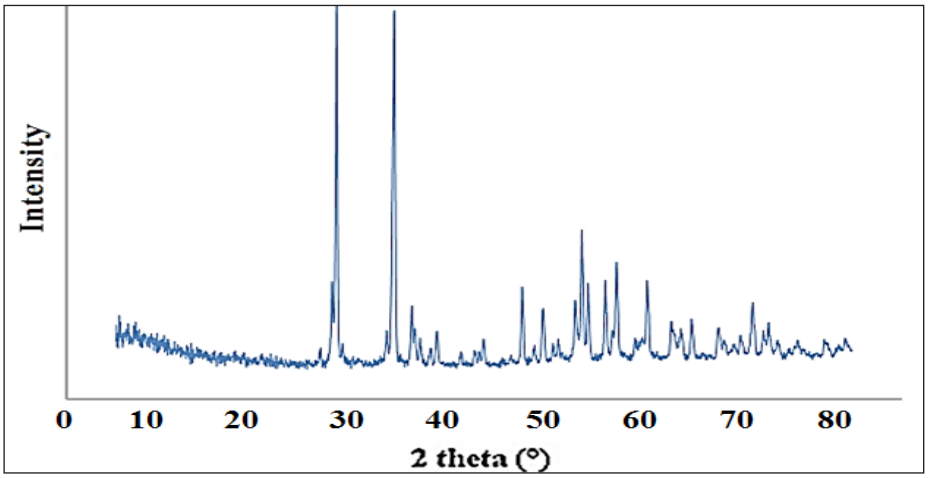

Fig. 2. XRD bismuth oxide nanostructures.

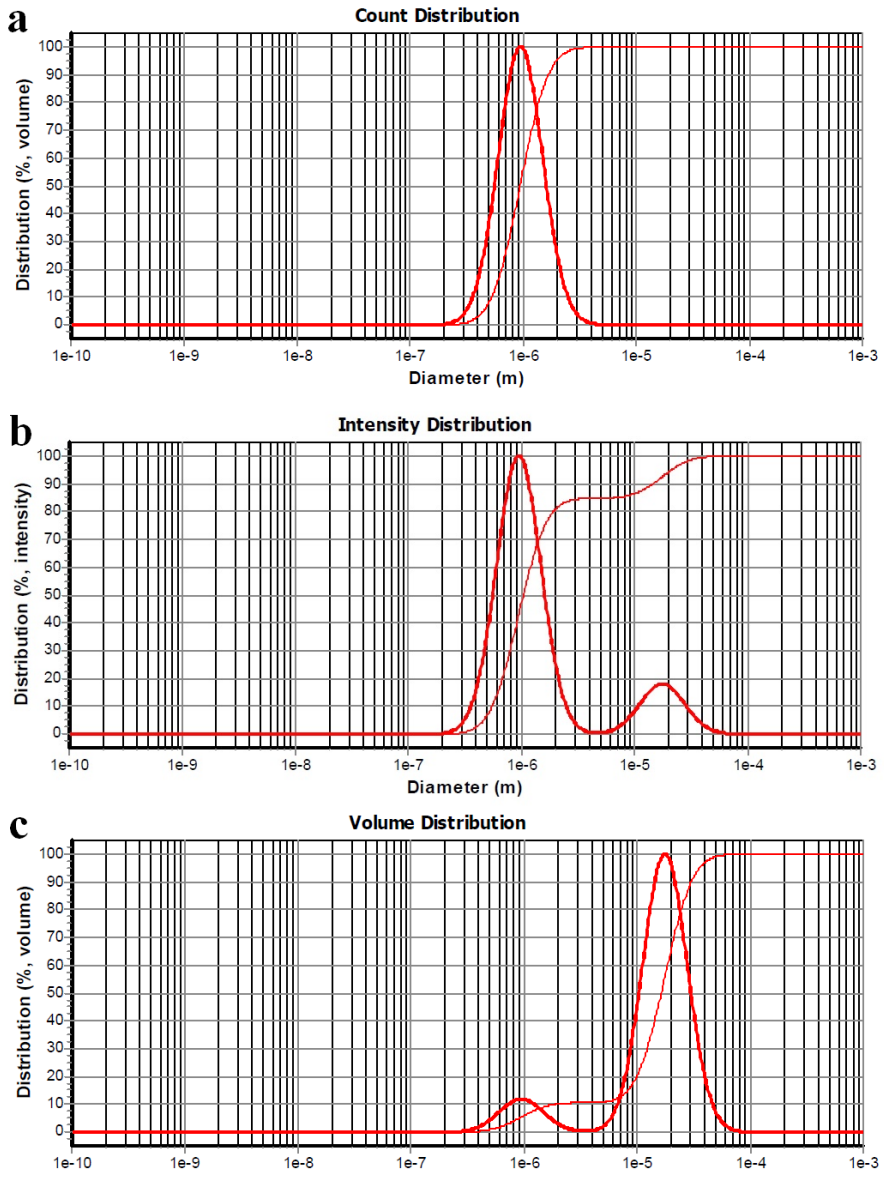

Fig. 3. DLS bismuth oxide nanostructures based on a) count, b) intensity, and c) volume.

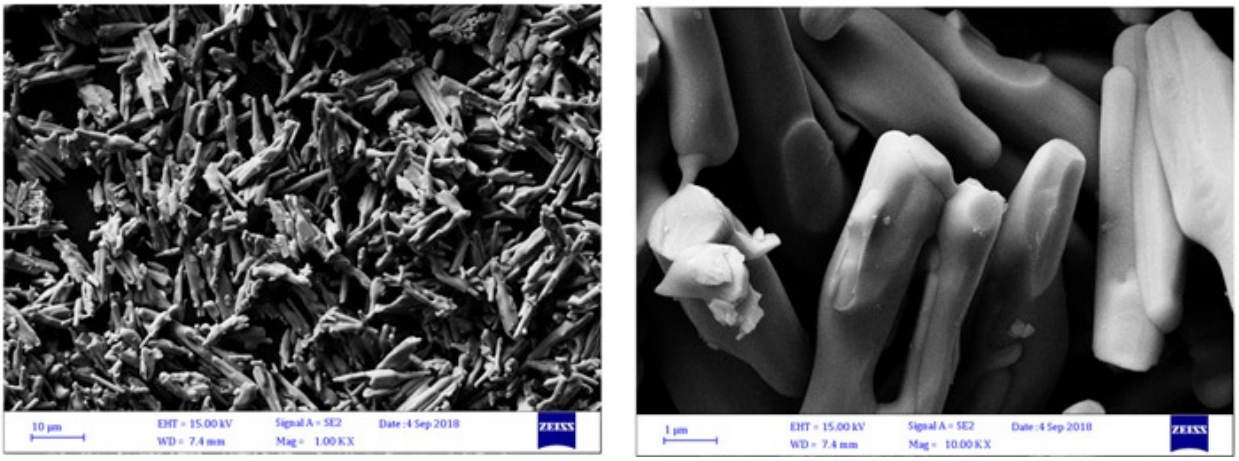

Fig. 4. SEM bismuth oxide nanostructures in different scale bar.

electrostatic forces and adhesion of the opposite charges of Gram-negative bacterium and bismuth oxide nanostructures. Based on teh result, bismuth oxide nanostructures are good candidates as antibacterial activity for research development.

3.8. Optimizing and validation

The IL-μSPE procedure based on the bismuth oxide (Bi_2O_3) nanostructures was used for extraction of benzene in water and wastewater samples. For increasing of efficient recoveries, all parameters such as, pH, sorbent mass, sample volume, adsorption capacity were studied and optimized. The pH of water sample has a main role for adsorption

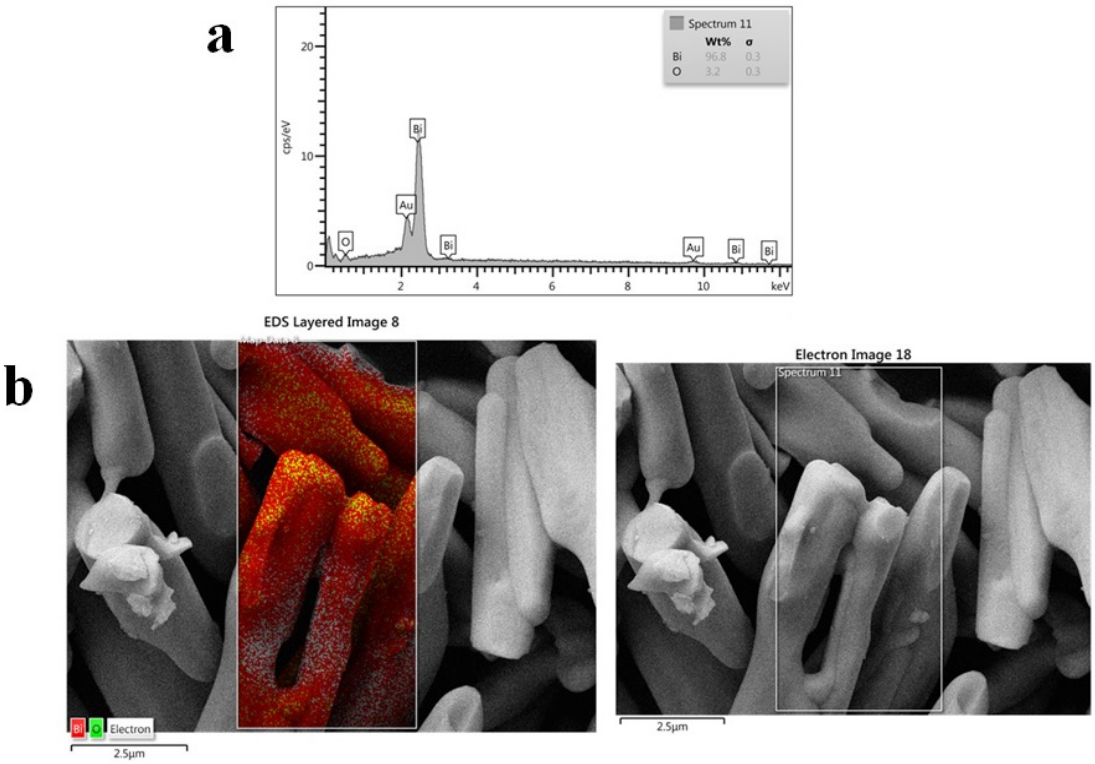

Fig. 5. a) EDS, and b) elemental map image of bismuth oxide nanostructures.

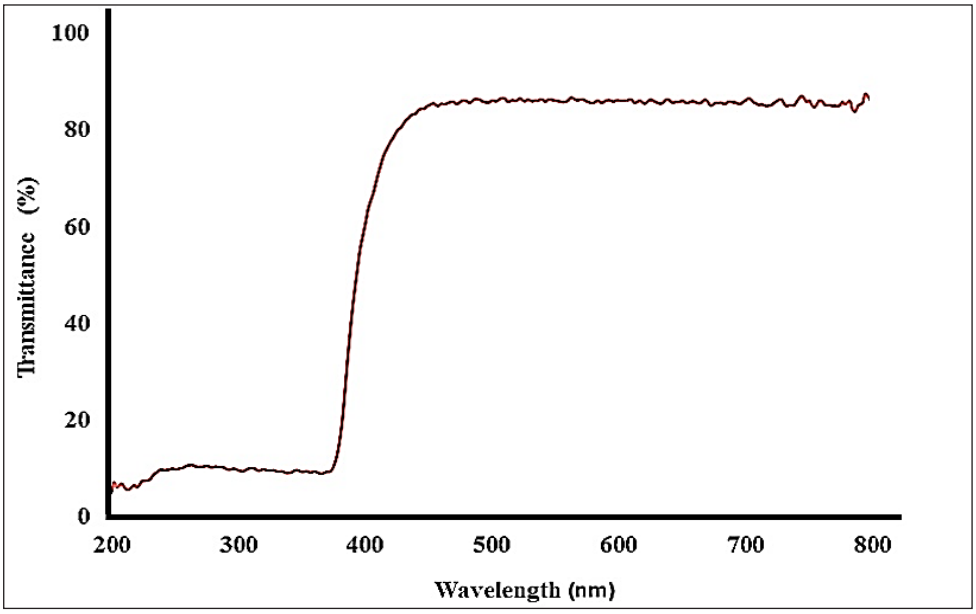

Fig. 6. DRS bismuth oxide nanostructures.

of benzene in water and wastewater by IL- Bi_2O_3 by IL-µSPE. The effect of pH range (2-11) on the extraction of benzene was studied containing 1 mg L^{-1} and 10 mg L^{-1} of C_6H_6. The results showed, the recovery of extraction for benzene were decreased at pH ranges (7<pH< 5) So, pH of 5-7 was selected as optimized pH for benzene extraction in waters (Fig. 7). By IL-µSPE method, the amount of Bi_2O_3 and ILwas optimized for extraction benzene in water and wastewater samples. Therefore, 5-50 mg of Bi_2O_3 and 0.05-0.4 g of IL was used and optimized. Based on results, more than 25 mg Bi_2O_3 and 0.15 g of IL can be extracted benzene in water samples in optimized pH. So, 30 mg and 0.2 g was selected as optimum value for Bi_2O_3 and IL, respectively (Fig.8). The sample volume effected on the extraction recoveries of benzene in water samples at pH=5-7. The different sample volumes from 1 to 20 mL (1-10 mgL^{-1} benzene) were used benzene extraction in water samples by IL-µSPE procedure. The results had good recoveries less than 15 mL of water samples. Therefore, 10 mL was used as the optimal sample volume by proposed procedure (Fig.9).

4. Conclusions

The bismuth oxide nanostructures synthesized by chemical method. The formation of nanostructures

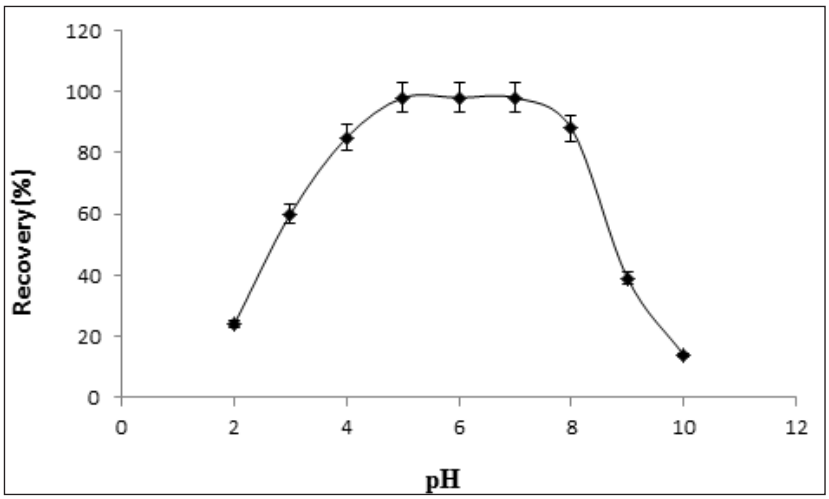

Fig. 7. The effect of pH on benzene extraction in water sample by IL-µSPE

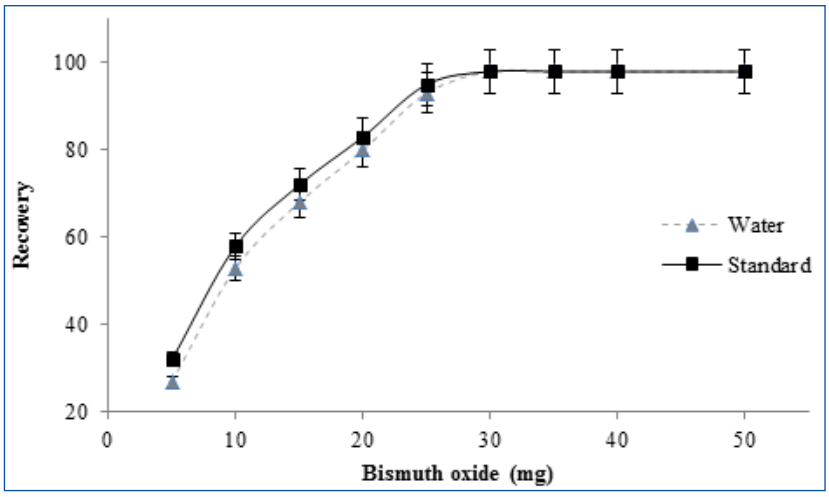

Fig. 8. The effect of bismuth oxide on benzene extraction in water sample by IL-µSPE

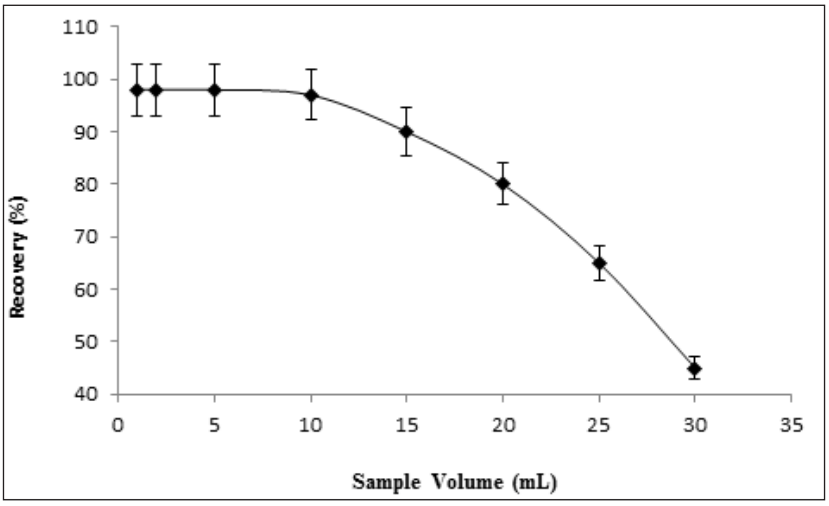

Fig. 9. The effect of Sample volume on benzene extraction in water sample by IL-µSPE

was emphasized by DLS with narrow distribution and SEM with rod morphology. XRD confirmed the monoclinic α-Bi_2O_3 crystalline structure for bismuth oxide nanostructures. In this study, benzene was extracted from water samples based on IL- Bi_2O_3 by IL-µSPE procedure at pH=5-7. The absorption capacity and mean of extraction efficiency for Bi_2O_3 was obtained 167.8 mg per gram and almost 96%, respectively. Also, we successfully observed UV blocking, and antibacterial activity applications of bismuth oxide nanostructures. These properties can be resulted to many advantages in the future with more safety and less toxicity to human health.

5. References

[1] M.R. Mehmandoust, N. Motakef-Kazemi, F. Ashouri, Nitrate adsorption from aqueous solution by metal–organic framework MOF-5, Iran. J. Sci. Technol. Trans A-Sci., 43 (2019) 443–449.

[2] B. Miri, N. Motakef-Kazemi, S.A. Shojaosadati, A. Morsali, Application of a nanoporous metal organic framework based on iron carboxylate as drug delivery system, Iran. J. Pharm. Res**.,** 7 (2018) 1164-1171.

[3] S. Hajiashrafi, N. Motakef Kazemi, Preparation and evaluation of ZnO nanoparticles by thermal decomposition of MOF-5, Heliyon 5 (2019) e02152.

[4] N. Motakef-Kazemi, S.A. Shojaosadati, A. Morsali, In situ synthesis of a drug-loaded MOF at room temperature, Micropor. Mesopor. Mater., 186 (2014) 73–79.

[5] N. Motakef-Kazemi, S.A. Shojaosadati, A. Morsali, Evaluation of the effect of nanoporous nanorods Zn_2 $(bdc)_2$(dabco) dimension on ibuprofen loading and release, J. Iran. Chem. Soc., 13 (2016) 1205–1212.

[6] P.R. Solanki, J. Singha, B. Rupavali, S. Tiwari, B.D. Malhotra, Bismuth oxide nanorods based immunosensor for mycotoxin detection, Mater. Sci. Eng. C 70 (2017) 564–571.

[7] X. Gou, R. Li, G. Wang, Z. Chen, D. Wexler, Room-temperature solution synthesis of Bi_2O_3 nanowires for gas sensing application, Nanotechnol., 20(2009) 495-501.

[8] W. Raza, M.M. Haque, M. Muneer, T. Harada, M. Matsumura, Synthesis, characterization and photocatalytic performance of visible light induced bismuth oxide nanoparticle, J. Alloys Compd., 648 (2015) 641-650.

[9] P. Malik, D. Chakraborty, Bi_2O_3-catalyzed oxidation of aldehydes with t-BuOOH, Tetrahedron Lett., 51(2010) 3521-3523.

[10] H.T. Fan, S.S. Pan, X.M. Teng, C. Ye, G.H. Li, L.D. Zhang, δ-Bi_2O_3 thin films prepared by reactive sputtering: Fabrication and characterization, Thin

Solid Films., 513 (2006) 142-147.

[11] WE. Mahmoud, A.A. Al-Ghamdia, Synthesis and properties of bismuth oxide nanoshell coated polyaniline nanoparticles for promising photovoltaic properties, Polym. Adv. Technol., 22 (2011) 877–881.

[12] MJ. Oviedo, OE. Contreras, Y. Rosenstein, R. Vazquez-Duhalt, Z.S. Macedo, GG. Carbajal-Arizaga, G.A. Hirata, New bismuth germanate oxide nanoparticle material for biolabel applications in medicine, J. Nanomater., 2016 (2016) 1-10.

[13] M. Abudayyak, E. Oztas, M. Arici, G. Ozhan, Investigation of the toxicity of bismuth oxide nanoparticles in various cell lines. Chemosphere., 169 (2017) 117-123.

[14] AMN. Jassim, S.A. Farhan, J.A.S. Salman, K.J. Khalaf, M.F. Al-Marjani, M.T. Mohammed, Study the antibacterial effect of bismuth oxide and tellurium nanoparticles, Int. j. Chem. Boil. Sci., 1 (2015) 81-84.

[15] H. Shirkhanloo, M. Saffari, S.M. Amini, M. Rashidi, Novel semisolid design based on bismuth oxide (Bi_2O_3) nanoparticles for radiation protection, Nanomed. Res. J., 2 (2017) 230-238.

[16] S. Condurache -Bota, V. Tiron, M. Praisler, Highly transparent bismuth oxide thin films deposition: Morphology-Optical properties correlation studies, J. Optoelectron Adv. Mater., 17 (2015) 1296-1301.

[17] Y.C. Chu, G.J. Lee, C.Y. Chen, S.H. Ma, J.J. Wu, T.L. Horng, K.H. Chen, J.H. Chen, Preparation of Bismuth Oxide Photocatalyst and Its application in white-light LEDs, J. Nanomater., 2013 (2013) 596324.

[18] A. Panda, R. Govindaraj, R. Mythili, G. Amarendra, Formation of bismuth iron oxide based core–shell structures and their dielectric, ferroelectric and magnetic properties, J. Mater. Chem. C 7 (2019) 1280-1291.

[19] F. Xia, X. Xu, X. Li, L. Zhang, L. Zhang, H. Qiu, W. Wang, Y. Liu, J. Gao, Preparation of bismuth nanoparticles in aqueous solution and its catalytic performance for the reduction of 4-nitrophenol, Ind. Eng. Chem. Res., 53 (2014) 10576–10582.

[20] J. La, Y. Huang, G. Luo, J. Lai, C. Liu, G. Chu, Synthesis of bismuth oxide nanoparticles by solution combustion method, Particul. Sci. Technolo., 31 (2012) 287-290.

[21] J. Wu, F. Qin, Z. Lu, H.J. Yang, R. Chen, Solvothermal synthesis of uniform bismuth nanospheres using poly(N-vinyl-2-pyrrolidone) as a reducing agent, Nanoscale Res. Lett., 6 (2011) 66.

[22] Z.A. Zulkifli, K.A. Razak, W.N.W.A. Rahman, S.Z. Abidin, Synthesis and characterisation of bismuth oxide nanoparticles using hydrothermal method: the effect of reactant concentrations and application in radiotherapy, J. Phys. Chem. Solid., 1082 (2018) 012103.

[23] L. Torrisi, L. Silipigni, N. Restuccia, S. Cuzzocrea, M. Cutroneo, F. Barreca, B. Fazio, G. Di Marco, S. Guglielmino, Laser-generated bismuth nanoparticles for applications in imaging and radiotherapy, J. Phys. Chem. Solid., 119 (2018) 62-70.

[24] P. Nazari, M.A. Faramarzi, Z. Sepehrizadeh, M.A. Mofid, R.D. Bazaz, A.R. Shahverdi, Biosynthesis of bismuth nanoparticles using Serratia marcescens isolated from the Caspian Sea and their characterization, IET Nanobiotechnol., 6 (2012) 58-62.

[25] M. Mallahi, A. Shokuhfar, M.R. Vaezi, A. Esmaeilirad, V. Mazinani, Synthesis and characterization of bismuth oxide nanoparticles via sol-gel method, Am. J. Eng. Res., 3 (2014) 162-165.

[26] L. Mädler, S.E. Pratsinis, Bismuth oxide nanoparticles by flame spray pyrolysis, J. Am. Ceram. Soc., 5 (2004) 1713–1718.

[27] S. Schulz, S. Heimann, C. Wölper, W. Assenmacher, Synthesis of bismuth pseudo cubes by thermal decomposition of Bi_2Et_4, Chem. Mater., 24 (2012) 2032–2039.

[28] L. Kumari, J.H. Lin, Y.R. Ma, Synthesis of bismuth oxide nanostructures by an oxidative metal vapour phase deposition technique, Nanotechnol., 18

(2007) 295605.

[29] B. Sirota, J. Reyes-Cuellar, P. Kohli, L. Wang, M.E. McCarroll, S.M. Aouadi, Bismuth oxide photocatalytic nanostructures produced by magnetron sputtering deposition, Thin Solid Film., 520 (2012) 6118-6123.

[30] M. Mehring, Molecules to bismuth oxide-based materials: Potential homo- and heterometallic precursors and model compounds, Coord. Chem. Rev., 251 (2007) 974-1006.

[31] J. Hou, C. Yang, Z. Wang, W. Zhou, S. Jiao, H. Zhu, In situ synthesis of α-β-phase heterojunction on Bi_2O_3 nanowireswith exceptional visible-light photocatalytic performance, Appl. Catal. B 142 (2013) 504–511.

[32] S. Hajiashrafi, N. Motakef-Kazemi, Green synthesis of zinc oxide nanoparticles using parsley extract, Nanomed. Res. J., 3 (2018) 44-50.

[33] D. Perez-Mezcua, R. Sirera, R. Jimenez, I. Bretos, C. De Dobbelaere, A. Hardy, M.K.V. Baelc, M. Lourdes Calzada, A UV-absorber bismuth(III) Nmethyldiethanolamine complex as a lowtemperature precursor for bismuth-based oxide thin films, J. Mater. Chem. C 2 (2014) 8750–8760.

Analytical Methods in Environmental Chemistry Journal Vol 2 (2019) 15-26

AMECJ

Research Article, Issue 4

Analytical Methods in Environmental Chemistry Journal

Journal home page: www.amecj.com/ir

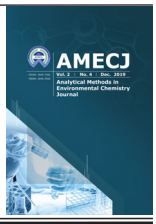

Removal of metanil yellow by batch biosorption from aqueous phase on egg membrane: Equilibrium and isotherm studies

Beniah Obinna Isiuku[a,*] and Francis Chizoruo Ibe[a]

[a] *Department of Chemistry, Imo State University, PMB 2000, Owerri, Imo State, Nigeria Obinna Isiuku*

ARTICLE INFO:

Received 25 Aug 2019

Revised form 21 Oct 2019

Accepted 17 Nov 2019

Available online 25 Dec 2019

Keywords:

Batch biosorption,
Hen egg membrane,
Isotherm modeling,
Metanil yellow,
Physisorption

ABSTRACT

The biosorption of metanil yellow on hen egg membrane from aqueous solution in a batch process was investigated at 29°C with a view to determine the potential of the membrane in removing metanil yellow from aqueous solution. The effects of contact time, initial biosorbate concentration, biosorbent dosage and initial biosorbate pH were determined. Various isotherm models were used to analyze experimental data. The highest experimental equilibrium biosorption capacity obtained was 129.88 mg g^{-1}. The optimum pH was 3. Adsorption capacity increased with increase in initial solution concentration but decreased with increase in time. The isotherm models applied were good fits based on correlation coefficients. Flory-Huggins isotherm was the best fit (R^2 =0.986). The biosorption was endothermic, good, physisorptive and spontaneous. This work shows that hen egg membrane is a potential biosorbent for the removal of metanil yellow from aqueous solution.

1. Introduction

The production of different kinds of chemical compounds due to rapid large-scale industrialization has created serious environmental pollution [1]. Dyes are organic compounds used for imparting color in textile, printing and paint industries. Due to their chemical structures, synthetic dyes dissolved in wastewaters are not degraded on exposure to light, chemical and biological treatments [2]. The discharge of dyes into water bodies cause immediate visible pollution and contamination due to their organic and toxic nature. The presence of dyes in water bodies hinders photosynthesis [3]. Dye_wastewaters_discharged from textile and dyestuff industries into water bodies generate growing public concern due to their toxicity and carcinogenicity [4]. Hen egg membrane comprises majorly of two parts: the egg membrane made up of protein fibers that are interwoven and spherical masses, and the calcified eggshell composed of interstitial calcite or calcium carbonate crystals [5]. Hen egg membrane is situated on the inner surface of the eggshell. The membrane is a dual membrane with structure that can be said to be an intricate

* Corresponding Author: Beniah Obinna Isiuku

Email: obinnabisiuku@yahoo.com

https://doi.org/10.24200/amecj.v2.i04.78

lattice meshwork of large and small fibers which interlock with each other to form a tenacious sheath. Apart from collagen, egg membrane contains polysaccharides [6]. Due to the polysaccharide and collagen contents which provide hydroxyl, amine and sulphonic functional groups on which adsorbate particles can stick, hen egg membrane exhibits good biosorption properties [7]. Eggs from hens are used in large quantities by food manufacturers, hatcheries, hotels and restaurants and the shells are disposed of as waste [8]. Metanil yellow is a water-soluble azo dye used in the beverages, leather, paper, and textile industries. It is also used as a stain and as an indicator in acid-base titrations [9]. Metanil yellow has detrimental health effects on humans [10]. It is toxic if absorbed through the skin, respiratory and intestinal tract and may act as a skin, eye or respiratory tract irritant. It is harmful when swallowed or inhaled and may be carcinogenic under long time exposure [11, 12]. Different methods have been developed to remove synthetic dyes from wastewater in order to reduce their impact on the environment. The methods include floatation, electro-coagulation, ozonation, photo-catalytic degradation, chemical oxidation, precipitation, filtration and adsorption [3, 13]. Adsorption is superior to the other mentioned methods due its low cost, flexibility, simplicity of design, ease of operation and insensitivity to toxic pollutants [13]. Biosorption is the type of adsorption whereby contaminants in air or water are removed using natural biological materials. Adsorption is mostly applied in cases where the contaminants do not readily undergo biological degradation and their concentrations are very low [14–17]. Batch adsorption experiments are usually done to measure the effectiveness of adsorption for removing specific adsorbates as well as to determine the maximum adsorption capacity [18]. Hen egg membrane had been used to remove metal ions and Levafix Brilliant Red E-4BA from aqueous solutions by biosorption [6]. Pramanpol and Nitayapat [8] used eggshell and egg shell containing the membrane to remove Reactive Yellow 205. Their results showed a 10 – 27 fold increase in biosorption capacity due the presence of the membrane. Hassan and Salih [7] used eggshell containing the membrane to effectively remove methylene blue, a cationic dye from aqueous solution. The aim of this work was to determine the performance of hen egg membrane in the removal of metanil yellow from aqueous solution. The impacts of initial dye solution concentration, contact time, biosorbent dosage and initial solution pH were investigated.

2. Experimental

2.1. Preparation of dye solution

The metanil yellow (Merck, Switzerland) of 70 % purity, used in this study was purchased at Onitsha, Nigeria and used directly without further treatment. The structure of metanil yellow, an anionic dye is shown in Figure 1. The stock solution was prepared by dissolving 1g dye per litre solution using distilled water. Different solution concentrations (25-100 mgL^{-1}) used in this work, were obtained by diluting the stock solution. 1M nitric acid and 1M sodium hydroxide solutions were used for pH adjustments.

2.2. Preparation of hen egg membrane

The hen eggshells were obtained from restaurants and hatcheries in Owerri, Imo State, Nigeria. The eggshells were washed with hot water and rinsed thrice with hot distilled water to remove odor and dirt. The eggshells were boiled for 30 min and cooled. While soaked, the membranes were

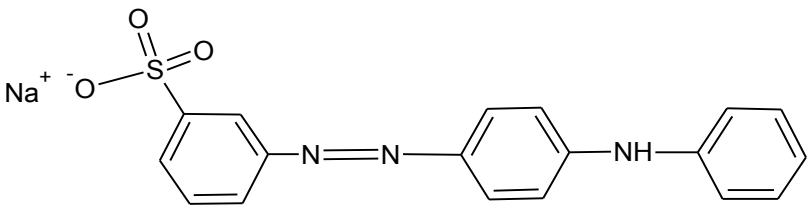

Fig. 1. The structure of metanil yellow (MY)

peeled off, packed in a lattice and allowed for water to drain off. The membrane biomass was dried at 110°C in a hot air oven for 1h, and cooled. The dried membrane biomass was ground with a blender and sieved to obtain 0.42 – 0.84 mm size particles and packed in an airtight plastic container.

2.3. Analysis of egg membrane

Infra-red spectrophotometric analysis was run with a sample of the hen egg membrane with (FTIR-8400S, Shimadzu, Japan) UV/Visible spectrophotometer. Proximate analysis of the biosorbent was carried out using the method of the Association of Official Analytical Chemists (AOAC) [19]. The surface structure of the egg membrane was examined with a scanning electron microscope (SEM model Phenom Prox, Phenom World, Netherlands).

2.4. Batch biosorption studies

Batch biosorption of metanil yellow from aqueous solution was carried out by agitating 0.01g membrane portions with 25mL portions of different initial concentration of the dye solution in 50 mL volumetric flasks. The stoppered sample flasks were put in a water-bath shaker (SHA-C DFS KW-1000BH) and agitated for 6 h at 29°C and a speed of 175rpm. A sample was collected each hour, filtered and the filtrate analyzed using UV-Visible spectrophotometer (Model 752 Shimadzu, Japan) at λ_{max} 440nm. Amounts of dye were absorbed on the biosorbent and determined by applying in Equations 1 -3.

$$q_t\,(mg/g) = \frac{(C_o - C_t)v}{1000\,m} \quad \ldots\ldots\ldots\ldots \quad (Eq.1)$$

$$q_e(mg/g) = \frac{(C_o - C_e)v}{1000\,m} \quad \ldots\ldots\ldots\ldots\ldots \quad (Eq.2)$$

$$\%\,Removal = \frac{(C_o - C_e)100}{C_o} \quad \ldots\ldots\ldots \quad (Eq.3)$$

3. Results and Discussion

3.1. Analysis of the hen egg membrane

Fourier Transform Infra-red spectrophotomeric analysis and proximate analysis were carried out on the egg membrane. Table 1 shows the protein, carbohydrate, fiber, and lipid contents of the biomass. Figure 2 shows the infra-red spectrum of the biosorbent. The infra-red peaks at 2341.66, 2843.17, 3036.06, 3255.95, and 3618.58 cm^{-1} show presence of (–NH) and (–OH) functional groups, while 1238.34, 1408.08, 1519.96, and1658.84 cm^{-1} show presence of –CO- functional group. The –NH- and –CO- functional groups are present as amide group in protein fibers; the (–OH) in carbohydrate; and (–CO; –CO–) , in carboxylate group. [20-22]. These functional groups are responsible for

Table 1. Proximate analytical data for hen egg membrane

Parameter	Value (%)
Ash	8.39
Moisture	11.70
Crude protein	2.11
Carbohydrate	36.57
Fiber	27.59
Lipid	13.65

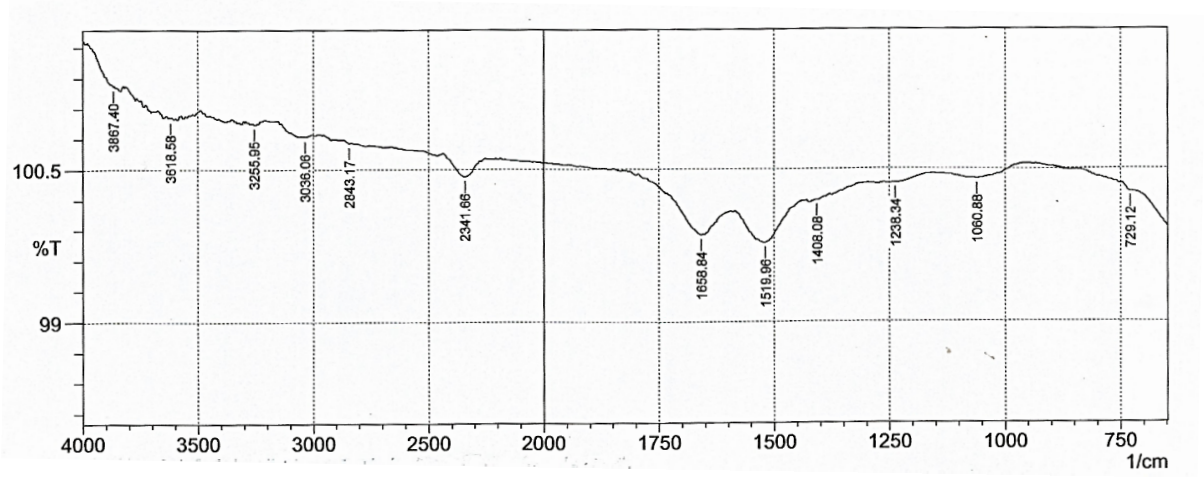

Fig. 2. FTIR spectrum of hen egg membrane

the biosorption. Figure 3 shows the morphology of the biosorbent; it shows a well arranged lattice structure of intertwined fibres. This creates a good network of pores contributing to biosorption [6].

3.2. Biosorption studies

3.2.1. Effect of initial dye concentration and contact time

The effects of initial biosorbate concentration and contact time at 29°C, agitation speed 175 rpm and pH 3 are shown in Figure 4. Maximum biosorption was within the first sixty minutes for all the concentrations. Generally the equilibrium biosorption capacities were high for all the initial concentrations. However, there was appreciable decline in biosorption with time for the initial concentration 100 mg/L. Results show increase in equilibrium biosorption capacity with increase in initial concentration. This agrees with the work of Njoku and Hameed [23]. The optimum time of biosorption for initial concentrations 25 and 50 mg/L was 120 min. For initial concentration 100 mg/L, equilibrium was not reached at 360 min. The appreciable decrease in equilibrium biosorption capcity with time for initial concentration 100 mg/L might be as a result of competition of the biosorbate anions for available binding sites [24, 25]. The increase in equilibrium biosorption

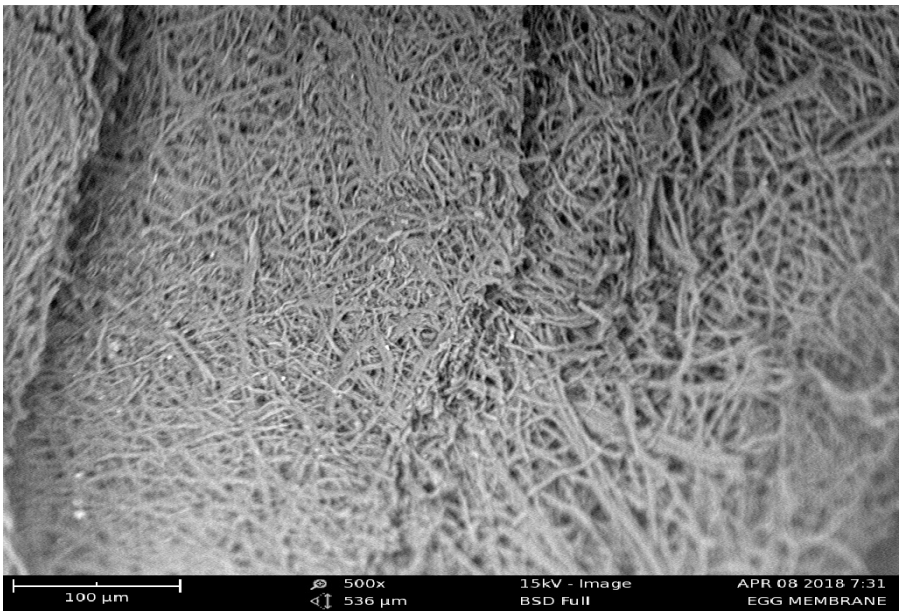

Fig. 3. Scanning electron micrograph of hen egg membrane 500x before biosorption

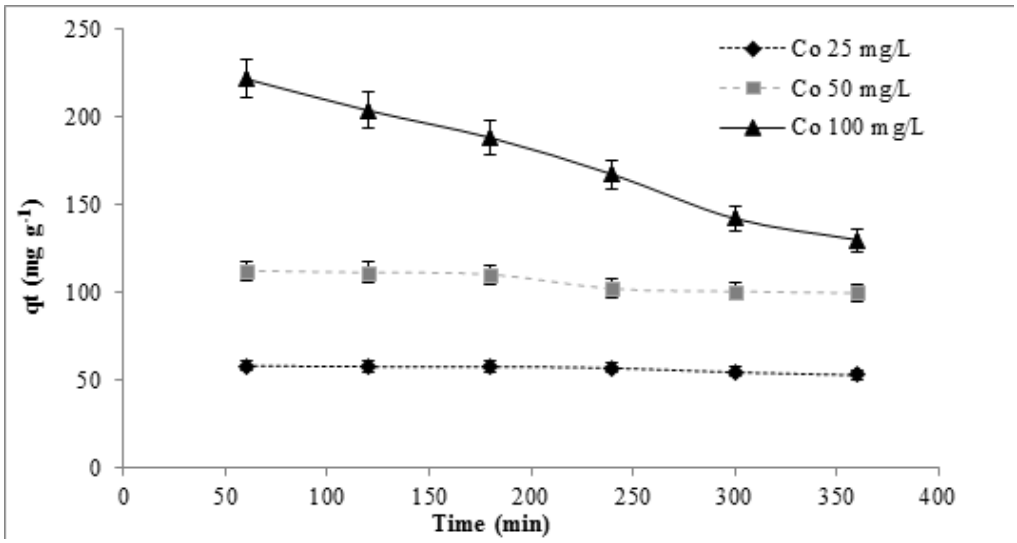

Fig. 4. Effect of initial concentration on the biosorption of metanil yellow on hen egg membrane

capacity with increase in initial concentration is as a result of the increase in the driving force from the concentration gradient. At highest initial concentration the active sites of the egg membrane were surrounded by much more biosorbate ions leading to more enhanced biosorption [26].

3.2.2. Effect of biosorbent dosage

Various dosages (0.04-1.28 % w/v) of the egg membrane were interacted with 25 mL portions of the dye of initial concentration 25 mg/L at pH 3, temperature 29 °C and agitation speed of 175 rpm for 6 h in order to study the effect of biosorbent dosage. The results of Figure 5 showed that equilibrium biosorption capacity decreased with increase in biosorbent dosage. This is in agreement with the work of Koumanova et al, [27]. At higher biosorbent dosage, there was a very fast superficial biosorption onto the biosorbent surface that produced a lower solute concentration in the solution than when biosorbent dosage was lower. Thus with increasing biosorbent dosage, the amount of metanil yellow biosorbed per unit mass of egg membrane reduced, hence leading to a decrease in equilibrium biosorption capacity. This is in conformity with the report of Han et al., [26]. Increasing the biosorbent dosage from 0.04 – 1.28 % led to a decrease in q_e from 54.38 to 1.80 mg g^{-1}. The optimum biosorbent dosage was found to be 0.04 % (w/v).

3.2.3. Effect of initial biosorbate pH

Solution pH affects the properties of both biosorbate and biosorbent and is therefore a very important parameter that affects biosorption in aqueous solutions [23]. The effect of initial solution pH on the biosorption of metanil yellow by hen egg membrane was investigated within the pH range 2-7 and the result is shown in Figure 6. The figure shows the highest equilibrium biosorption capacity of 29.40 mg g^{-1} for pH 3, initial dye concentration 25 mgL^{-1}, biosorbent dosage 0.08 % w/v, and temperature 29°C. There was decrease in equilibrium biosorption capacity with increase in pH. At pH 7, there was virtually no biosorption. The pH values 3 was optimum for the biosorption process. The equilibrium biosorption capacity decreased from 29.40 mg g^{-1} at pH 3 to 26.45 mgL^{-1} at pH 2. The reason for the decrease was attributed to the increase in H^+ concentration leading to the formation of aqua complexes thereby retarding the biosorption process. This agrees with the report of Mas Haris and Sathasivam, [28]. At low pH, the carboxylate anion of the protein fiber present in

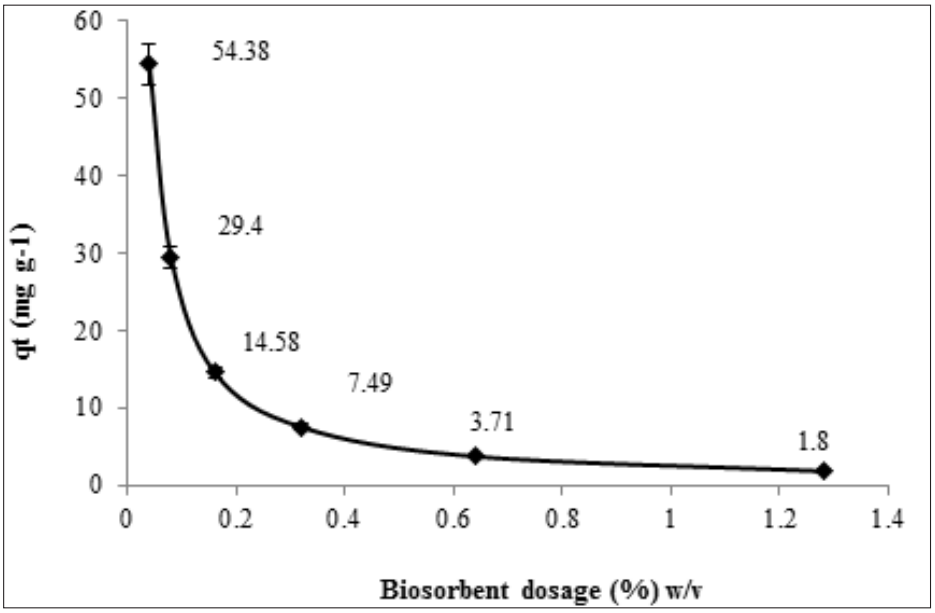

Fig. 5. Effect of adsorbent dosage on the biosorption of metanil yellow on hen egg membrane

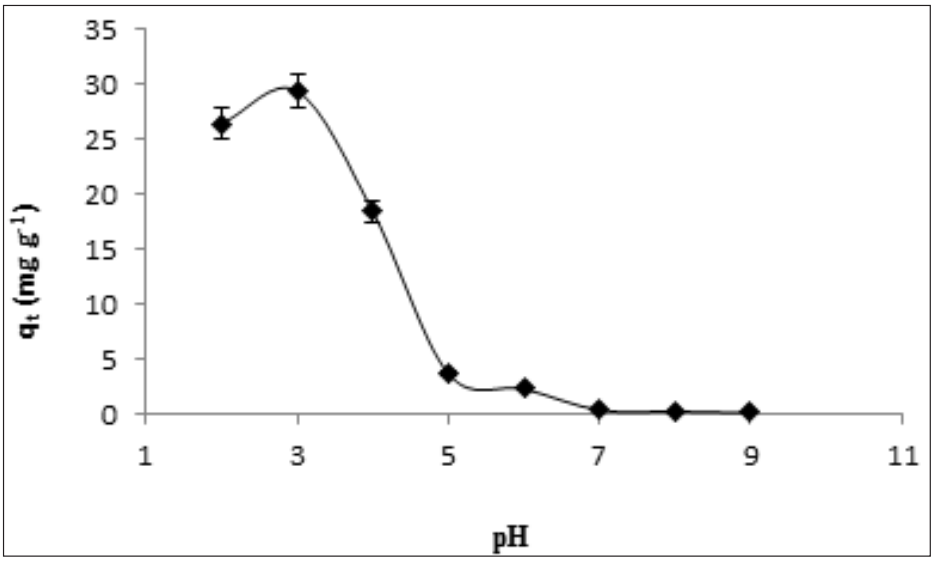

Fig. 6. Effect of initial pH on biosorption of metanil yellow on hen egg membrane

the membrane as part of the amino acid functional group was protonated and the amino acid existed primarily in the ammonium ion form; the oxo functional group present in the polysaccharide was also protonated. These conditions created positively charged surface on the biosorbent hence, high biosorption; as the pH was raised, the ammonium ion site in the protein was deprotonated, and the molecule existed as the carboxylate anion; the oxo functional group was hydrated generating hydroxyl ions which repelled the metanil yellow anions [21, 29]. These conditions were responsible for poor biosorption at higher pH values.

3.3. Adsorption Isotherm modeling

An adsorption isotherm indicates how adsorbed particles distribute between the liquid phase and the solid phase when the adsorption process reaches an equilibrium state [26]. To enhance the description of an adsorption process in terms of batch equilibrium process a finite amount of adsorbent is brought into contact with various concentrations of the adsorbate. Batch equilibrium studies yield information as to the total capacity of an adsorbent for a particular material in single component systems. However, isotherms are obtained under equilibrium conditions, whereas in most adsorption treatment applications the retention time is too short for equilibrium to be attained [6].

The analysis of the isotherm data by fitting them to different isotherm models is an important step to find the suitable model that can be used for design purposes [5, 26]. An adsorption isotherm is critical in optimizing the use of adsorbents. In this study many isotherm models were used to model experimental data. The applicability of the isotherm models to the biosorption was compared by judging the correlation coefficient values.

3.3.1. Langmuir isotherm model

The Langmuir isotherm assumes a homogenous surface with identical sites in terms of energy for the biosorbent [30, 31]. It is represented by Eq. 4:

$$q_e = \frac{q_m K_L C_e}{1 + K_L C_e} \quad (4)$$

The type 2 linearized Langmuir equation is given as Eq. 5:

$$\frac{1}{q_e} = \frac{1}{K_L q_m}\frac{1}{c_e} + \frac{1}{q_m} \quad (5)$$

A plot of $1/q_e$ against $1/C_e$, gave a straight line with slope $1/K_L$ and intercept $1/q_m$ as shown in Figure 7. Table 2 shows the model parameters (K_L, q_m and R_L). R^2 value (0.977) shows that the experimental results fitted well into the Langmuir isotherm model. The essential characteristics of the Langmuir isotherm can be expressed in terms of a dimensionless constant, the Hall separation factor R_L [32] expressed as Eq. 6:

The value of R_L indicates the type of isotherm to be either favorable ($0<R_L<1$), unfavorable ($R_L>1$), linear ($R_L=1$) or irreversible ($R_L = 0$). R_L value was found to be 0.314. The result shows the isotherm to be favorable. The Langmuir constant K_L was used to determine the spontaneity of the adsorption by calculating the Gibbs free energy (33) applying Eq. 7:

$$\Delta G^o_{ads} = -RT\,(InK_L + 4.02) \quad (7)$$

The free energy value (-5.009 kJ mol^{-1}) shows that the process was spontaneous.

3.3.2. Freundlich isotherm model

The Freundlich isotherm model is empirical. Assumptions made in applying this model are that, multilayer adsorption occurs on a heterogeneous adsorbent surface, and that the concentration of the adsorbate on adsorbent increases infinitely with increase in the concentration of the adsorbate [34]. The adsorbent surface has unequal available sites with different energies of adsorption [35]. It does not predict any saturation of the adsorbent by the adsorbate [30]. The Freundlich model is mathematically expressed as Eq. 8:

$$q_e = K_F C_e^{1/n} \quad (8)$$

Its linear logarithmic form [31] is Eq. 9:

$$Inq_e = InK_F + \frac{1}{n} InC_e \quad (9)$$

A plot of In q_e against In C_e, gave a straight line, with slope 1/n, and intercept In K_F.

K_F is the adsorption or distribution coefficient and represents the quantity of dye adsorbed onto the membrane for a unit equilibrium concentration. The mechanism and the rate of adsorption are functions of 1/n and K_F. For a good adsorbent, $0.2 < 1/n < 0.8$, while a smaller value of 1/n indicates better adsorption and formation of stronger bond between the adsorbate and adsorbent [36]. The plot of In q_e against In C_e (Fig.8) gave values of 1/n, n, K_F and R^2 as shown in Table 2. The 1/n value ($0.34 < 1$) shows that the biosorption was physisorptive; n ($2.941 > 1$) shows that the biosorption was good

Table 2. Isotherm parameters for batch biosorption of of metanil yellow on egg membrane at 29°C

Model	Parameter	Value
Langmuir	q_m (mgg^{-1})	129.880
	$q_{e\ expt}$ (mgg^{-1})	158.730
	K_L (mgL^{-1})	0.132
	R_L	0.070
	R^2	0.977
	ΔG^o_{ads} (kJ mol^{-1})	-5.009
Freundlich	1/n	0.34
	n	2.941
	K_F [$mgg^{-1}(L/mg)^{-1/n}$]	37.487
	R^2	0.872
Temkin	B (J mol^{-1})	29.525
	b_T (J/mol/K)	85.041
	A_T (L g^{-1})	3.025
	R^2	0.935
Dubinin-Radushkevich	q_m (mg g^{-1})	123.273
	R^2	3
	E (J mol^{-1})	408.248
	R^2	0.98
Elovich	q_m (mg g^{-1})	50.505
	K_E	0.912
	R^2	0.809
Harkin-Jura	A_{HJ} (g^2 L^{-1})	3333.33
	B_{HJ} (mg^2 L^{-1})	1.667
	R^2	0.743
Halsey	n_H	0.034
	K_H (mg L^{-1})	3.025
	R^2	0.935
Flory-Huggins	n_{FH}	2.551
	K_{FH} (L mol^{-1})	616.464
	ΔG^o_{ads} (kJ mol^{-1})	-16.13
	R^2	0.986

[34]. The R^2 value (0.872) shows that Freundlich isotherm model simulated experimental data well.

3.3.3 Temkin isotherm model

The Temkin model presumes that the heat of

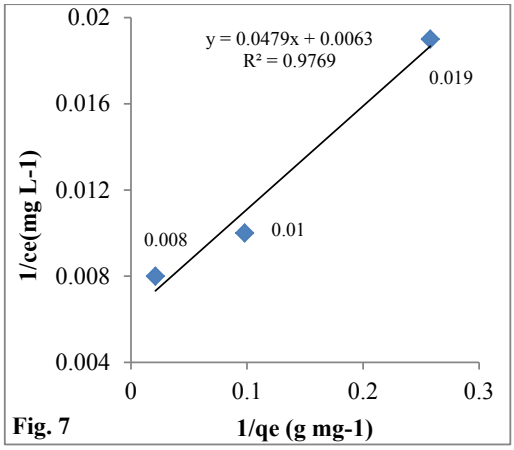

Fig. 7

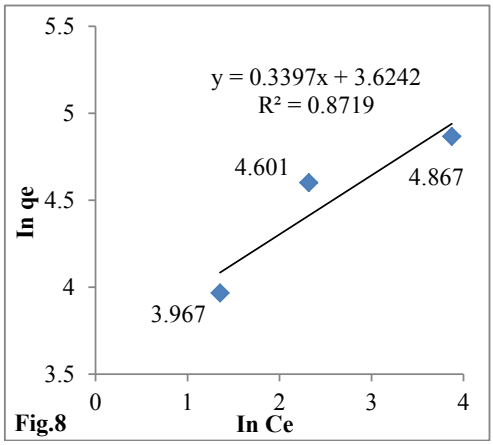

Fig.8

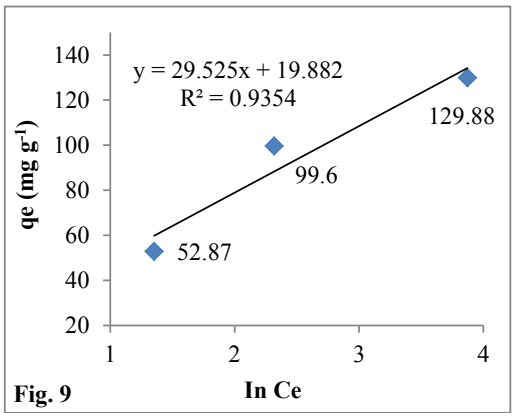

Fig. 9

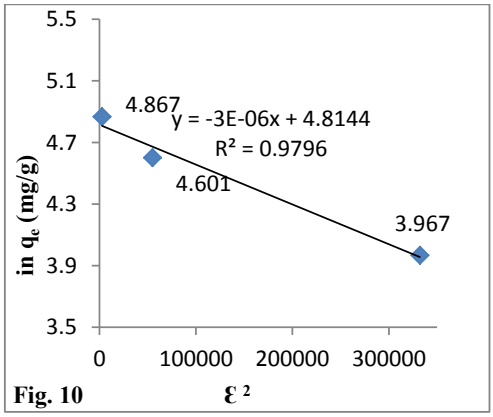

Fig. 10

Fig. 7-10. The isotherm plot for biosorption of metanil yellow on hen egg membrane: Langmuir (**Fig. 7**), Freundlich (**Fig.8**), Temkin isotherm (**Fig.9**) and Dubinin-Radushkevich (**Fig. 10**)

adsorption of adsorbate particles in the layer decreases linearly with coverage with consideration of the effects of indirect adsorbent-adsorbate interaction, and adsorption process is characterized by a uniform distribution of binding energies, up to some maximum binding energy [13, 37]. The linear form of Temkin equation [13, 38] is expressed as Eq. 10:

$$q_e = BInA + BInC_e \quad (10)$$

$$B = {RT}/{b_T} \quad (11)$$

A plot of q_e against In C_e (Fig. 9) gave a straight line with slope B and intercepts B In A. The B, A, b_T and R^2 values are shown in Table 2. The correlation coefficient R^2 (0.935) shows that the Temkin model is a good fit for simulating experimental data.

3.3.4. Dubinin-Radushkevich isotherm model

This model is applied in estimating the characteristic porosity of an adsorbent and the apparent adsorption energy. The model neither assumes homogenous adsorbent surface nor a constant adsorption potential as the Langmuir model [32]. The model equation is expressed a Eq.12:

$$q_e = q_m e^{-B_D \varepsilon^2} \quad (12)$$

The linearized logarithmic expression [39] of Eq.12 is Eq.13:

$$In\ q_e = In\ q_m - B_D \varepsilon^2 \quad (13)$$

$$\varepsilon = RT\ In\ [1 + (1/C_e)] \quad (14)$$

A plot of ln q_e against ε^2 (Fig. 10) gave a straight line with slope B_D and intercept ln q_m. The values of q_D and B_D are in Table 2.

The free energy of adsorption E (J/mol) is related to the porosity factor B_D by Eq. 15:

$$E = {1}/{(\sqrt{2B_D})} \quad (15)$$

E values less than 8kJ/mol indicate physisorption [32]. The value of E in this work was 0.408 kJ/mol showing physisorption. Positive E values show that the adsorption was endothermic and that higher

temperatures would favor the adsorption [40]. B_D ($3x10^{-6}$ mol^2/J^2) is less than unity, indicating microporous adsorbent surface [41] and that the adsorbent may require less number of cycles to reduce the concentration of the adsorbate below regulatory levels [42].

3.3.5. Elovich isotherm

The Elovich isotherm model [43] was originally designed to describe chemisorptions of gas on solids [44]. The model assumes that there is exponential increase in adsorption sites with the adsorption process showing multilayer adsorption [45]. The Elovich isotherm model is expressed as Eq. 16:

$$q_e/q_m = K_E C_e exp(q_e/q_m) \quad (16)$$

The linear logarithmic form of Eq. 16 is Eq. 17:

$$In\,(q_e/C_e) = In\,(K_E q_m) - q_e/q_m \quad (17)$$

A plot of In (q_e/C_e) versus q_e (Fig. 11) gave a straight line with slope $1/q_m$ and intercept In ($K_E q_m$) from which K_E and q_m were calculated. Table 2 shows the parameters K_E, q_m and R^2. The R^2 value (0.809) proves the Elovich model a good fit for experimental data.

3.3.6. Harkin-Jura isotherm

In the application of Harkin-Jura isotherm model, it is assumed that the adsorbent surface is heterogeneous in pore distribution and that adsorption is multilayer [43]. The model is expressed as Eq. 18:

$$1/q_e^2 = (B_{HJ}/A_{HJ}) - (1/A_{HJ}) log C_e \quad (18)$$

A plot of $1/q_e^2$ against log C_e (Fig. 12) gave a straight line with slope $1/A_{HJ}$ and intercept B_{HJ}/A_{HJ}. The values of A_{HJ} and B_{HJ} are shown in Table 2. The R^2 value (0.743) shows that this model is a good fit for experimental data.

3.3.7. Halsey isotherm

The Halsey isotherm model is applied in measuring multilayer adsorption at a relatively large distance from the adsorbent surface [43]. This model is expressed as Eq. 19:

$$q_e = (1/n_H) InK_H - (1/n_H) InC_e \quad (19)$$

A plot of q_e versus In C_e (Fig. 13) gave a straight line with slope $1/n_H$ and intercept $1/n_H InK_H$. The values of n_H and K_H are in Table 2. The R^2 value (0.935) shows that the model is a good fit for experimental data.

3.3.8. Flory-Huggins isotherm

The relationship between behavior of the surface of the adsorbent and adsorption in terms of surface coverage is expressed applying the Flory-Huggins isotherm model [46]. The isotherm model is expressed as Eq. 20:

$$In\,(\theta/C_e) = In\,K_{FH} + n_{FH} In\,(1-\theta) \quad (20)$$

$$\theta = 1 - (C_e/C_o) \quad (21)$$

A plot of In (θ/C_e) versus In (1-θ) (Fig. 14) gave a straight line with slope nFH and intercept In K_{FH}. The values of K_{FH} and n_{FH} are in Table 2. The R^2 value (0.986) shows that Flory-Huggins isotherm model is a good fit for the biosorption experimental data. The Gibbs free energy was calculated applying K_{FH} according to Eq. 22:

$$\Delta G^o_{ads} = -RTInK_{FH} \quad (22)$$

The magnitude of the free energy value (16.13 kJ/mol), which is lower than 20 kJ/mol shows that the biosorption was physisorptive. The negative value of ΔG^o_{ads} shows that the process was spontaneous.

4. Conclusions

Hen egg membrane was successfully applied in the removal of metanil yellow from aqueous solution by batch biosorption. Experimental equilibrium data were simulated with Langmuir, Freundlich, Temkin, Dubinin-Radushkevich. Elovich, Harkin Jura, Halsey and Flory Huggins isotherms. Correlation coefficient values show that the Flory-Huggins isotherm model analyzed experimental data most while the Harkin-Jura model was the least good fit. Results show that the biosorption was endothermic, good, physisorptive and spontaneous. Egg membrane is a good adsorbent for removing metanil yellow from aqueous phase.

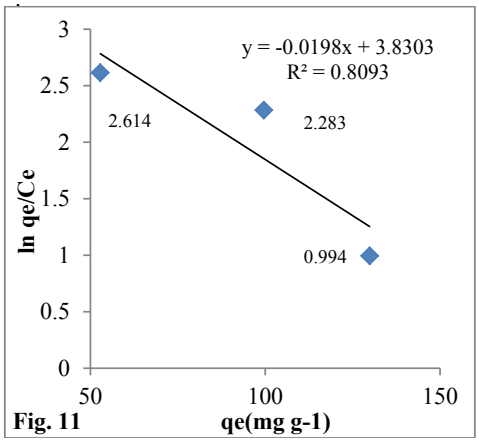

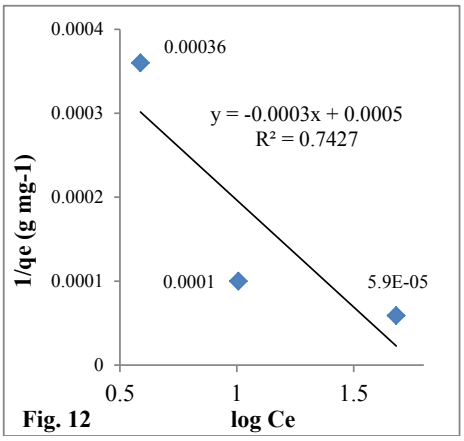

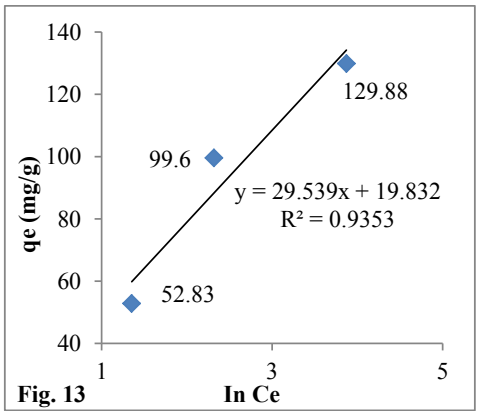

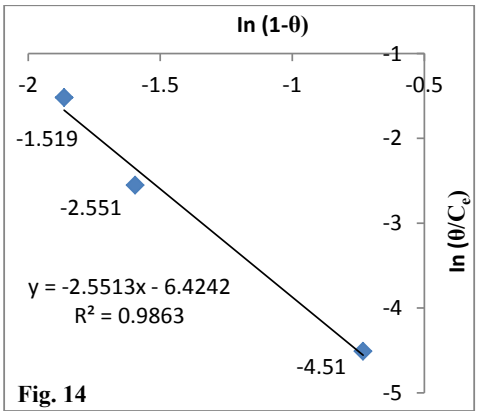

Fig. 11-14. The isotherm plot for biosorption of metanil yellow on hen egg membrane: Elovich (**Fig. 11**), Harkin-Jura (**Fig. 12**), Halsey (**Fig. 13**) and Flory-Huggins (**Fig. 14**)

5. Glossary

A_{HJ} ($g^2\ L^{-1}$) Harkin-Jura isotherm parameter

A_T ($L\ g^{-1}$) Temkin constant corresponding to the maximum binding energy

B ($J\ mol^{-1}$) Temkin constant related to the heat of adsorption

B_D ($mol^2\ J^{-2}$) Dubinin-Radushkevich constant related to average free energy per mole of adsorbate

B_{HJ} ($mg^2\ L^{-1}$) Harkin-Jura isotherm model constant

b_T (J/mol/K) Temkin isotherm constant related to heat of adsorption, showing whether the process is endothermic or exothermic

C_e ($mg\ L^{-1}$) Equilibrium un-adsorbed adsorbate concentration

C_o ($mg\ L^{-1}$) Initial adsorbate concentration

C_{om} ($mg\ L^{-1}$) Maximum initial concentration

C_t ($mg\ L^{-1}$) Un-adsorbed adsorbate concentration at time t

E ($kJ\ mol^{-1}$) Dubinin-Radushkevich isotherm model average energy of adsorption

K_E Elovich isotherm constant

K_F [$mg\ g^{-1}(L/mg)^{-1/n}$] Freundlich isotherm model adsorption or distribution coefficient

K_{FH} ($L\ mol^{-1}$) Flory-Huggins equilibrium constant

k_H ($mg\ L^{-1}$) Halsey isotherm model constant

K_L ($L\ mg^{-1}$) Langmuir constant related to the affinity of the binding sites and energy of adsorption

m (g) mass of adsorbent

$1/n_F$ Freundlich constant indicating adsorption intensity and degree of heterogeneity of adsorbent surface

n_F Freundlich isotherm model constant

n_{FH} Flory-Huggins constant indicating number of adsorbate particles occupying adsorption sites

n_H Halsey isotherm exponent

q_D ($mg\ g^{-1}$) Dubinin-Radushkevich maximum adsorption capacity

q_e ($mg\ g^{-1}$) Equilibrium adsorption capacity

q_m ($mg\ g^{-1}$) Equilibrium adsorption capacity for a complete monolayer

q_t ($mg\ g^{-1}$) Adsorption capacity at time t

R (J/mol/K) Universal gas constant
R_L Hall separation factor or dimensionless constant
R^2 Correlation coefficient
T (K) Kelvin temperature
v (mL) Adsorbate volume
ε (kJ mol^{-1}) Polanyi potential
θ Adsorbent surface coverage

6. References

[1] J. H. Li, H. Yu, Y. Luan, Metal-analysis of the copper, zinc and cadmium absorption capacities of aquatic plants in heavy metal-polluted water. Int. J. Environ. Res. Public Health, 12 (2015) 14958 – 14973. doi: 10.3390/ijerph121214959

[2] N. Gopal, M. Asaithambi , P. Sivakumar , V. Sivakumar, Continuous fixed bed adsorption studies of Rhodamine-B dye using polymer bound adsorbent. Ind. J. Chem. Technol., 23 (2016) 53 – 58.

[3] A. S. Olawale, O. A. Ajayi, M. S. Olakunle, M. T. Ityokumbul, S. S. Adefila, Preparation of phosphoric acid activated carbons from *Canarium schwienfurthii* nutshell and its role in methylene blue adsorption, J. Chem. Eng. Mater. Sci., 6 (2015) 9 – 14.

[4] O. B. Isiuku, M. Horsfall , A. I. Spiff, Adsorption of metanil yellow on chemically-activated carbon in a packed bed column: Effect of activation reagent, J. Eng. Appl. Sci., 8 (2013) 282-289.

[5] W.T. Tsai, K. J. Hsien, H.C. Hsu, C.M. Lin, K.Y. Lin, C.H. Chiu, Utilization of ground eggshell waste as an adsorbent for the removal of dyes from aqueous solution, Bioresour. Technol., 99 (2008) 1623-1629.

[6] B. Koumanova, P. Peeva, S. J. Allen, K. A. Gallagher, M. G. Healy, Biosorption from aqueous solutions by eggshell membrane and Rhizopus oryzae: Equilibrium and kinetic studies, J. Chem. Technol. Biotechnol., 77 (2002) 539-545.

[7] A. A. Hassan, Z. A. Salih, Methylene blue removal from aqueous solution by adsorption on eggshell bed Euphrates, J. Agric. Sci., 5 (2013) 11 – 23.

[8] N. Pramanpol, N. Nitayapat, Adsorption of reactive by eggshell and its membrane, Kasetsart J. Nat. Sci., 40 (2006) 192-197.

[9] B. O. Isiuku, C. N. Nwosu, Fixed-bed adsorption of metanil yellow from aqueous solution on HNO_3-treated-H_3PO_4-activated carbon from gmelina bark, Asian J. Chem., 20 (2017) 475 – 479.

[10] S. Gupta, M. Sundarrajan, K. V. K. Rao, Tumour promotion by metanil yellow and malachit1e green during rat hepatocarcinogenesis associated with dysregulated expression of cell cycle regulatory proteins, Tetragon, Carcin. Mut., (2003) 301-312.

[11] R. Sivashankar, V. Sivasubramanian, A. B. Sathya, S. Pallipad, Biosorption of hazardous azo dye metanil yellow using immobilized aquatic weed. Proceedings of the International Conference on Future Trends in Structural, Civil, Environmental and Mechanical Engineering – FTCEM, 153-157, India, 2013.

[12] R. Jain, N. Sharma, K. RadhapyariRemoval of hazardous azo dye, metanil yellow from industrial wastewater using electrochemical technique, Euro, Water, 27 (2009) 43-52

[13] Z. Tong, P. Zheng, B. Bai H. Wang, Y. Suo, Adsorption performance of methyl violet via α-Fe_2O_3 @ porous hollow carbonaceous microspheres and its effective regeneration through a Fenton-like reaction, Catalysts, 6 (2016) 58. doi: 10.3390/catal6040058

[14] V. O. Njoku, A. A. Ayuk, E. E. Oguzie, E. N. Ejike, Biosorption of Cd (II) from aqueous solution by cocoa pod husk biomass: Equilibrium, kinetic and thermodynamic studies, Sep. Sci. Technol., 47 (2012) 753-761.

[15] J. L. Wang, C. Chen, Biosorbents for heavy metals removal and their future. Biotchnol. Adv., 27 (2009)195.

[16] R. Pelech, F. Milchert, M. Bartkowink, Fixed-bed adsorption of chlorinated hydrocarbons from multicomponent aqueous solution onto activated carbon: Equilibrium column model, J. Colloid Interface Sci., 296 (2006) 458-464.

[17] B. Volesky, Biosorption for the next century, Hydrometallurgy, 59 (2001) 203.

[18] B. O. Isiuku, M. Horsfall, A. I. Spiff, Colour removal from a simulated methyl red wastewater by adsorption on carbon in a fixed bed, Res. J. Appl. Sci., 9 (2014) 202-207.

[19] Association of official analytical chemists (AOAC), official methods of analysis, 15th Ed., Arlington, VA, 1990.

[20] D. H. Williams, I. Fleming, Spectroscopic methods in organic chemistry, 3rd Ed., McGraw Hill book Company (UK) Ltd, pp. 49-58, 1980.

[21] I. L. Finar, Organic chemistry, vol. 1: The Fundamental Principles, 6th Ed., Longman Group Ltd., pp. 207, 1973.

[22] I. L. Finar, Organic chemistry, vol. 2, 5th Ed., ELBS, Longman Group Ltd., pp. 651- 660,1975.

[23] V. O. Njoku, B. H. Hameed, Preparation and characterization of activated carbon from corncob by chemical activation with H_3PO_4 for 2,

4-dichlorophenoxyacetic acid adsorption. Chem. Eng. J., 173 (2011) 391-399.

[24] O. A. Ekpete, M. Horsfall, A. I. Spiff, Removal of chlorophenol from aqueous solution using fluted pumpkin and commercial activated carbon, Asian J. Nat. Appl. Sci., 1 (2010) 96 – 105.

[25] A. Mahvi,A. Maleki, A. Eslami, Potential of rice husk and rice husk ash for phenol removal in aqueous systems, Amer. J. Appl. Sci., 14 (2004) 321-326.

[26] R. Han, W. Zou, W. Yu, S. Cheng, Y. Wang, J. Shi, Biosorption of methylene blue from aqueous solution by phoenix tree leaves, J. Hazard. Mater., 141 (2007) 156 – 162.

[27] B. Koumanova, P. Peeva-Antova, Z. Yaneva, Adsorption of 4-chlorophenol from aqueous solution on activated carbon: Kinetic, J. University Chem. Technol. Metallurg., 40 (2005) 213-218.

[28] M-R. H. Mas Haris, K. Sathasivam, The removal of methyl red from aqueous solution using banana pseudo fibers. Amer. J. Appl. Sci., 6(2009) 1690-1700.

[29] M. Jones Jr, Organic chemistry, W. W. Norton and Company, 2nd Ed., pp. 715, 2000.

[30] P. D. Rocha, A. S. Franca, L. S. Oliveira, Batch and column studies of phenol adsorption by an activated carbon based on acid treatment of corn cobs, IACSIT Int. J. Eng. Technol., 7 (2015) 459 – 464.

[31] M. A. Yousif, A. A. Atia, O. F. Zaid, I. A. Ibrahim, Efficient and fast adsorption of phosphates and sulphates on prepared modified cellulose, J. Dispersion Sci. Technol., 36 (2015) 1628 – 1638.

[32] O. S. Bello, T. A. Fatona, F. S. Falaye, O. M. Osuolale, V. O. Njoku, Adsorption of eosin dye from aqueous solution using groundnut hull-based activated carbon: kinetic, equilibrium and thermodynamic studies, Environ. Eng. Sci., 29 (2012) 186 – 194.

[33] I. Ismi, H. Elaidi, A. Lebkiri, A. Skalli, E.H. Rifi. Adsorption of silver (Ag^{+}) from aqueous solution by the sodium polyacrylate form, Int. J. Adv. Res. Technol., 3 (2014) 121-127.

[34] B. O. Isiuku, C. U. Nwogu, Cationic dye (methyl violet) removal from aqueous solution by egg membrane in a batch biosorption process, Asian J. Green Chem., 3 (2019) 236-257.

[35] V. O. Njoku, C. Obi, E. E. Oguzie, A. A. Ayuk, O. S. Bello, Removal of Cr (III) and Zn (II) from aqueous solutions by a Nigerian natural clay, Int J. Chem., 22(2012) 57-65.

[36] J. U. K. Oubagaranadin, Z. V. P. Murthy, P. S. Rao, Applicability of three-parameter isotherm models for the adsorption of mercury on fuller's earth and activated carbon, Ind. Chem. Eng., 49 (2007) 196 – 204.

[37] M. I. Temkin, V. Pyzhev, Kinetics of ammonia on promoted iron catalysts. Acta Physiochim. URSS, 12 (1940) 217 – 222.

[38] M. Dutta, J. K. Basu, M. H. Faraz, N. Gautam, A. Kumar, Fixed –bed column study of textile dye Direct Blue 86 by using a composite adsorbent, Archives of Appl. Sci. Res., 4 (2012) 882 – 891.

[39] J. C. Igwe, A. A. Abia, A bioseparation process for removing heavy metals from waste using biosorbents, J. Biotechnol., 5 (2006) 1167-1179.

[40] T. A. Khan, S. Sharma, I. Ali, Adsorption of Rhodamine B dye from aqueous solution onto acid activated mango mangifera indica leaf powder: Equilibrium, kinetic and thermodynamic studies. J. Toxicol. Environ. Health Sci., 3 (2011) 286-297.

[41] U. Israel, U. M. Eduok, Biosorption of Zn from aqueous solutions using coconut (Cocus nucifera L.) coir dust, Archives Appl. Sci. Res., 4 (2012) 809-819.

[42] Z. Aksu, J. Yener, A comparative adsorption/ biosorption study of monochlorinated phenols onto various sorbents, Waste Manage., 21(2001) 695 – 702.

[43] N. Ayawei, A. Ebelegi, D. Wankasi, Modeling and interpretation of adsorption isotherms, J. Chem., (2017)1-11. https://doi.org/10.1155/2017/3039817

[44] O. Hamdaou, E. Naffrechoux, Modeling of adsorption isotherms of phenols and chlorophenols onto granular activated carbon. Part II: Models with more than two parameters. J. Hazard. Mater., 147 (2007) 401-411.

[45] M. Gubernak, W. Zapala, K. Kaczmarski, Analysis of amylbenzene adsorption equilibria on an RP-18e chromatographic column, Acta Chromatogr., 13(2003) 38-59.

[46] B.O. Isiuku, D. C. Anyanwu, C. N. Nwosu, S. C. Iroamaka, Batch adsorptive removal of metanil yellow from simulated dye wastewater using nitric acid-modified-H_3PO_4-activated carbon (NAMPAAC) from *Gmelina arborea* bark: equilibrium and isotherm studies, Desal. Water Treatment 70 (2017) 380-386.

Analytical Methods in Environmental Chemistry Journal Vol 2 (2019) 27-38

AMECJ

Research Article, Issue 4

Analytical Methods in Environmental Chemistry Journal

Journal home page: www.amecj.com/ir

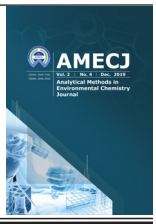

Enhancing the effect of zinc oxide on the absorption of heavy metals from wastewater by using silica in graphene bed

Ahmad Ghozatloo[a,*], Atefeh Enayatollahi[a]

[a] *Research Institute of Petroleum Industry (RIPI), West Blvd. Azadi Sport Complex P.O. Box: 14665-137, Tehran, Iran*

ARTICLE INFO:

Received 2 Sep 2019

Revised form 26 Oct 2019

Accepted 16 Nov 2019

Available online 26 Dec 2019

Keywords:

Graphene,
Silica,
Adsorbent,
Heavy metals,
Wastewater

ABSTRACT

In this study, the effects of nanostructure absorbent of zinc oxide (ZnO) in graphene bed for wastewater treatment were studied. Initial analysis was undertaken to identify the existing metals and their concentration in the prepared wastewater. It was seen that the diluted solution consisted of the ambivalence ions of lead, copper, nickel, cadmium, and silver with the concentration of 73.31, 81.19, 54.6, 98.1and 76.1 milligram per liter, respectively. Trivalent chrome, with a concentration of 98.1 milligram per liter was also observed. Therefore, by adding various amounts of absorbent (20, 30 and 50 mg) to the wastewater sample and adjusting the pH to 5 and 6, each metal was separately absorbed. Consequently, the concentration of the remaining metals was measured, and it was observed that absorbent was effective for the absorption of lead, copper and silver (with a reduction of up to 80%), however, the absorbent was weak in the absorption of nickel and chrome. Hence, the silicon nanoparticles added to absorbent and the experiments repeated. It was observed that the presence of silicone resulted in higher absorption of nickel and chrome but negatively affected the absorption of copper and silver. Electrical charges at lower pH's have an inverse impact on the absorption of metal ions that is due to the electrostatic repelling forces between the positive charges. In more acidic solutions, the carbonyl groups in the surface of composite create positive charges and hence repel the metal ions. Hence, the performance of the absorbent improves by reducing the acidity of the solution. At the pH of six, the number of hydroxide increases and the capacity of absorbing metal cations increase.

1. Introduction

During the past decades, due to population growth and industrial development, the demand for freshwater and wastewater treatment has significantly increased. This includes the treatment of industrial wastewater that contains considerable amounts of heavy metals, such as; lead, copper, chrome, cadmium, nickel, iron, zinc, arsenic, manganese and mercury. Among the various industries, the weaving industries produce a significant amount of chemically contaminated wastewater. The concentration of these chemicals depends on the raw materials and the methods of production. Due to the variety of different processes and their demand for large amounts of water, these industries are responsible for the production of considerable contaminated water. Production of textile requires several mechanical processes such as spinning, weaving, knitting, etc. [1]. Besides, there exist the "wet processes" that include wool washing, bleaching, and dying. During the production processes of fibers, cloth and, clothes several contaminators will be added

*Corresponding Author. Ahmad Ghozatloo
E-mail: ghozatlooa@ripi.ir
https://doi.org/10.24200/amecj.v2.i04.88

to the wastewater. As such, during the dying process, heavy metals such as chrome and copper contaminate wastewater. It is vital to reduce and remove these metals, as these will disable the bacteria's in the biological treatment units. Additionally, these metals can contaminate surface and underground water sources, which due to their toxicity can cause death by affecting nerves and kidneys [2]. There are national and international codes and standards that define a limit for disposing of the wastewater containing heavy metals to the water resources. Exceeding these limits could be fatal and harm the environment. The main concern in wastewater treatment in weaving industries is the quantity of disposed wastewater. Dispose of wastewater in these industries are often to the absorbent wells, which will cause irreversible damages to the environment. The sampling results show high values of pH, BOD, COD and dye. The quantity of COD, BOD and TSS was reported 750 - 3500 milligram per liter, 300-1800 milligram per liter, 18-155 milligram per liter, respectively [3]. In the same study, the pH was observed to be varying from 5 to 12 and the quantity of dye was reported to be from 30 to 550 units. The dying weaves produce a significant amount of wastewater. If these were disposed to the environment without proper treatment, the damages to the environment would be significant. This reveals a pressing need for efficient methods of treatment. Cadmium and nickel are examples of toxic elements, which traces of these are seen in wastewater from mining, alloying and battery production industries. Adsorption is one of the methods used to reduce these elements. Nowadays various adsorbents are used with the capability of removing organic and inorganic contaminators, which the most common adsorbent is activated carbon. The activated carbon is not an economical solution for large scale treatment units, as there are significant losses of carbon in the regeneration process [4]. The critical elements for selecting the reduction methods are environmental issues, regeneration and economic matters. In the past few years, improvement in nanotechnologies helped in the production of nanostructures that are distinct due to their larger surface. The unique structure of nano adsorbents caused them to be high capacity adsorbents. On this basis, wastewater treatment is considered one of the main applications of nanotechnologies that have the potential to considerably improve the quality and capacity of the water and wastewater treatment units.

2. Experimental

2.1. ZnO nanostructure synthesis in graphene bed

Firstly, synthesis of the graphene sheets by oxidation process in accordance with hummer's method in the concentrated acidic media that contains mixing ratio of 1:2:46 of concentrated sulphuric acid, graphite powder, and sodium nitrate, respectively in 2°C temperature with continuous mixing. Afterward, potassium permanganate to a ratio of 6 added to mixture slowly and after oxidation reaction, mixture temperature rose to 40°C and mixing plateaued for 1 hour. Added distilled water and sodium hypochlorite solution stopped the reaction and trended the pH to neutral and then filtration, washing and drying mixture, respectively. The yellowish powder remained was graphene. In order to extend synthesized graphene sheets completely, pour 1mg graphene oxide powder in 100ml distilled water and apply ultrasound for 3 hours. The resulting solution, centrifuged for half an hour by 6500rpm in order to get out unexpended graphene sheets by sedimentation process from the solution. Then added 3 grams of zinc oxide salt powder ($6H_2O*Zn(NO_3)_2$) to remain solvent and apply ultrasound spanned 1 hour then stirred it slowly for more than 3 hours in 90 centigrade degrees. Poured the produced mixture in an autoclave tank and carried out a hydrothermal synthesis method for 6 hours at 180 °C. Then cooled it down to room temperature naturally and washed it with extra ethanol. The amount of resulting graphene was about 20 percent [1]. The final structure was a hybrid form of zinc monoxide at the surface of

graphene (GO/ ZnO) that was used as the first type of absorbent. Figure (1) illustrates the TEM of this structure. As shown in Figure (1) use of graphene sheets leads to produce an appropriate culture for bonding nanoparticles of zinc oxide on it without aggregation of zinc particles, in the second step silica nanoparticles added on this hybrid structure. Therefore, in order to build graphene/zinc/silica nano-composite firstly applied ultrasound for the solution of 0.5 grams synthesized GO/ZnO in 100 ml of Dionysius water for half an hour in room temperature. After that added 2 g of CTAB and mixed completely, then by using caustic soda adjusted pH around 9 and dropped 1mg of tetraethyl orthosilicate solution and heated by 40°C of temperature the mixture in a closed system with magnetic agitator for 24 hours. The next step was to dry out the solution after filtration the resulting mixture and washed it with extra Dionysius water in Avon with 60 °C for one day. This resulting powder is the second type absorbent of this study. Figure (2) illustrates the TEM of that. As shown in Figure (2) darkness particles of SiO_2 bonded and distributed correctly within ZnO nanoparticles that stabilized on graphene culture.so it can be seen that the second type absorbent structure formed as well.

2.2. Apparatus and Reagents

The furnace atomic absorption spectrophotometer (GF-AAS, GBC 932 plus, Australia) were used for the determination of Cu, Ni, Cd, Pb, Cr and Ag in samples. First, the manufacturer's manual book of GF-AAS was prepared. The hollow cathode lamp (HCL) with wavelength and current favorite for

Table 1. The instrumental conditions of heavy metals by GF-AAS

Element	Current(mA)	Wavelength(nm)	Slit(nm)	*LR	*LOD	*LOQ
Cu	4.0	327.4	0.5	1-30	0.3	1.0
Ni	9.0	229.0	0.2	1.5-60	0.4	1.5
Cd	3.0	228.8	0.5	0.2-6.5	0.05	0.2
Pb	3.0	283.3	0.4	2.0-70	0.5	2.0
Cr	7.0	357.9	1.5	1.0-15	0.3	1.0
Ag	4.0	328.1	0.5	0.2-4.2	0.05	0.2

*Linear range (LR, µg L^{-1}); Limit of detection (LOD, µg L^{-1}); Limit of quantification (LOQ, µg L^{-1})

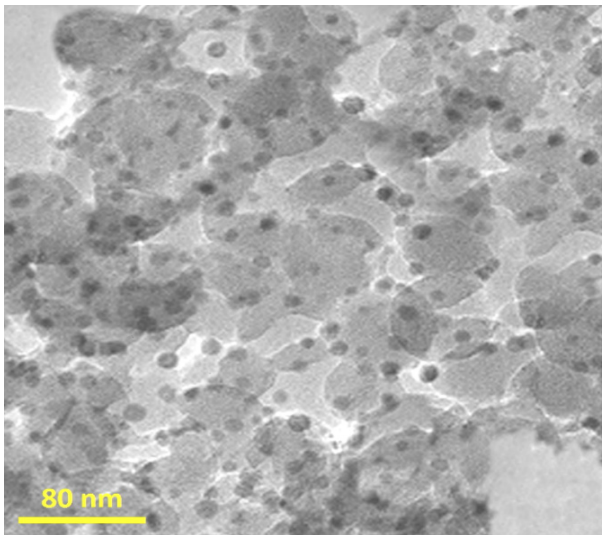

Fig. 2. TEM nanostructure of GO /ZnO/SiO_2

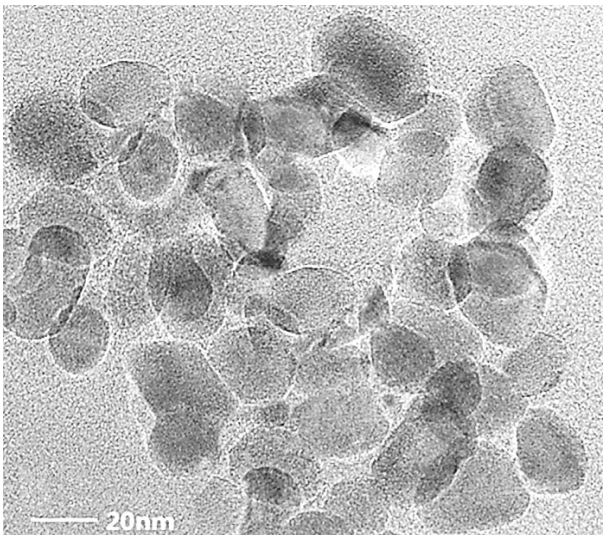

Fig. 1. TEM nanostructure of GO /ZnO

Table 2. The initial quantity of metal ions in sample wastewater

Pollutant	Metal ions	Initial quantity
Copper	Cu^{++}	19.8
Nickel	Ni^{++}	6.5
Cadmium	Cd^{++}	2.3
Lead	Pb^{++}	31.7
Chromium	Cr^{3+}	1.98
Silver	Ag^{++}	1.76

Cu, Ni, Cd, Pb, Cr and Ag was applied by 20 µL of sample injection to graphite tube of GF-AAS. For measuring pH, a Metrohm pH meter based on glass electrode was used (E-744, Switzerland) in wastewater samples**.** The instrumental conditions are listed in Table1.

2.3. Analytical Procedure

The adsorption of heavy metals such as, Cu, Ni, Cd, Pb, Cr and Ag based on GO/ZnO and GO/ZnO-SiO2 as sorbent were studied. All metals determined by electrothermal atomic absorption spectrometry (GBC, 932; ET-AAS). The different concentration heavy metals (1-50 ppm) in waters was used based on GO/ZnO and GO/ZnO-SiO2 (10-50 mg) for heavy meal adsorption at pH=5 and 6. After shacking, the heavy metals separated and adsorbed by GO/ZnO or GO/ZnO-SiO2. Other parameters such temperature, pH and sonication time were studied and optimized. In optimized conditions, temperature (25^{o}C), pH=5-6, and shacking of 5 min was achieved.

3. Results and Discussion

3.1. Dilution process

The wastewater used in this study belongs to an active center of the dyeing and printing industry, which kept motionless in a closed container for 24 hours span until sedimentation had been done. Then add an equal amount of Dionysius water into solution in order to half the pollutants concentration. Firstly, in order to assess the wastewater condition, measured the levels of metal ions by the atomic absorption method as listed in a Table (2). According to Table (1) the despite the dilution of prepared wastewater a large variety of heavy metals in significant amounts exists. In order to pursue the used absorbent function firstly added 0.2, 0.3 and 0.5 grams of it into 50 ml of selected wastewater. For pH adjustment used 0.1solution of NaOH. Each test carried out on 5-6 pH range.

Table (3) represents the samples and pH of experiments. In every experiment samples put on the ultrasonic device for 12 hours and afterward the liquid part of solution separated from the solid part by centrifuge equipment and then the concentration of remaining metals in solutions measured by atomic absorption machine. All experiments carried out at room temperature.

3.2. Discussion

As represented in Table (3), the existence of silica nanoparticles within the absorbent structure generally improves the adsorption function and increases adsorption efficiency that strongly subordinates with pH level, so that, in general view, the maximum efficiency of adsorption occurs when pH equals 6. Results in adsorption rate deal with pH value represent that it was rose up by increasing of the adsorbent amount, that the main reason for it is due to the total increase in adsorption valence for each adsorbent unit, in other words, by increasing of the adsorbent content, more adsorption bed provided for heavy metals. Also, it can be seen that the adsorption value varies for different metals which process differently within the dissimilar experimental conditions for each metal. Hence, in the following, the adsorption conditions for metals were investigated.

3.3. Lead adsorption

Results of Pb adsorption on used adsorbent shows that in pH of 5 the rate of adsorption increases by rising in amount of adsorbent, which is adsorbed 57.8% of Pb in case of 20 mg of adsorbent existence and by increase this till 30 mg, adsorption rate rises to 64.9%, in other way the adsorption rate improves 12 percent. Also in the concentration of

Table 3. Samples and pH status at the experiments

Adsorbent	conc.	pH	Remained concentration(mg L^{-1})					
			pb^{2+}	cu^{2+}	Ni^{2+}	cd^{2+}	Cr^{3+}	Ag^{2+}
Non	0		31.73	19.81	6.54	2.32	1.98	1.76
GO/ZnO-20	20		11.10	4.36	6.24	1.23	1.86	0.49
GO/ZnO-30	30		9.19	3.37	6.24	1.25	1.84	0.29
GO/ZnO-50	50	6	6.34	2.18	6.18	1.23	1.82	0.19
GO/ZnO-SiO2-20	20		8.94	8.12	3.12	1.18	1.43	0.68
GO/ZnO-SiO2-30	30		7.39	6.93	2.75	1.13	1.20	0.46
GO/ZnO-SiO2-50	50		5.05	5.38	2.62	1.04	1.15	0.34
Non	0		31.73	19.81	6.54	2.32	1.98	1.76
GO/ZnO	20		13.39	4.82	6.37	1.78	1.92	0.90
GO/ZnO	30		11.14	3.63	6.37	1.80	1.89	0.67
GO/ZnO	50	5	7.79	2.19	6.31	1.78	1.87	0.55
GO/ZnO-SiO2	20		12.85	10.36	4.00	1.72	1.81	1.13
GO/ZnO-SiO2	30		10.02	8.95	3.56	1.66	1.74	0.87
GO/ZnO-SiO2	50		6.27	7.26	3.41	1.55	1.68	0.73

50 milligrams of adsorbent, it reaches 75.4% that is equivalent to 30 percent of enhancement. Therefore, the first type adsorbent structure (graphene hybrid/ zinc oxide) represents an appropriate adsorbent for lead adsorption. Although the existence of silica within this adsorbent amplifies their ability of adsorption, this may not be significant, in a way, that adsorption improves 3% and 6% in the concentration of 20 milligrams and 50 milligrams, respectively, the results demonstrate in the Figure (3).

According to Figure (3), the presence of silica within the GO/ZnO adsorbent structure was ineffective to reach more adsorption of

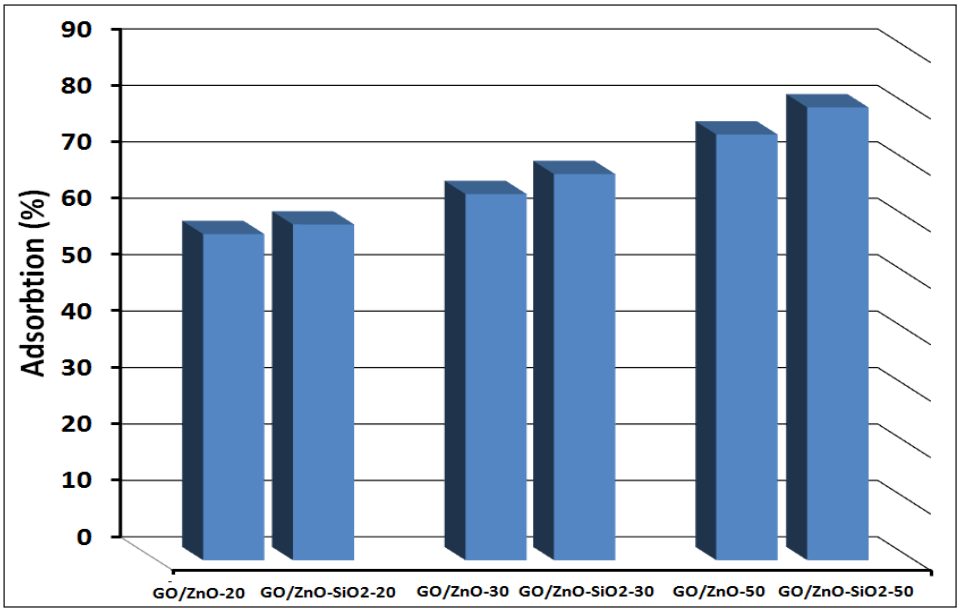

Fig. 3. Silica effect in GO/ZnO structure for Pb adsorption (pH=5)

Pb. Therefore, in existence 20 mg of adsorbent in wastewater 65%of Pb has adsorbed and by increasing this quantity to 30 mg adsorption yield rose up to 71%, in the other word adsorption improved 9% and in 50 milligrams of adsorbent, it reached 80%, equivalent 23% of increase. The same results obtained in pH of 6. Although the adsorption shows a little improvement in this pH, it is not noticeable. Figure (4) demonstrate the pH effect in different quantities of the second type of adsorbent in which silica added to their structure.

As illustrated the adsorption process is better in all amount of adsorbent (second type) in pH of 6 than 5, but the effect of pH in lower amounts of adsorbent (20 mg) is more significant, in a way, in higher concentrations 4% improvement has seen whereas in lower points of adsorbent's concentration it has been more than 20% (Fig.4).

3.4. Copper adsorption

Results of Cu adsorption on used adsorbent shows that in pH of 5 the rate of adsorption increases by rising in amount of adsorbent, which is adsorbed 75.7% of Pb in case of 20 milligrams of adsorbent existence and by increase this till 30 milligrams, adsorption rate rises to 81.7%, in other way the adsorption rate improves 8 percent. Also in the concentration of 50 milligrams of adsorbent, it reaches 88.9% that is equivalent to 17 percent of enhancement. Therefore, the adsorbent structure (GO/ZnO) is considered as an approximately appropriate adsorbent for copper adsorption. The existence of silica within this adsorbent structure reduces their function and abilities significantly, in a way that in this situation,20 milligrams of adsorbent low off about 37% in adsorption or 29% reduction for 50 milligrams of adsorbent's concentration. The results represent in Figure (5).

According to the bar chart in Figure (5) it is considered that added silica nanoparticles to GO/ZnO structure in order to more adsorption of copper not only didn't be efficient but also reduced it. The same results obtained in pH of 6. Although the adsorption level is better in this pH, it's behavior and the proceeding similarly continues, for 20 mg concentration of adsorbent in wastewater solution,78% of copper adsorbed and by its increase to 30 mg adsorption rose up to 83%, in other words, adsorption efficiency improved 6% improved. Also, 50 milligrams of adsorbent lead to 89% copper adsorption that is equivalent to 14% of improvement. Due to the function of both adsorbent structure, the existence of silica within this adsorbent structure strongly reduces the copper

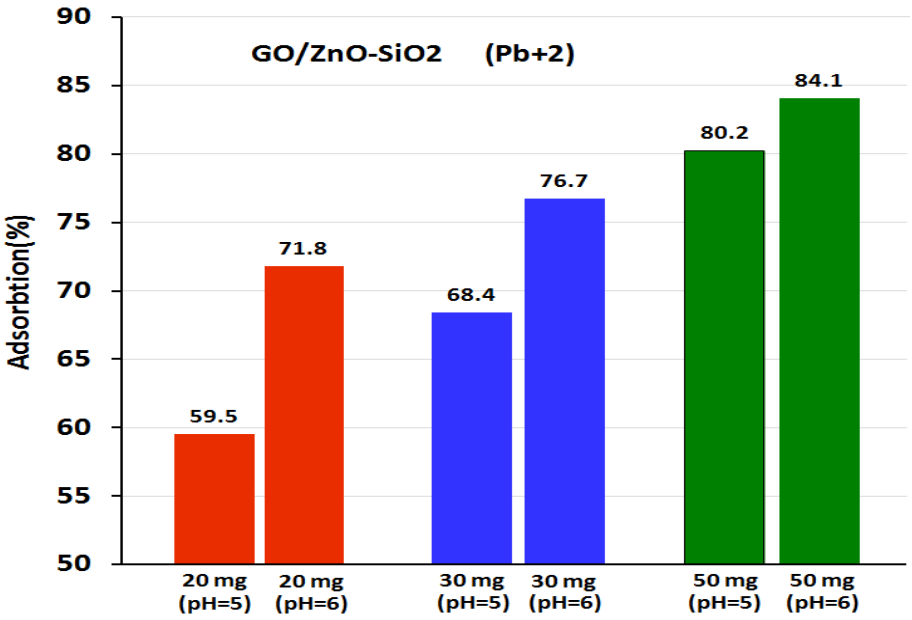

Fig. 4. Comparison of the pH effect by the different quantity of adsorbent GO/ZnO/SiO2

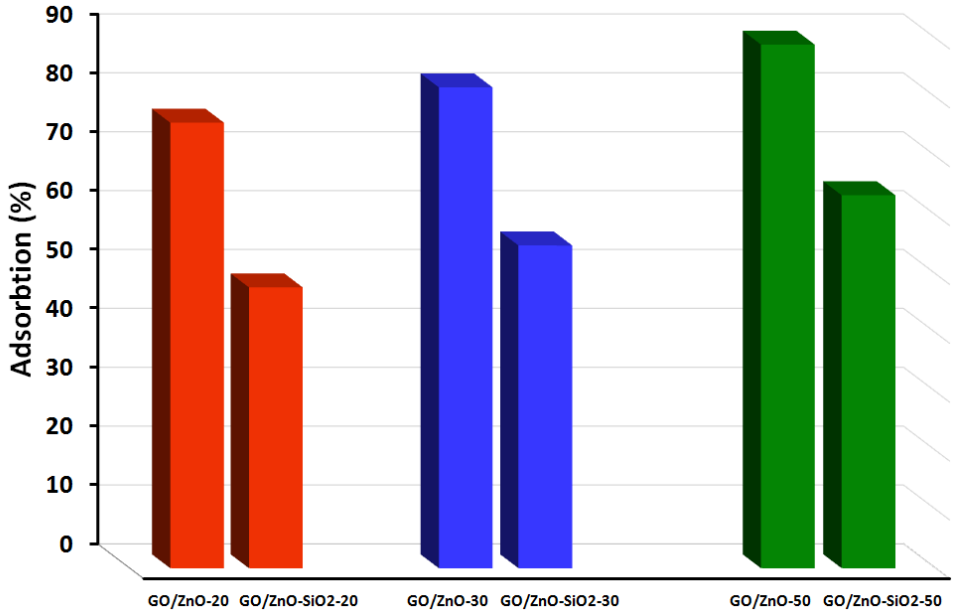

Fig. 5. Effect of silica within the GO/ZnO adsorbent structure to copper adsorption(pH=5)

adsorption which is subordinating to wastewater pH. Figure (6) represents the effect of pH for defined quantities of the second type adsorbent.

As represented in the Figure (6), the adsorption process is better in all amount of adsorbent (second type) in pH of 6 than 5. But, the similar to lead adsorption the effect of pH in lower amounts of adsorbent (20 mg) is more significant, in a way, in higher concentrations 14% improvement has seen whereas in lower points of adsorbent's concentration it has been more than 23%.

3.5. Nickel adsorption

Results of nickel absorption by the specified adsorbents express that in the pH of 5, adsorption rate rises by increasing adsorbent concentration.

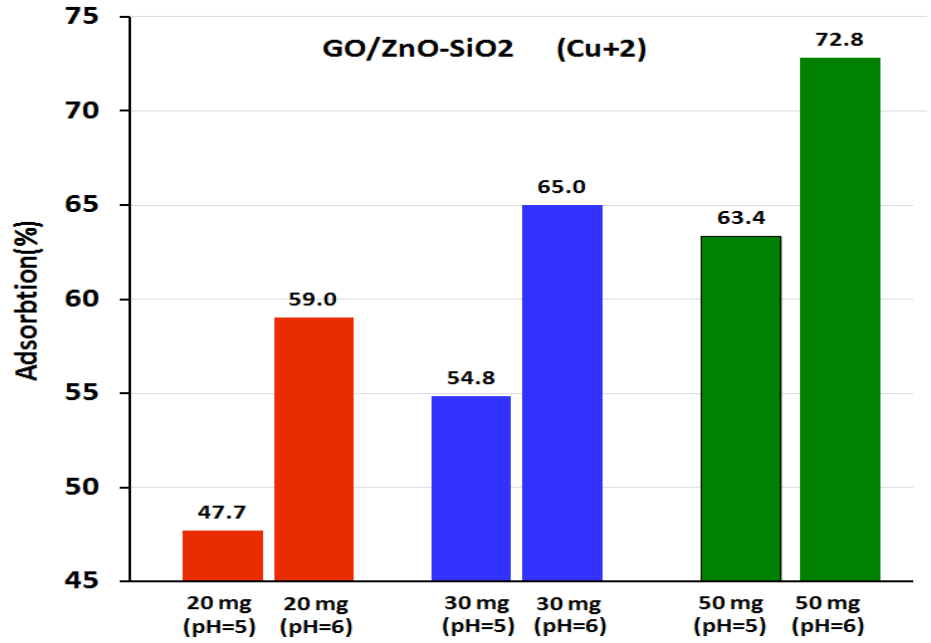

Fig. 6. Comparison of the pH effect on Cu adsorption by the different quantity of adsorbent GO/ZnO/SiO2

The first type of adsorbent acts weakly in nickel adsorption, in a way that due to the existence of 20 milligrams of adsorbent in wastewater, only 2.6% of nickel adsorbed and by rising its concentration to 30 milligrams adsorption plateaued and then went up slowly till 3.5% for 50 mg of the adsorbent concentration. Therefore, GO/ZnO structures have known as an inefficient adsorbent for nickel. Chang the adsorbent structure to GO/ZnO/SiO_2 strongly improved its ability in nickel adsorption, in a way that by added 20 milligrams of this structure into wastewater adsorption yield reached to 38.8%, despite of it is not acceptable yet but it shows that silica is the main factor to the nickel adsorption from wastewater. Also in 50 milligrams of adsorbent, the adsorption amount raised up to 45.6% that equivalent by 17% more nickel adsorption. The results demonstrate a bar chart in Figure (7).

As shown in Figure (7) the existence of silica nanoparticles within the GO/ZnO in order to more adsorption of nickel act effectively and strongly increased the adsorption results. Similar proceeding to this has shown in the pH of 6 meanwhile the results are better. Results showed that the adsorbent concentration of 20 milligrams in per liter of wastewater, adsorbed 52.3% of its nickel and by increasing that until 30 mg adsorption range reach to 58%, means adsorption efficiency improved 10 percent and also in 50 milligrams of adsorbent concentration, the adsorption amount was 59.9% that is equal to 14% increase in adsorption yield. On the other hand, the existence of silica in the adsorbent structure enhances nickel adsorption efficiently. As considered in both types of adsorbent function, it is obvious that silica leads to a significant increase of nickel adsorption. it is subordinated to the pH of wastewater. The pH effect on nickel adsorption in different quantities of the second type of adsorbent that is included silica represented as a bar chart in Figure (8).

As represented in the Figure (8) adsorption process is better in all amount of adsorbent (second type) in pH of 6 than 5, but unlike with lead metal adsorption, the pH's effect shows off with the same pattern in different quantities of the adsorbent, which shows 14% of improvement for higher concentration and 23% for lower ones.

3.6. Cadmium adsorption

The study results of cadmium adsorption on defined adsorbent represent that in pH of 5 adsorptions weren't changed by increasing of

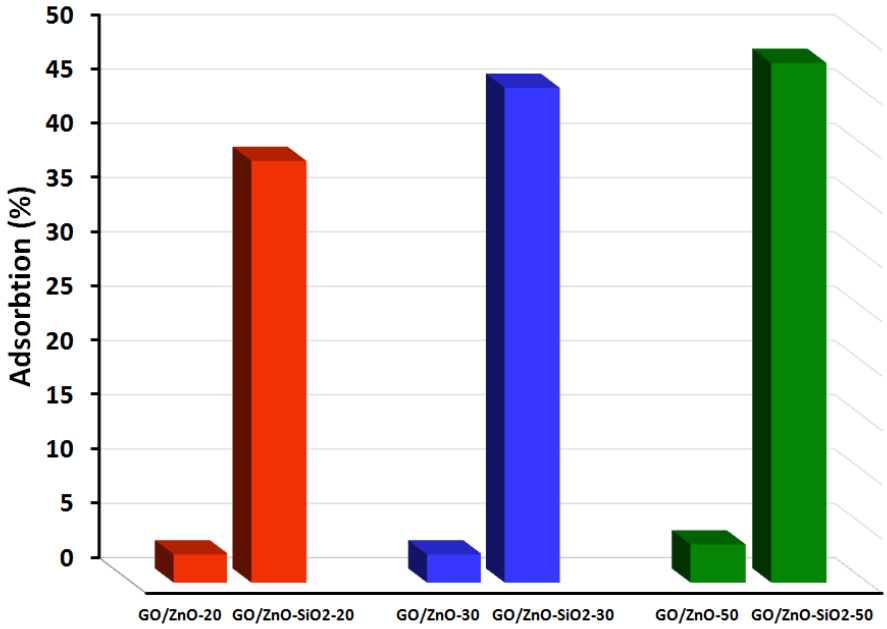

Fig. 7. Effect of silica within the GO/ZnO adsorbent structure to nickel adsorption (pH=5)

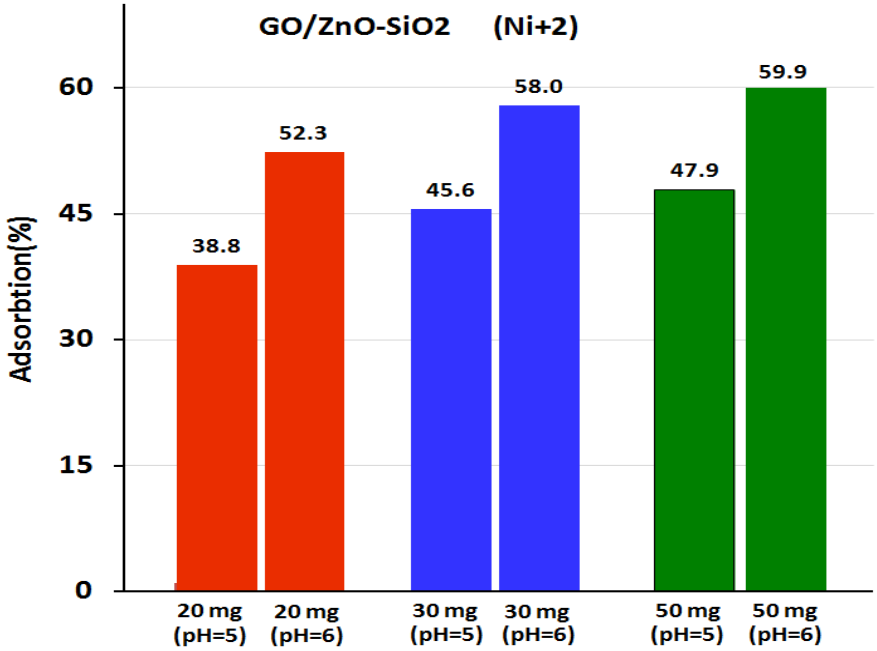

Fig. 8. Comparison of the pH effect on Ni adsorption by the different quantity of adsorbent GO/ZnO/SiO_2

adsorbent concentration. The first type of adsorbent ‘s function was weakness, in which,20 milligrams of its concentration leads to adsorb 23.3% of cadmium and by increasing that to 30 and then 50 milligrams per liter of wastewater the adsorption of cadmium plateaued. So, the GO/ZnO structure had seen as an adsorbent with moderate efficiency that absorbs a few amounts of cadmium at low levels and then remains constant. Even added silica to adsorbent structure did not change their ability to adsorb cadmium. The existence of 20 milligrams of adsorbent with silica could adsorb 25.9 % of cadmium that didn’t have noticeable difference by the first type of adsorbent. so, it seems that not only silica isn’t be adsorbing factor of cadmium in wastewater, but also due to steric hindrance of cadmium ions with atomic number of 48, adsorption of this heavy metal is based on surface of nanostructure that most of the time adsorption quantities overmatch by steric competition on adsorbent surface by increasing of adsorbent concentration. Also in 50 milligrams of adsorbent, the quantity of adsorption reaches 33.2% that it is 42 percent more cadmium adsorption than the case of silica absence. The results illustrated in Figure (9).

According to Figure (9), it showed that the existence of silica nanoparticles in the GO/ZnO structure in order to more cadmium adsorption act slowly and somewhat increases the adsorption. Similar results with about double improvement obtained that represents the strong effect of pH on the adsorption process. For this number of pH, 20 milligrams GO/ZnO/SiO_2 ،adsorbed 47% of cadmium from wastewater and by increasing in adsorbent concentration, the adsorption trends up insignificantly. Moreover, silica in the structure didn’t change the adsorption rate noticeable. Figure (10) demonstrates the effect of pH in different concentrations of the second type of adsorbent and it represents that in all quantities of GO/ZnO/SiO_2 adsorption yield is better in pH of 6 than 5, in a way that in high concentration of adsorbent 66% and in its lower concentration 89% improvement is seen. Therefore, adsorption gets better in the lower concentrations of adsorbent and changes the pH number makes it double.

4. Conclusions

The most important parameter in absorbing heavy

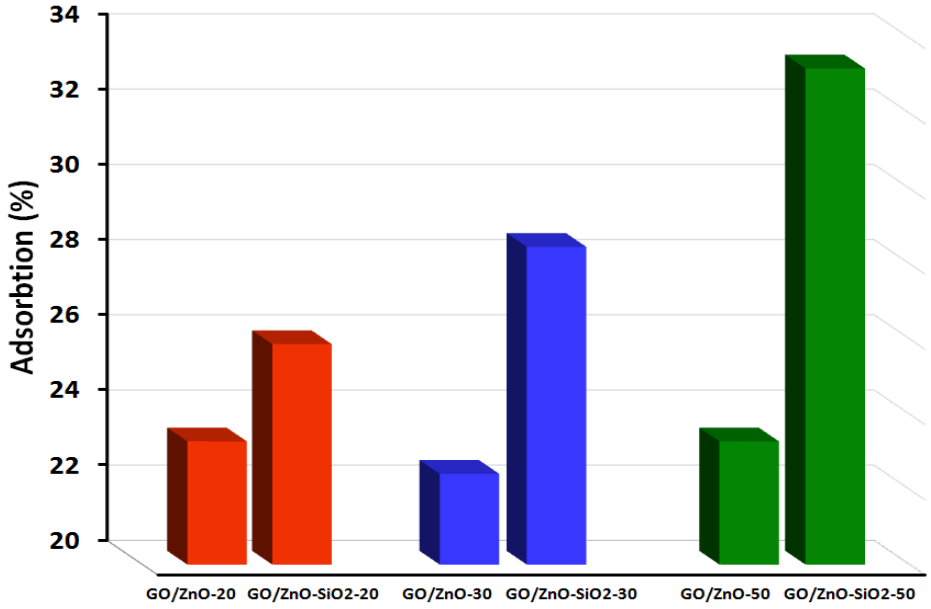

Fig. 9. Effect of silica within the GO/ZnO adsorbent structure to cadmium adsorption (pH=5)

metals in industrial wastewaters that contain a high concentration of metals is the acidity of the wastewater. The results of this experiment have shown that metals often exist in wastewater as ions, in which their interactions are controlled by the acidity of the wastewater. The metal cations in acidic environments are repelled by the cations in the solution, and hence their effects are converged. Under these circumstances, the adsorption processes are emulative and hence the adsorption efficiency diminishes [11]. Hence, one would be able to enhance the efficiency by adjusting pH, that is a function of metal ions in the wastewater. However, it must be considered that both basic and acidic environments are negatively affecting the adsorption efficiency. Hence the type and quantity of the existing metals and the adsorbent used can affect the adsorption process. In this study, it was also observed that the best adsorption process takes place at pH of around 6. The effect of silicon on the structure of nanocomposite, causes the absorbing surface to be positively charged, which are inappropriate for heavy metals. The electro-statically force between anions and cations, at increased pH, causes the efficiency of adsorbing nickel and cadmium to improve [12]. Additionally, the silicon nanostructure used in the adsorbent, oddly resulted in higher adsorption in pH of 6 as compared to pH of 5. Presence of silicon significantly increases the adsorption chrome but reduces the copper adsorption, and has a neutral effect on cadmium adsorption. From this, it can be concluded that the adsorption processes depend on chemistry of the adsorbs as well as the reaction of the existing dissolved metals. Therefore, in order to improve the performance of the graphene-based adsorbents with ZnO, it recommended that the heavy metals removed first, then reduced the chrome, and nickel using silicon. Also in pH of around 6, improves the performance of graphene bases to some extent and enhances the efficiency. Overall, the graphene-ZnO recommended for pre-treatment of wastewater by adsorbing heavy metals. Afterwards, there is a need for the main treatment to reduce the metals to their acceptable limits according to the standards. During the initial stages of adsorption, several adsorbing sites are available. However, as time passes, due to repelling forces between the absorbed matter and the dissolved molecules, the free sites are hardly usable. It was also observed that increasing the concentration of metals, causes the absorbing efficiency to drop. In lower concentrations the chance of adsorption increases and ions are able to react with the

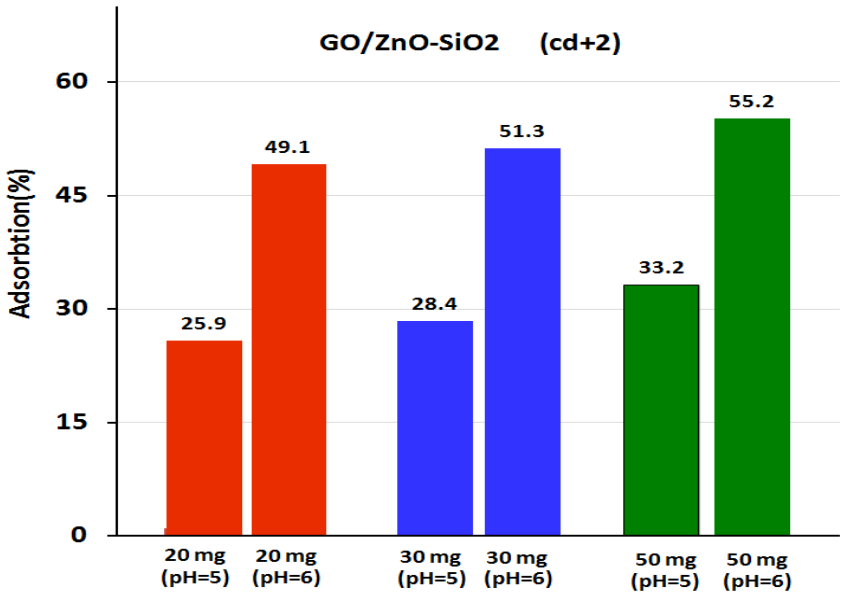

Fig. 10. Comparison of the pH effect on Cd adsorption by the different quantity of adsorbent GO/ZnO/SiO_2

adsorbing surface, which improves efficiency.

5. References

[1] D. Gumuş, F. Akbal, Photocatalytic degradation of textile dye and wastewater, Water Air Soil Pollut. Focus., 216 (2011) 117–124.

[2] M.R. Al-Mamun, S. Kader, M.S. Islam, M.Z.H. Khan, Photocatalytic activity improvement and application of UV-TiO2 photocatalysis in textile wastewater treatment: A review, Environ. Chem. Eng., 7 (2019) 48-61.

[3] C.R. Holkar, A.J. Jadhav, D.V. Pinjari, N.M. Mahamuni, A.B. Pandit, A critical review on textile wastewater treatments: possible approaches, Environ. Manage., 182 (2016) 351–366.

[4] M.C.M. Ribeiro, M.C.V.M. Starling, M.M.D. Leao, C.C. De Amorim, Textile wastewater reuse after additional treatment by Fenton's reagent, Environ. Sci. Pollut. Res., 24 (2017) 6165–6175.

[5] M. Punzi, F. Nilsson, A. Anbalagan, B.M. Svensson, K. Jonsson, B. Mattiasson, M. Jonstrup, Combined anaerobic-ozonation process for treatment of textile wastewater: removal of acute toxicity and mutagenicity, Hazard. Mater., 292 (2015) 52–60.

[6] S. Thangavel, S. Thangavel, N. Raghavan, Visible-light driven photocatalytic degradation of methylene-violet by rGO/Fe3O4/ZnO ternary nanohybrid structures, J. Alloys Compd., 665 (2016) 107-112.

[7] Y. Areerob, C.J. Yong, J. Won Kweon, W. C. Oh, Enhanced sonocatalytic degradation of organic dyes from aqueous solutions by novel synthesis of mesoporous Fe3O4-graphene/ZnO@SiO2 nanocomposites, Ultrason. Sonochem., 1 (2017) 1-44.

[8] N. Bougdour, R. Tiskatine, I. Bakas, A. Assabbane, PHotocatalytic degradation of industrial textile wastewater using S2O82−/Fe2+ process, Mater. Today: Procee., 22 (2020) 69-72.

[9] X. Zhang, Y. Xu, K. Cao, Q. Zhang, Structure–activity relationships of functional absorbents: Effects of absorption capacity, selective and retention behavior, Mater. Design, 90 (2016) 1044-1049.

[10] D. Kong, X. Du, S. Wei, H. Zhang, Y. Yang, S. P. Shah, Influence of nano-silica agglomeration on microstructure and properties of the

hardened cement-based materials, Constr. Build. Mater., 37 (2012) 707-715.

[11] M. Marques Fernandes, B. Baeyens, Cation exchange and surface complexation of lead on montmorillonite and illite including competitive adsorption effects, Appl. Geochem., 100 (2019) 190-202.

[12] G. Zhu, Z. Chen, B. Wu, N. Lin, Dual-enhancement effect of electrostatic adsorption and chemical crosslinking for nanocellulose-based aerogels, Ind. Crops Prod., 139 (2019) 80-96.

Analytical Methods in Environmental Chemistry Journal Vol 2 (2019) 39-48

AMECJ

Research Article, Issue 4

Analytical Methods in Environmental Chemistry Journal

Journal home page: www.amecj.com/ir

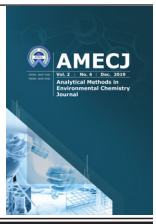

Speciation of arsenic (III,V) based on methyltrioctylammonium mercaptobenzoate and centrifuging dispersive liquid-liquid microextraction in water and blood

Ahmad Riahi [a], Elham Mosafayian Jahromy[b] and Bahareh Fahimirad [C,*]

[a] *Department of Chemistry, Australian Community of Science, Hobart,Tasmania, Australia*
[b] *Islamic Azad University of Pharmaceutical Sciences (IAUPS), Medical Nano Technology Tehran, Iran*
[C,*] *Department of Chemistry, Semnan University, Semnan, Iran*

ARTICLE INFO:

Received 22 Aug 2019
Revised form 3 Nov 2019
Accepted 28 Nov 2019
Available online 27 Dec 2019

Keywords:
Arsenic speciation,
Water and human blood,
Task-specific ionic liquids,
Centrifuging dispersive liquid-liquid microextraction

ABSTRACT

A novel analytical method based on centrifuging dispersive liquid-liquid microextraction (CD-LLME) procedure for pre-concentration of As (III) has been developed prior to determine by hydride generation atomic absorption spectrometry (HG-AAS). In this method, 0.1 g of a task specific ionic liquids (methyltrioctylammonium 2-mercaptobenzoate; TOMAS; TSIL) as the extracting and complexing solvent and acetone as dispersant solvent were rapidly added into the water and blood samples at pH 4.5. The As (V) is simply calculated by difference between total concentration and inorganic forms As (III) in liquid samples. By optimizing parameters, the enrichment factor (EF) was obtained 9.8 and 49.6 for blood and water samples, respectively. The limit of detection (LOD) of 22.4 ngL^{-1} and 4.3 ngL^{-1} were achieved for 10 mL and 50 mL of As(III) in blood and water samples, respectively (RSD<%5). The real samples were validated by certified reference material (CRM) by proposed procedure.

1. Introduction

Analytical methods has important role for determining hazardous heavy metal in different matrixes such as human blood and environmental samples. Analytical methods based on nanotechnology and ionic liquids was used for determination arsenic concentration in the blood, urine and serum samples by different instruments such as ICP-MS, ET-AAS and HG-AAS [1]. Inorganic arsenic compounds are toxic in human body but organic arsenic is usually less harmful [2]. Therefore, speciation and determination of arsenic in human blood and water samples is very important [3]. The toxicity of arsenic compounds is generally linked to the soluble inorganic trivalent forms, which is controlled by pH. Human exposure assessment in workers to arsenic containing substances includes short term (recent or acute exposure) and long term (chronic exposure) tests that can be performed to monitor detoxification efficiencies. Exposure of arsenic can lead to progressive peripheral and central nervous changes, such as, numbness and muscle tenderness. Normal arsenic concentrations in blood and urine are typically below 50 $\mu g\ L^{-1}$ and 7 $\mu g\ L^{-1}$, respectively [4]. Threshold limit value

* Corresponding author: Bahareh Fahimirad
Email: bahareh.fahimi@yahoo.com
https://doi.org/10.24200/amecj.v2.i04.83

(TLV) of arsenic concentration in human blood is less than 2.5 µg dL^{-1} [5].

So, the sensitive analytical techniques, such as; high performance liquid chromatography coupled to inductively coupled plasma mass spectrometry (HPLC-ICP-MS)[6], inductively coupled plasma atomic emission spectrometry (ICP-AES)[7], Cold vapor/hydride generation atomic absorption spectrometry (HG-AAS)[8], hydride generation and atomic fluorescence spectrometry (HGAFS)[9] and electro-thermal atomic absorption spectrometry (ET-AAS)[10]. Gas Chromatography-Inductively Coupled Plasma-Mass Spectrometry (GC-ICP-MS) or Ion Chromatography Coupled to inductively coupled plasma mass spectrometry (IC- ICP-MS) was required for determination and speciation of arsenic in blood and water samples. Among them, HG-AAS is a conversional instrument which was widely used for arsenic determination in human biological samples and waters. But, sample preparation was needed for preconcentration and separation ions from real samples before using analytical techniques. The ionic liquids (ILs) as green solvent were used for separation and determination metals in liquid phases. The different hydrophobic/hydrophilic ILs can be extracted ions from waters with ligand by spectrometry methods [11-14]. The cadmium, chromium and mercury were removed from water samples by TSILs. The sample preparation procedures based on ionic liquids (ILs) was used for this purposed. Recently, the liquid–liquid extraction (LLE)[15], cluod point extraction (IL-CPE)[16], ionic liquid based on solid phase extraction (IL-SPE) [17] was reported by previous papers. Arsenic speciation and determination by GC-ICP-MS or IC- ICP-MS were too much expensive. On the other hands, the arsenic speciation with conversional instruments needs to prepare difficult samples at low time. In this study, a new analytical method based on TOMAS ($C_{32}H_{59}NO_2S$) was used for arsenic speciation in water and human blood samples by CD-LLME procedure. Based on results, many advantages such as, low time, efficient extraction and high recovery were obtained.

2. Experimental

2.1. Apparatus

The experiments were performed using a GBC-932 atomic absorption spectrometer equipped with a cold vapor/hydride generation module (HG3000-AAS -AUS). The operating parameters for the metal of interest were set as recommended by the manufacturer. Mercury and arsenic determined by HGAAS respectively. Arsenic hollow cathode lamp based on 8 mA, 193.7 nm and the spectral bandwidth of 1 nm was used. The pH values of the solutions were measured by a digital pH meter (Metrohm 744). In all analysis the deuterium background correction was turn on (Table 1). The instrumental calibration curve was linear between 0.5 –30 µg L^{-1}. All containers (quartz crucibles, plastic tubes) were cleaned with detergent and treated successively by the HNO_3(2%) and rinsed with de-ionized water(DW). The pure argon gas (99.99%) was used as a carrier gas for HGAAS analysis. The reduced flame was turn on by HG-AAS.

2.2. Materials

All chemicals of analytical grade such as nitric acid, hydrochloric acid, Polyoxyethylene octyl phenyl ether (TX-100), sodium acetate, sodium hydroxide, and sodium borohydride ($NaBH_4$) were from Merck Germany. Reducing agents (aqueous solution of 0.6% sodium borohydride in 0.5% sodium hydroxide) were prepared freshly and filtered before use. Arsenic standard solutions were prepared from a stock solution of 1000 mg L^{-1} as ultra-trace in 2% nitric acid from Fluka Switzerland (No; 39436). Working standard solutions were prepared by dilution of stock and intermediate standards. Buffer solutions were prepared from 1-2 mol L^{-1} sodium acetate and acetic acid for pH= 3-7. Ultrapure water was obtained from a Water System of Iranian research Institute of Petroleum Industry (Millipore RIPI). Alderich. The TSIL, Ethyltrioctylammonium 2-mercaptobenzoate or Trioctylmethylammonium thiosalicylate (TOMAS, CAS Number 1027004-61-0) was purchased from Sigma Aldrich.

Table 1. Instrumental Conditions for arsenic

Parameter	Arsenic
Wavelength (nm)	193.7
Lamp current (mA)	8.0
Slit (nm)	1.0
LOD (µg L^{-1})	0.22
Linear Range (µg L^{-1})	0.5-58
Mode	Peak area

2.3. Sampling

For sampling, the clean glass tubes and container were purchased from Iranian company. The 10 mL of human blood samples were collected from industrial factory of Iran. For sampling, all glass tubes were washed with a 0.5 mol L^{-1} HNO_3 solution for at least 24 h and thoroughly rinsed 10 times with ultrapure water (UPW) before using. As concentrations of arsenic in blood / serum are very low, even minor contamination at any stage of sampling, sample storage and handling, or analysis has the potential to affect the accuracy of the results. For analysis in blood 10 µL, pure heparin (free metals) is added to a 10 mL blood sample. The human blood sample was maintained at –20 °C in a cleaned glass tube. The water prepared in 250 mL of polyethylene bottle (PEB) based on ASTM for sampling and storage by acidifying.

2.4. General procedure

The developed method based on centrifuging dispersive liquid-liquid microextraction (CD-LLME) was used for arsenic speciation in human blood and water samples at pH=4.5. By proposed procedure, the concentrations of As (III, V) in range of 1-5.8 µg L^{-1} were determined by HG-AAS in human blood and water samples. As (III) can be extracted with TOMAS in liquid phase without any chelating agent at optimized pH. Flame condition tuned based on 1.2 L min^{-1} of fuel with low air flowrate for As by HG-AAS. By CD-LLME procedure, 0.12 g of TOMAS diluted with 0.2 mL of acetone and injected into 10 mL of blood and standard samples which was included the arsenic

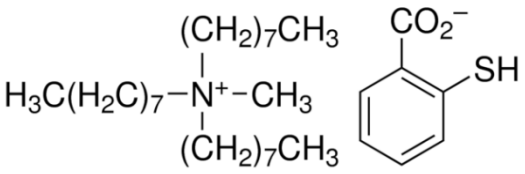

Fig. 1. The schema of TSIL (TOMAS)

concentration of 1-5.8 µg L^{-1}. Then, the pH was adjusted to 4.5 with buffer solution, shaking for 5 min and then transferred to a centrifuge tube. Arsenic (III) was complexed with TSIL (As-TOMAS) and then, the TSIL were separated from liquid phase by centrifuging of turbid solution at 3 min with 3500 rpm. The upper phase of TOMAS, with olive green color layer, was removed with a transfer pipette to PEB (5 mL). The As(III) was back-extracted from TOMATS at acidic pH by 0.5 mL of hydrochloric acid solution (2 M) which was shaken for 1.0 min and diluted with ultrapure water up to 1mL. Then, the TOMAS phase was removed by centrifuging and pipette and aqueous phase was determined by HG-AAS. The same procedure was done on sample blank for water and human serum/blood samples without As(III,V). Finally, the As (V) was reduced to As (III) with KI (1M) and ascorbic acid, the total arsenic (TAs) was determined. In addition, the concentration of As (V) was calculated by subtracting the content of As (III) from total arsenic content. The extraction conditions based on TOMAS were explained in Table 2.

3. Results and Discussion

In proposed method, for increasing higher sensitivity, selectivity and precision, of determining and speciation arsenic (As) in blood and water samples, we studied and optimized thoroughly, the effect of the main parameters, like the type of disperser and extraction solvent, sample volume, sample acidity, amount of TOMAS as chelating agent, and extraction time.

Human sampling based on ethical rules was confirmed by the Ethical Committee of Islamic Azad University, Tehran Medical Sciences (Ethical Code: R.IAU.PS.REC.1399.106)

Table 2. The extraction conditions of As(III) based on TOMAS by CD-LLME method

Features (Human blood)	**Value As**
Mean RSD% (blood, n=10)	3.2
LOD of CD-LLME(blood, µg L^{-1})	0.022
Enrichment factor(blood)	9.8
Volume of blood (mL)	10
Linear range of blood, PA (µgL^{-1})	0.05 –5.9
Correlation coefficient of DLLME	R = 0.9965
Features (Water)	**Value As**
Mean RSD% (water, n=10)	2.8
LOD of CD-LLME(water, µg L^{-1})	0.004
Enrichment factor(water)	48.6
Volume of water(mL)	50
Linear range of water, PA (µgL^{-1})	0.01-1.1
Correlation coefficient of DLLME	R = 0.9983

PA = Peak Area

3.1. Instrumental

The repeatability of results was investigated for speciation and determination arsenic in blood and water samples by hydride generation atomic absorption spectrometer (HGAAS) in present of flame. After mixing reagents and samples, the mixture solution moved to reaction coil where the metal hydride is formed and then passed through a gas-liquid separator where the hydride vapor is removed from the bulk liquid using an inert carrier gas. The hydride is then fed into a fused quartz absorption cell. For arsenic determination the cell is mounted over a burner and heated by an air-acetylene flame (HGAAS). Flame conditions were with 1.2 $Lmin^{-1}$ fuel and minimum flow air.

3.2. Effect of pH range

The complexation phenomenon is strongly conditioned by the pH of solutions and subsequently affects the extraction efficiency of the As(III) by complexing of TOMAS. As previously research, ionic liquids such as TOMAS was decomposed in lower pH (less than pH=3). Therefore, the effect of pH was studied and evaluated in the pH range of 3 –11 as a lower limit of quantification (LLOQ) and upper limit of quantification (ULOQ) for 0.05-5.0 µg L^{-1} for As(III). The results show that the high extraction efficiency for As (III) were achieved in pH=4.5 and As(V) had no extraction in optimized pH (less than 5%). So, the procedure was applied to speciation of arsenic in water and blood samples (Fig. 2).

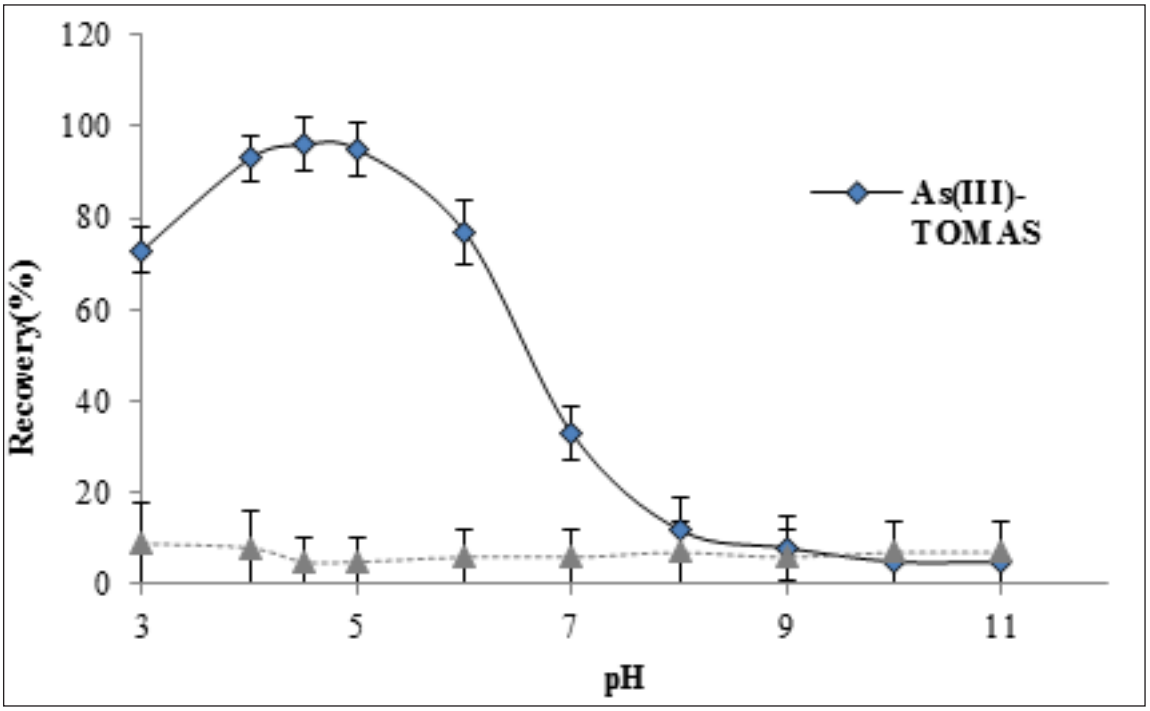

Fig. 2. The effect of pH on As(III) extraction based on TOMAS by CD-LLME method

3.3. Optimization of amount of TSIL and extraction time

The variation of extraction efficiency upon TOMAS amount as TSIL was examined within the range of 0.02-0.2 g for arsenic concentration from 0.05 to 5.0 µg L^{-1} in blood samples. It was observed that the extraction efficiency of the system was remarkably affected by the TSIL amount. Quantitative extraction of As(III) based on TOMAS was observed more than 0.08 g and 0.1 g for 10 mL and 50 mL of blood and water samples, respectively. So, 0.12 g of TOMAS was selected as optimum amount of TSIL for arsenic speciation in both samples (Fig.3). Triton X-100, an emulsifier and anti-sticking agent, was added to the solution in order to raise the efficiency of the extraction procedure. After added TX-100 [1% (w/v)] the quantitative extraction was observed for arsenic by TOMAS in human blood samples. The effectiveness of As(III) extraction under the influence of shaking and centrifugation time was studied. The different shaking and centrifuging times (3500rpm) were studied and optimized by CD-LLME procedure. The results showed us, the 5.0 min of shaking and 3.0 min of centrifuging had efficient extraction for proposed method.

3.4. Effect of sample volume

Sample volume is one of the most important parameter to be studied when real samples are analyzed by a pre-concentration technique, since it conditions the sensitivity enhancement of the method. The effect of sample volume was examined in a range of 1–100 mL for 5.0 µg L^{-1} and 1.0 µg L^{-1} As(III) ions in blood and water samples, respectively. It was found that the As(III) could be quantitatively extracted in blood samples for 12 mL of the sample solution. At higher a volume the recoveries are decreased. It was also noticed that higher sample volumes partially solubilized the TOMAS in liquid phase and lead to non-reproducible results. Therefore sample volume of 10 mL was selected for further experiments for human blood samples. Also, the results showed, the As(III) was efficient extracted based on TOMAS in 60 mL of water samples. So, 50 mL of water samples selected for further study (Fig. 4).

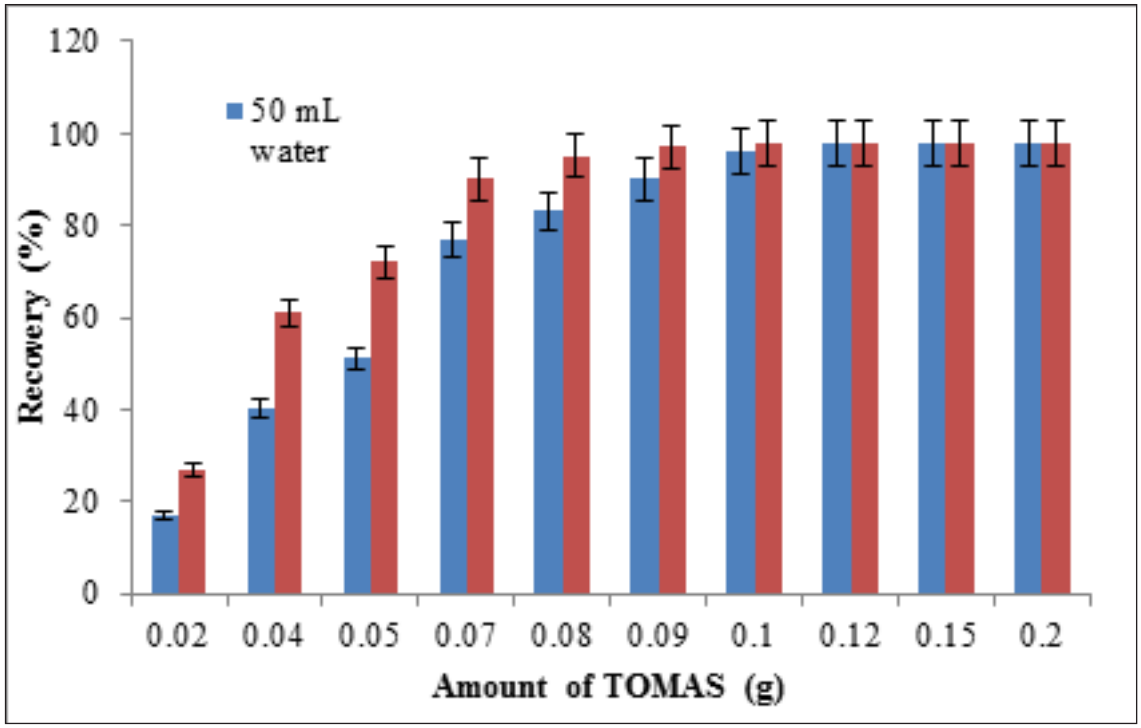

Fig. 3. The effect of amount of TOMAS on As(III) extraction by CD-LLME method

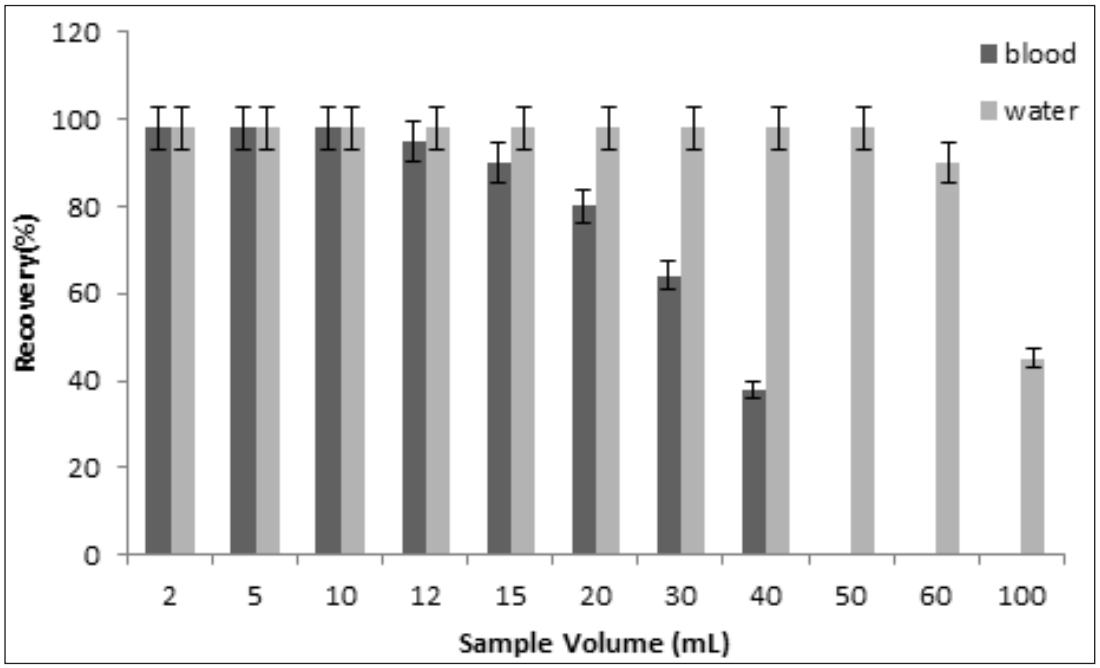

Fig. 4. The effect of sample volume for As(III) extraction by CD-LLME method

3.5. Interferences study.

TOMAS is a TSIL with thiol (HS) group which was acted as a chelating agent for many transition metals. Thus, for extraction of As(III) with TOMAS, the interferences coexisting ions such as mercury, lead, copper, zinc, vanadium, and silver should be considered. The effect of potential interfere occurring in blood and water samples on the determination of As(III) were tested in optimized conditions by CD-LLME procedure. The extraction recovery of TOMAS for 0.05-5.9 µg L^{-1} and 0.01-1.0 µg L^{-1} of As(III,V) was tested in blood and water samples with individual ions interferences. The results showed that many ions could be tolerated up to at least 1-3 mg L^{-1}. Mercury and silver had low tolerated up to at least 80-400 µg L^{-1} by using TOMAS in water and blood samples. High concentrations of alkali metals, alkaline earth metals, CO_3^{2-} and PO_4^{3-} which are usually found in blood samples, were tested by 0.5-1.0 mg L^{-1} and did not effect on extraction recovery of As(III) by CD-LLME procedure (Table 3).

Table 3. The effect of interferences coexisting ions on extraction of As(III) in human blood and water samples by CD-LLME method

Interfering Ions in blood(M)	**Mean ratio ($C_M/C_{As(III)}$)**	**Recovery (%)**
	As(III)	**As(III)**
Cr^{3+}, Al^{3+}, Mn^{2+}, Cd^{2+}, V^{3+}, Pb^{2+}	750	98.8
Zn^{2+}, Cu^{2+}, Ni^{2+}, Co^{2+} , Mo^{2+}	500	95.9
I^- , Br^-, F^-, Cl^-	1000	98.5
Na^+, K^+, ,Ca^{2+}, Mg^{2+}	900	99.1
CO_3^{2-}, PO_4^{3-}, $HCO3^-$	700	96.7
Ag^+	300	98.2
Hg^{2+}	80	96.6
$NO3^-$, SO_4^{2-}	800	97.5
Interfering Ions in water (M)	**Mean ratio ($C_M/C_{As(III)}$)**	**Recovery (%)**
	As(III)	**As(III)**
Cr^{3+}, Al^{3+}, Mn^{2+}, Cd^{2+}, V^{3+}, Pb^{2+}	900	97.7
Zn^{2+}, Cu^{2+}, Ni^{2+}, Co^{2+} , Mo^{2+}	650	97.2
I^- , Br^-, F^-, Cl^-	1200	97.4
Na^+, K^+, ,Ca^{2+}, Mg^{2+}	1000	98.6
CO_3^{2-}, PO_4^{3-}, $HCO3^-$	950	96.6
Ag^+	400	99.2
Hg^{2+}	150	97.3
$NO3^-$, SO_4^{2-}	1000	98.1

3.6. Method validation

For validation of proposed method, 10 mL and

Table 4. Validation of the methodology was performed by standard reference material (NIST SRM 2670)

SRM	As(III)	As(V)	Found [a] As(III)	Found [a] As(V)	Recovery As(III)	Recovery As(V)
Urine [b]	2.50 ± 0.2	1.50 ± 0.2	2.52 ± 0.18	1.45 ± 0.11	100.8 %	96.6%
Blood [C]	2.07 ± 0.63	-----	1.98 ± 0.12	-----	95.7%	-----

[a] Mean value ± standard deviation based on three replicate measurements

[b]NIST, SRM 2670, arsenic in frozen dried urine, pH 4.0 ,-20°C

[C] NIST, SRM 955c, Caprine Blood, Level 1

50 mL of blood and water samples were used. Results showed that there are no interferences from major consistent of blood samples, therefore we have explored the feasibility of the methodology using proposed method for the determination of As(III) ions in different matrices. Validation of the methodology was performed by standard reference material (NIST SRM 2670) with certified values for arsenic speciation (Table 4). Also, the spiked of standard arsenic solutions with real human blood and water samples were done to demonstrate the reliability of the method for determination and speciation of As (III) and As (V) (Table 5). In addition, the ability of different methods compared to CD-LLME method in Table 6. The TOMAS based on CD-LLME-HGAAS technique can be used for determination and speciation of arsenic (As^{3+}, As^{5+}) in human samples as compared to HG-AAS or ET-AAS (project Ethical Code: R.IAU.PS.REC.1399.106).

3.7. Comparing to other methods

The figures of merit of the CD-LLME method compared to the alternative methods for arsenic speciation (III, V) in different matrixes (Table 7). Recently, the different techniques for extraction/ separation/detemination arsenic spcies in human biological fluids and waters have been reported. Some techniques such as dispersive liquid–liquid microextraction (DLLME), cloud point extraction, and solid phase extraction have already used for extraction and speciation arsenic [18-21]. In this work, the TSIL (TOMAS) based CD-LLME combined with CV-AAS for speciation and determination of As (II, V) in human blood and water samples. The LOD, RSD and linear range values compared to other published method. Wen et al. used cloud point extraction with ICP-optical emission spectrometry for speciation of AS (III, V) with LOD of 0.72 and RSD of 3.5 which was higher than CD-LLME procedure [18]. Based on

Table 5. Evaluation of accuracy and precision of results in human blood and water samples by spiking of arsenic standard (III, V) based on CD-LLME method

Sample	Added		Found [a]			Recovery (%)		
	As(III)	As(V)	As(III)	As(V)	Total As	As(III)	As(V)	Total As
CRM*	-------	-------	2.45 ± 0.14	1.42 ± 0.11	3.87± 0.21	98.0	94.6	96.7
	2.0	-------	4.41 ± 0.23	1.44 ± 0.12	5.85± 0.28	98.1	-------	99.0
	-------	1.5	2.43 ± 0.15	2.95 ± 0.16	5.38± 0.25	-------	102	100.6
Water	-------	-------	0.88 ± 0.04	0.59 ± 0.02	1.47 ± 0.07	-------	-------	-------
	1.0	-------	1.85 ± 0.09	0.61 ± 0.03	2.46 ± 0.13	97.0	-------	98.8
	-------	0.5	0.87 ± 0.05	1.07 ± 0.05	1.94 ± 0.11	-------	95.7	94.5
Blood	-------	-------	1.77± 0.08	ND	1.77± 0.08	-------	-------	-------
	1.5	-------	3.24± 0.14	ND	3.24± 0.14	98.0	-------	98.0
	-------	1.5	1.74± 0.08	1.48± 0.07	3.22± 0.18	-------	98.6	96.5
Urine	-------	-------	1.15± 0.06	1.06± 0.05	2.21± 0.11	-------	-------	-------
	1.0	-------	2.17± 0.08	1.02± 0.05	3.19± 0.15	102	-------	97.9
	-------	1.0	1.13± 0.05	2.03± 0.10	3.16± 0.16	-------	97.0	95.0

[a]Mean value ± standard deviation based on three replicate measurements

*NIST SRM 2670, arsenic in frozen dried urine, pH 4.5,-20°C

Table 6. Comparing of different techniques with CD-LLME method for determination and speciation of arsenic (III, V) in real samples

As species	Sample	HG-AAS*	CD-LLME/HG-AAS*	LC-MS/MS*
Water	As (V)	-----	0.304 ± 0.016	0.296 ± 0.012
	As (III)	-----	0.197 ± 0.011	0.201 ± 0.008
	Total	± 0.027 0.485	± 0.024 0.501	± 0.015 0.497
Blood	As(V)	-----	0.865 ± 0.043	0.844 ± 0.032
	As (III)	-----	2.641 ± 0.127	2.702 ± 0.096
	Total	3.317 ± 0.175	3.486 ± 0.166	3.546 ± 0.121

*Mean value ± standard deviation based on three replicate measurements (N=5, P= 0.95)

Table 7. Comparison of the published methods with the proposed method in this work

Method	Separation	Matrixes	LR*	DL*	RSD%	References
ICP-OES [a]	APDC-CPE [b]	Snow water	2-50	0.72	3.5	[18]
ETAAS	HF-LPME[C]	Hair water	1-50	0.12	8.0	[19]
LC-HG-AFS[D]	1-octyl-3-methylimidazolium chloride(IL)	wine	1-2000	0.81	2.98	[20]
ET-AAS	DDTP -CLLME[H]	plasma urine	0.1-50	0.03-0.05	4.0- 5.7	[21]
HGAAS	TOMAS- CD-LLME	Blood	0.05 – 5.9	0.022	3.2	This work
HGAAS	TOMAS/ CD-LLME	Water	0.01 –1.1	0.004	2.8	This work

* Linear rang (LR, µg L−1); Detection limit (DL, µg L−1)

[a] inductively plasma-optical emission spectrometry(ICP-OES)

[b] Ammonium 1-pyrrolidinedithiocarbamate(APDC) - Cloud point extraction (CPE)

[C] Hollow fiber liquid phase microextraction combined

[D] liquid chromatography - hydride generation atomic fluorescence spectrometry

[H] Diethyldithiophosphoric acid (DDTP)-Centrifuging liquid-liquid microextractio

Table 7, the sensitivity of the developed method is similar to other reported methods. The linear range was perfectly adequate for the analyzed human blood samples. Lower LOD values are related with higher sensitivity of proposed method which was used in this study. Also, some methods have higher PF that analyzed by ICP in water or human blood samples with large sample volume. TSIL (TOMAS) based CD-LLME combined with CV-AAS showed a rapid and easy extraction and speciation of As (III,V) using a user-friendly instruments.

4. Conclusions

The procedure here studied takes advantage of the combination of a very simple, reliable way of pre-concentrating in sea water and blood samples for arsenic determination and speciation with the sensitive TOMAS@HG-AAS technique. The increase in sensitivity resulting of sample pre-concentration, good sample frequency and possibility of speciation of As (III), As (V) forms of these analytes, means the procedure can be considered an alternative to high-performance liquid chromatography (HPLC) in combination with inductively coupled plasma mass spectrometry (ICP-MS) , Ion Chromatography Coupled to inductively coupled plasma mass spectrometry (IC-ICP-MS) and ICP-MS. The results showed that the quantitative extraction (QE) and enrichment factor (EF) for water samples were more than 95% and 49.6, respectively (RSD<5%). Linear range of arsenic in blood and water samples was obtained 0.05 –5.9 and 0.01-1.1µgL^{-1}, respectively by CD-LLME method. By proposed procedures, the satisfactory results of ultra-trace analysis for arsenic species in blood and water samples were achieved.

5. Acknowledgements

The authors thank from the Islamic Azad University of Pharmaceutical Sciences (IAUPS)

Iran (Ethical Code:R.IAU.PS.REC.1399.106).

6. References

[1] A.T. Townsend, K.A. Miller, S. McLean, S. Aldous, The determination of copper, zinc, cadmium and lead in urine by high resolution ICP-MS, J. Anal. Atom. Spec., 13 (1998) 1213-1219.

[2] J.S. Petrick, F. Ayala-Fierro, W.R. Cullen, D.E. Carter, H.V. Aposhian, Monomethylarsonous acid (MMAIII) is more toxic than arsenite in Chang human hepatocytes, Toxicol. Appl. Pharm., 163 (2000) 203-207.

[3] X. Zhang, R. Cornelis, J. de Kimpe, L. Mees, Speciation of toxicologically important arsenic species in human serum by liquid chromatography–hydride generation atomic absorption spectrometry, J. Anal. Atom. Spec., 11 (1996) 1075-1079.

[4] H. Shirkhanloo, A. Rouhollahi, H.Z. Mousavi, Ultra-trace arsenic determination in urine and whole blood samples by flow injection-hydride generation atomic absorption spectrometry after preconcentration and speciation based on dispersive liquid-liquid microextraction, Bull. Korean Chem. Soc., 32 (2011) 3923-3927.

[5] A. Hussam, M. Alauddin, A. Khan, S. Rasul, A. Munir, Evaluation of arsine generation in arsenic field kit, Environ. Sci. Technol., 33 (1999) 3686-3688.

[6] M. Van Hulle, C. Zhang, X. Zhang, R. Cornelis, Arsenic speciation in chinese seaweeds using HPLC-ICP-MS and HPLC-ES-MS, Analyst, 127 (2002) 634-640.

[7] X. Li, B.J. Coles, M.H. Ramsey, I. Thornton, Sequential extraction of soils for multielement analysis by ICP-AES, Chem. Geology, 124 (1995) 109-123.

[8] A. Shraim, B. Chiswell, H. Olszowy, Speciation of arsenic by hydride generation–atomic absorption spectrometry (HG–AAS) in hydrochloric acid reaction medium, Talanta, 50 (1999) 1109-1127.

[9] J.T. van Elteren, Z. Šlejkovec, M. Svetina, A. Glinšek, Determination of ultratrace dissolved arsenite in water–selective coprecipitation in the field combined with HGAFS and ICP–MS measurement in the laboratory, Fresenius' j. Anal. Chem., 370 (2001) 408-412.

[10] F. Shemirani, M. Baghdadi, M. Ramezani, M.R. Jamali, Determination of ultra trace amounts of bismuth in biological and water samples by electrothermal atomic absorption spectrometry (ET-AAS) after cloud point extraction, Anal. Chim. Acta, 534 (2005) 163-169.

[11] S. Smirnova, T. Samarina, I. Pletnev, Hydrophobic–hydrophilic ionic liquids for the extraction and determination of metal ions with water-soluble reagents, Anal. Method., 7 (2015) 9629-9635.

[12] A.A. Miranbeigi, M. Yousefi, M. Abdouss, Room temperature imidazolium-based ionic liquids as scavengers for hydrogen sulfide removal of crude oil, Anal. Method. Environ. Chem. J., 1 (2018) 11-22.

[13] S. Davari, F. Hosseini, H. Shirkhanloo, Dispersive solid phase microextraction based on aminefunctionalized bimodal mesoporous silica nanoparticles for separation and determination of calcium ions in chronic kidney disease, Anal. Method. Environ. Chem. J., 1 (2018) 57-66.

[14] A. Khaligh, H. Shirkhanloo, Food Analysis: Task specific ionic liquids for separation of nickel and cadmium from olive oil samples by thermal ultrasound-assisted dispersive multiphasic microextraction, Anal. Method. Environ. Chem. J., 2 (2019) 55-64.

[15] M. Chamsaz, M.H. Arbab-Zavar, S. Nazari, Determination of arsenic by electrothermal atomic absorption spectrometry using headspace liquid phase microextraction after in situ hydride generation, J. Anal. Atom. Spec., 18 (2003) 1279-1282.

[16] J. Ping, J. Wu, Y. Ying, M. Wang, G. Liu, M. Zhang, Evaluation of trace heavy metal levels in soil samples using an ionic liquid modified carbon paste electrode, J. Agri. food Chem., 59 (2011) 4418-4423.

[17] M. Gharehbaghi, F. Shemirani, Ionic liquid modified silica sorbent for simultaneous separation and preconcentration of heavy metals from water and tobacco samples prior to their determination by flame atomic absorption spectrometry, Anal. Method., 4 (2012) 2879-2886.

[18] S. Wen, X. Zhu, Speciation of inorganic ***As***(III) and ***As***(V) by a facile dual-cloud point extraction coupled with inductively plasma-optical emission spectrometry, Talanta 181(2018) 265-270.

[19] H. Jiang, B. Hu, B. Chen, L. Xia, Hollow fiber

liquid phase microextraction combined with electrothermal atomic absorption spectrometry for the speciation of arsenic (III) and arsenic (V) in fresh waters and human hair extracts, Anal. Chim. Acta 634 (2009) 15-21.

[20] A. Castro Grijalba, E.F. Fiorentini, L.D. Martinez, R.G. Wuilloud, A comparative evaluation of different ionic liquids for arsenic species separation and determination in wine varietals by liquid chromatography - hydride generation atomic fluorescence spectrometry, J. Chromatogr. A 1462 (2016) 44-54.

[21] L. Haghnazari, N. Mirzaei, H. Arfaeinia, K. Karimyan, H. Sharafi, N. Fattahi, Speciation of As(III)/As(V) and total inorganic arsenic in biological fluids using new mode of liquid-phase microextraction and electrothermal atomic absorption spectrometry, Biol. Trace Elem. Res., 183 (2018) 173–181.

AMECJ

Research Article, Issue 4

Analytical Methods in Environmental Chemistry Journal

Journal home page: www.amecj.com/ir

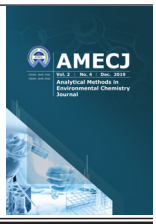

Mercury determination in work place air and human biological samples based on dispersive liquid-liquid micro-extraction coupled with cold vapor atomic absorption spectrometry

Seyed Mojtaba Mostafavi [a] and Ali Ebrahimi [b,*]

[a] *Department of Chemistry, Iranian-Australian Community of Science, Hobart, Tasmania, Australia*
[b] *Occupational Health Engineering Department, School of Public Health, Qom University of Medical Sciences, Qom, Iran*

ARTICLE INFO:

Received 13 Sep 2019
Revised from 18 Nov 2019
Accepted 11 Dec 2019
Available online 28 Dec 2019

Keywords:
Mercury,
Analysis,
Dispersive liquid-liquid micro-extraction,
Human blood,
Work place air

ABSTRACT

Mercury as a toxic heavy metal is important factor must be determined and controlled in work place air and human biological samples. It should be mentioned that, mercury (Hg) get distinguished from other toxic environment pollutants, due to their non-biodegradability which accumulate in living tissues of human body. By NIOSH method, the briefing work place air of worker was measured by flow injection cold vapor atomic absorption spectrometry (FI-CV-AAS). For separation and preconcentration mercury from blood/urine samples, a new procedure based on benzyl 1H-pyrrole-1-carbodithioate (BPDC; $C_{12}H_{11}NS_2$) was used by ultrasonic liquid-liquid micro-extraction (ULLME) coupled with cold vapor atomic absorption spectroscopy (CV-AAS). The influences of various analytical parameters including pH, BPDC concentration, sample volume and ionic liquid volume were investigated. The quantitative recoveries and enrichment factor were obtained more than 95% and 9.8, respectively at pH=7. The detection of limit (LOD) and detection of quantification (LOQ) of mercury were 30 ng L^{-1} and 0.1 µg L^{-1} respectively. In order to calculate the validation and accuracy of proposed method, the certified reference materials (NIST, CRM 3133 Lot 061204) was used and analyzed by ULLME-CVAAS. So, proposed method had good potential for preparation and preconcentration mercury in human blood / urine samples of worker and workplace air before analysis.

1. Introduction

Heavy metal is important factor must be controlled in environmental air and patients. There are some heavy metals with toxic effects such as mercury, cadmium, nickel, vanadium, arsenic, lead and aluminum which have no known beneficial effect on organisms. Mercury has been documented to cause autoimmune and neurological diseases. Mercury simply vaporizes at room temperature and easily enters to the environment and human lungs. High concentration of mercury vapors in work place air can accumulate in human tissues as compared to non- occupationally exposed individuals. Adverse health effects of this exposure including subtle neurological side-effects have also been well documented in most Petrochemical workers even at the lowest levels of exposure; consequently, measurement of mercury and methyl mercury in blood, urine, hair and air briefing seems to be important [1-7]. Chlor-alkali workers are mostly exposed through breathing air of mercury vapors which was released from electrochemical system to human body such as lungs and skin.

* Corresponding Author: Ali Ebrahimi E-mail: Ali.Ebrahimi.ohe@gmail.com
https://doi.org/10.24200/th amecj.v2.i04.81

Family members of these workers may also become exposed to mercury through personnel's clothes contaminated with mercury particles. Ingested metallic mercury enters the body through the stomach or intestines but even in large amounts very little enters the body. On the other hand, breathing mercury vapors results in direct absorption of most it (about 80%) from the lungs which rapidly moved to other organs, including the brain and kidneys. Mercury get distinguished from other toxic pollutants due to their non-biodegradability can accumulate in living tissues of human body. Even a very small amount of them can cause severe physiological or neurological damage to the human body [8-14]. The concentration of mercury vapor in air reported by occupational safety and health administration guidelines (OSHA, 0.1 mg m^{-3}). In addition, national institute for occupational safety and health (NIOSH) has established a recommended exposure limit for mercury vapor of 0.05 mg m^{-3} for up to an 8-hour workday and a 40-hour workweek. American conference of governmental industrial hygienists (ACGIH) has assigned mercury vapor a threshold limit value of 0.025 mg m^{-3} for a normal eight-hour workday and a 40-hour work week .Mercury levels in blood can be used to help diagnose recent mercury exposure and to evaluate patient response to chelation therapy. Normal mercury concentration in human blood/urine is less than 10-20 µg L^{-1} [15-19]. Many analytical methods such as atomic fluorescence spectrometry [20-24] high-performance liquid chromatography [25] Gas-chromatographic [26] plasma mass spectrometry [27] high-performance liquid chromatography on-line coupled with cold-vapor atomic fluorescence spectrometry [28, 29] gas chromatography-mass spectrometry [30] ion chromatography using photo-induced chemical vapor generation atomic fluorescence spectrometric detection [31] ion chromatography coupled with ICP-MS [32] liquid chromatography hyphenated to cold vapor atomic fluorescence spectrometry [33] UV–Vis spectrophotometric [34] were used for mercury spices determination. Samples preparation and preconcentration before analysis is an important factor for determination of pollutants in different matrixes. Recently, the various methods for the preparation and preconcentration of mercury compounds, including solid phase extraction (SPE) [35-43], gold trap [44], ionic liquid-based dispersive liquid-liquid microextraction (IL-DLLME) [45, 46], cloud point extraction (CPE) [47,48], electromembrane extraction [34], dispersive solid phase micro-extraction [49], single-drop microextraction [50], and Liquid–liquid extraction (LLE) [51], were reported. Since 2010, the DLLME method has been used for extraction and/or preconcentration of different analytes from aqueous samples [52, 53]. By DLLME method, extraction solvent such as ionic liquids, liquid phase (sample) and disperser solvent (acetone) was used [54]. The DLLME procedure has many advantages including simple, rapid, low time and cost, and efficient extraction. The green analysis such as, decrease solvent volume and less waste generation due to preparation and analysis samples was achieved [53-54]. In this study, the mercury concentration in human blood and urine samples based on BPDC –IL was determined by FI-CVAAS after ULLME procedure in 50 samples. In addition, 50 briefing air based on Hopcalite was analyzed by NIOSH method (6009).

2. Experimental

2.1. Apparatus

The experiments were performed using the flow injection cold vapor atomic absorption spectrometer (FI-CVAAS, GBC – 932, 3000, Australia). All containers (quartz crucibles, plastic tubes) were cleaned with detergent and treated successively by the hydrochloric acid and rinsed with de-ionized water. Microwave digestions were carried out with a multi-wave 3000 (Anton Paar, 100 mL, 20 bars; Austria). The pure argon gas (99.99%) was used as a carrier gas for CV-AAS analysis and the pH values of the solutions were measured by a digital pH meter (Metrohm 744). Personal sampling pump, Sampler (glass tube, 7 cm long, 6-mm OD, 4 mm ID, flame sealed ends with plastic caps containing one section of 200 mg Hopcalite held in place by

glass wool plugs (SKC, Inc., Cat. Num. 226-17-1A, or equivalent) and BOD bottle were used for collection of air and blood/urine in the industrial factory respectively.

2.2. Reagents and Materials

All chemicals of analytical reagent grade such as nitric acid, hydrochloric acid, benzyl 1H-pyrrole-1-carbodithioate (BPDC; $C_{12}H_{11}NS_2$) (CAS no 60795-38-2), Polyoxyethylene octyl phenyl ether (TX-100), and sodium borohydride (NaBH4) were from Merck Germany. Mercury standard solutions were prepared from a stock solution of 1000 mg L^{-1} in 1% nitric acid from Fluka Switzerland. Reducing agents (aqueous solution of 0.6% sodium borohydride in 0.5% sodium hydroxide) were prepared freshly and filtered before use. Ionic liquid (1-butyl-3-methylimidazolium hexafluorophosphate; [BMIM][PF6]; $C_8H_{15}F_6N_2P$) (1-Ethyl-3-methylimidazolium hexafluorophosphate ;[EMIM][PF6]; $C_6H_{11}F_6N_2P$) (Trimethyl imidazolium hexafluorophosphate ; [DMMIm][PF6]) was purchased from Sigma Aldrich. Buffer solutions were prepared from 2-1 mol L^{-1} sodium acetate and acetic acid for pH= 3-7. Ultrapure water was prepared from Millipore (Germany).

2.3. Sampling

For sampling, all glass tubes (sampling vessel) were washed with a 1 moL L^{-1} HNO_3/HCl solution for at least 24 h and rinsed 10 times with DW before using. Due to low mercury concentrations in whole blood/urine, even minor contamination at any stage of sampling, sample storage and handling, or analysis has the potential to effect on the accuracy of the results. 10 mL blood and 100 mL urine samples were collected from factory workers and healthy matched controls (20-55 years), living in Abadan (IRAN). For analysis of 45 blood samples, 5 microliter of heparin (free metals) was added. The human blood and urine sample was maintained at –20 °C in a cleaned glass tube.

45 air samples were collected in an employee's breathing zone according to 6009 NIOSH analytical method. Each personal sampling pump was calibrated with a representative sampler and the end of sampler was broken immediately prior to sampling. Samplers were attached to the pumps with flexible tubing and air was collected at a rate of 200 to 300 mL min^{-1}.

2.4. General procedure

In this research, human blood and urine and briefing air samples of factory workers were studied. The determination of mercury in blood/urine and air was carried out using a flow injection cold vapor atomic absorption spectrometry system after sample treatment according to the ULLME procedure. Based on procedure, the BPDC as complexing agent was added to human samples and mercury extracted by ULLME as a new mode of liquid phase extraction with high recovery and extraction efficiency. In this work, 0.5 mL of 2% (w/v) BPDC solution was prepared and added to 10 mL of blood and urine samples and pH was adjusted to 7 with buffer solution in a centrifuge tube. Then, 0.2 g of different IL was added to the mixtures and they were shaken with a vortex apparatus for 5 min. Mercury (Hg^{II}) was complexed and pre-concentrated as Hg-BPDC-IL ([BMIM][PF6]). The phases were separated by centrifuging of turbid solution at 4 min with 3500 rpm. After separation of ionic liquid from liquid phase, the remained solution (Hg-BPDC-IL) was back extracted with nitric acid (0.5 M, 0.5 mL) and the mercury concentration in blood/urine samples was determined by FI-CV-AAS (Fig 1).

Air samplers were capped and pack securely for shipment. Based on NIOSH procedure, the Hopcalite sorbent and the front glass wool plug from each sampler were placed in separate 50-ml volumetric flasks and mixture of 2.5 mL of HNO_3/HCl concentration added to volumetric flasks. Hopcalite sorbent was dissolved in acids and diluted to 50 mL of deionized water (blue color), then the mercury concentration was determined with FI-CV-AAS.

3. Results and Discussion

Analytical conditions for mercury determination

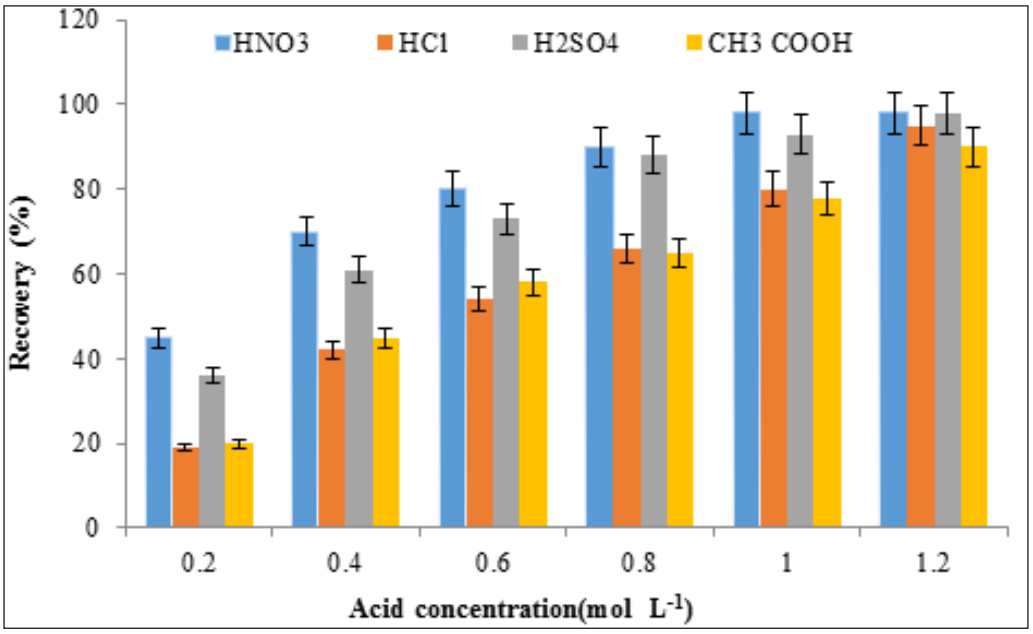

Fig. 1. Back extraction of Ionic liquid with different acids

were performed in briefing air and human blood and urine samples of chemical factory workers at this work. Absorption (S/N) and repeatability of the results were investigated for the determination mercury by FI-CVAAS. The instrumental and extraction conditions are listed in Table 1. Working range was between 0.05- 7.1 µg L^{-1} for samples at peak area.

The complexation phenomenon is strongly conditioned by the pH. The results showed us the pH from 5.5 to 7.5 was good recovery for mercury extraction by BPDC. So pH=7 selected as favorite pH for further analysis in blood samples (Fig 2). The minimum BPDC concentration necessary to achieve maximum extraction efficiency is 1.4×10^{-6} moL L^{-1}. So the 15×10^{-6} moL L^{-1} was used by ULLME procedure (Fig 3).

Table 1. Instrumental and extraction conditions for mercury determination by FI- CVAAS

Instrumental Parameters	**Mercury**
Wavelength (nm)	253.7
Lamp current (mA)	3-4
Spectral bandwidth (nm)	0.5
LOD (µg L^{-1})	0.2
LOQ (µg L^{-1})	0.6
Working range(µg L^{-1})	0.5-70
ULLME method by BPDC	**Mercury**
LOD (µg L^{-1})	0.015
LOQ (µg L^{-1})	0.05
Working range (µg L^{-1})	0.05-7.1
Enrichment Factor	9.8
Volume sample (mL)	10
Amount of IL (g)	0.2
pH	7

Different ionic liquids were used by ULLME method. Based on Figure 4, maximum extraction was occurred by [BMIM][PF6]. The high extraction was observed by volume higher than 0.2 mL for [BMIM][PF6] (Fig. 4). The effect of sample volume was evaluated with different volume of blood and urine samples from 1-25 mL and quantitative extraction was observed in 10 mL of blood/urine sample (Fig. 5).

The concentration of Hg(II) based on BPDC as ligand was determined by ULLME procedure in blood and human samples which was coupled to spectrometer of FI-CVAAS. In optimized conditions, the means of five times determinations, for Hg (II) were obtained by proposed method. The real samples were spiked with standard concentration of Hg(II) in LLOQ and ULOQ of linear range at pH=7 (Table 1). As validation methodology, the good accuracy results was achieved by spiking standard mercury species (0.1-7.0 μg L^{-1}) to human

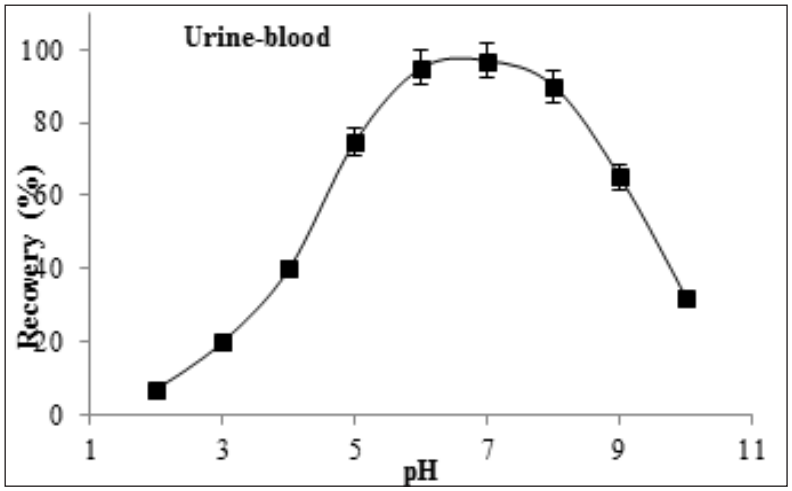

Fig. 2. Effect of pH on mercury extraction in human blood /urine samples

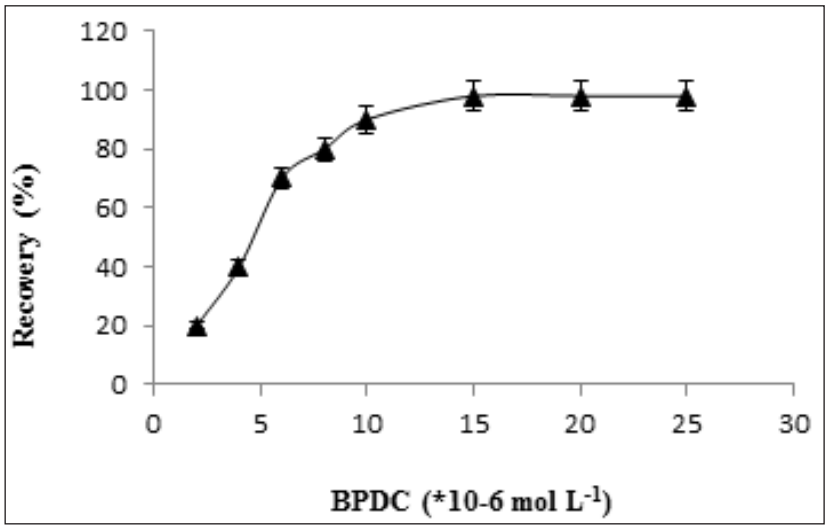

Fig. 3. Effect of BPDC on mercury extraction in human blood /urine samples

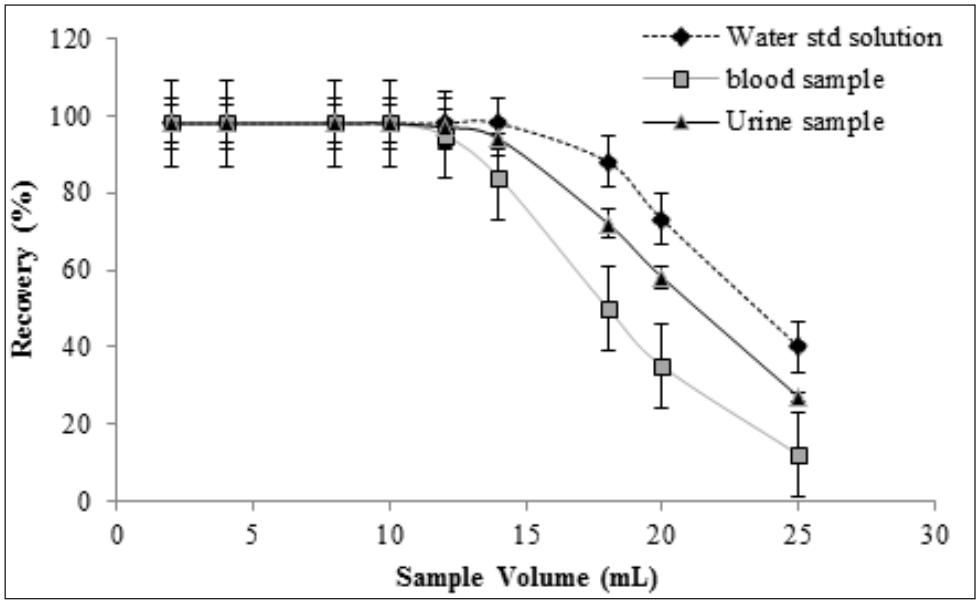

Fig. 4. Effect of sample volume on mercury extraction in human blood /urine samples

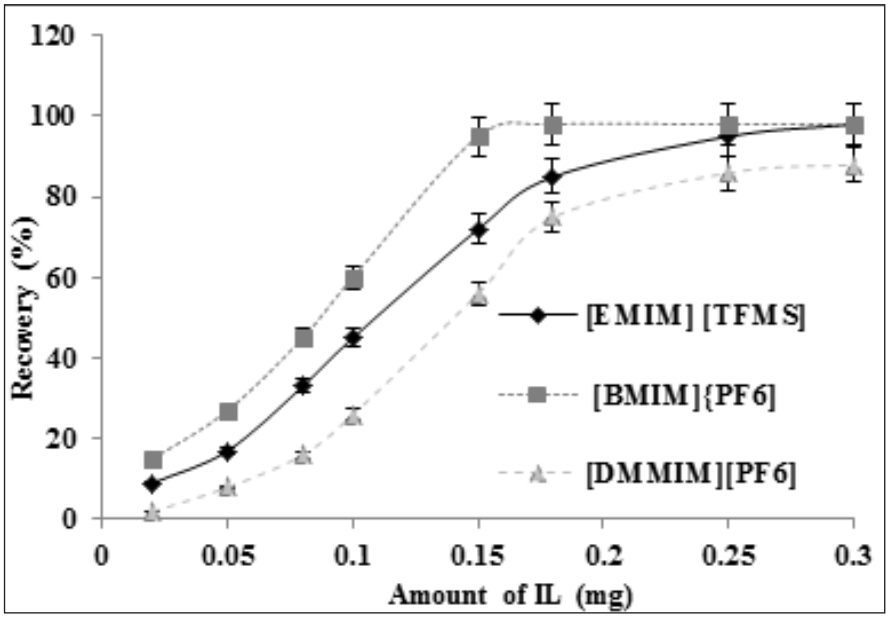

Fig. 5. Effect of ionic liquid on mercury extraction in human blood /urine samples

samples. Mercury concentrations in workers have higher than threshold limit value (TLV) and all of them have almost clinical problem. Validation of proposed method for determining blood and urine mercury was shown by CRM, NIST in Table 2.

Also Statistical parameters for determining mercury in blood and briefing air sample were calculated in Table 3. In addition, the results of mercury concentration in blood samples of worker and control were shown in Figure 6.

Table 1. Validation of proposed method for determining blood mercury by BPDC (μg L^{-1})

Sample	Added mercury	Found mercury	Recovery (%)
Blood A	-----	2.33± 0.09	-----
	2	4.26 ± 023	96.5
	4	6.28 ± 035	98.7
Blood B	-----	1.78 ± 0.07	-----
	1	2..80 ± 0.14	102
	2	3..73 ± 0.18	97.5
Urine A	-----	3.12 ± 0.16	-----
	2	5.15 ± 0.28	101.5
	3	6.09 ± 0.32	99.0
*Urine B	-----	7.45 ± 0.33	-----
	5	12.32 ± 0.65	97.4
	10	17.38 ± 0.32	99.3

[a] Mean of five determinations ± confidence interval (P = 0.95)
• Urine diluted with DW(1::5)

4. Conclusions

Mercury has toxic effect in humans. In high exposures, observed mostly in occupational settings, the severity of response correlates with the duration and intensity of the exposure. Increase mercury exposure depended on time of working and volume of air briefing which was determined based on NIOSH 6009. The results showed us, the mercury concentration in human blood/urine and briefing air in workers were higher than control group. Also, the increasing mercury doses in human blood and briefing air may be lead to an important neuropsychological problem in workers. Therefore, the concentration of mercury in human blood and briefing air is very important factor that must be

Table 2. Analytical results of mercury determination in certified reference material (CRM)

Analyte	CRM	Certified Value (μg L^{-1})	Found (μg L^{-1})	Recovery%
Mercury	NIST SRM 3133 Lot 061204	6.50 ± 0.29	6.38 ± 0.33	98.2

Mean value ± standard deviation based on three replicate measurements.

Table 3. Statistical parameters for determining mercury in blood and briefing air sample by BPDC

sample	Mean Conc.	Median Conc.	RSD%	Range Conc.
[a] Worker	25.37± 0.93	20.15± 0.57	3.6	4.0-52
[a] control group	1.15± 0.08	0.94± 0.04	4.2	0.7-5.0
[b] Worker	32.72± 2.24	29.81± 1.08	2.7	8.0-64
[b] control group	0.74± 0.03	0.62± 0.02	2.9	0.2-1.1
[c] Worker	0.045± 0.01	0.038± 0.01	4.4	0.01-0.05
[c] control group	ND	ND	---	ND

[a] Blood concentration, BPDC (µg L^{-1})

[b] Urine concentration, BPDC (µg L^{-1})

[c] Briefing air concentration (mg m^{-3})

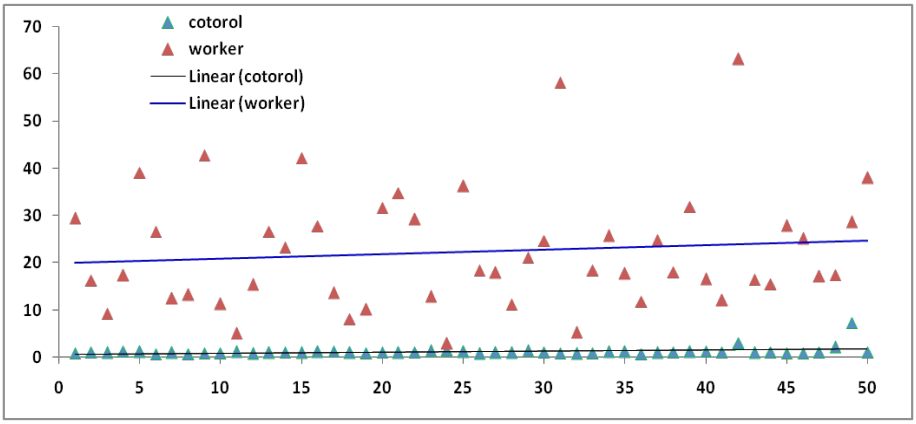

Fig. 6. Dispersive of blood mercury concentration in worker and control group

controlled and determined in industrial workers. In this study the precise and accurate method based on BPDC was used for mercury determination in blood and urine samples by ULLME coupled with FI-CVAAS. The experimental showed, the concentration mercury in worker were higher than OSHA/ACGHI references.

5. Acknowledgements

Approval was obtained from the Kerman University of medical science Occupational Health Committee (R. KUMS.PN: 96.10.60.11712).

6. References

[1] WHO. Elemental Mercury and Inorganic Mercury Compounds, Human Health Aspects, Concise International Chemical Assessment Document 50. World Health Organization, Geneva, 2003.

[2] T. Ohno, M. Sakamoto, T. Kurosawa, M. Dakeishi, T. Iwata, K. Murata, Total mercury levels in hair, toenail and urine among women free from occupational exposure and their relations to renal tubular function, Environ. Res., 103 (2007)191-198.

[3] A. Kingman, T. Albertini, LJ. Brown, Mercury concentrations in urine and whole blood associated with amalgam exposure in a US military population. J. Dent. Res., 77 (1998) 461-471.

[4] M.Kampa, E. Castanas, Human health effects of air pollution, In. Environ Pollut., 151 (2008) 362-367.

[5] LL. Booze, Elemental mercury exposure: an evidence-based consensus guideline for out-of-hospital management, Clin. Toxicol., 46 (2008) 21-28.

[6] SC. Foo, Neurobehavioral effects in Occupational Chemical Exposure. Environ. Res., 60 (1993) 267-73.

[7] WHO, Mercury environmental aspects, environmental health criteria. world health organization, Geneva, 2008.

[8] IARC, beryllium, cadmium, mercury and exposures in the glass manufacturing industry, mercury and mercury compounds, International Agency for Research on Cancer, Vol 58, 1997.

[9] H V. Warren, S J. Horksy, C E Gould, Quantitative analysis of zinc, copper, lead, molybdenum, bismuth, mercury and arsenic in brain and other tissues from multiple sclerosis and non-multiple sclerosis cases, Sci. Total Environ., 29 (1983) 163-171.

[10] T W. Clarkson, L. Magos, G J. Myers, The toxicology of mercury current exposures and clinical manifestation, New Eng. J. Med., 349 (2003) 1731-1737.

[11] M E. Vahter, N K Mottet, L T. Friberg, S B. Lind, J S. Charleston, T M. Burbacher, Demethylation of methyl mercury in different brain sites of Macaca fascicularis monkeys during long-term subclinical methyl mercury exposur, Toxicol. Appl. Pharm., 134 (1995) 273-284.

[12] M B. Pedersen, J C. Hansen, G. Mulvad, H S. Pedersen, M Gregersen, G. Danscher, Mercury accumulations in brains from populations exposed to high and low dietary levels of methyl mercury. Concentration, chemical form and distribution of mercury in brain samples. Int. J. Circumpolar Health, 58 (1999) 96-107.

[13] M. Nylander, L. Friberg, J Weiner, Muscle biopsy as an indicator for predicting mercury concentrations in the brain, Br. J. Ind. Med., 47 (1990) 575-576.

[14] G. Turabelidze, Multiple sclerosis prevalence and possible lead exposure. J. Neurol. Sci., 269 (2009) 158-162.

[15] OSHA, Guidelines for mercury vapor. Occupational safety and health administration, 2008. Available at: www.osha-slc.gov

[16] NIOSH, Centers for disease control and prevention. National Institute for Occupational Safety and Health, guide to chemical hazards, 3th Ed, 2007.

[17] ACGIH, U.S Documentation of the threshold limit values and biological exposure. American Conference of Governmental Industrial Hygienists, 7th Ed, 2011.

[18] N M. Tietz, Clinical Guide to Laboratory Tests. W. B. Saunders, Philadelphia, PA, 8rd Ed, 2010.

[19] NIOSH, Documentation of the threshold limit values and biological exposure indices. National Institute for Occupational Safety and Health, Cincinnati, OH., 7th Ed., 2001.

[20] Y. Cai, Speciation and analysis of mercury, arsenic, and selenium by atomic fluorescence spectrometry, TrAC Trends Anal. 19 (2000) 62-66.

[21] Gao, Ying, Determination and speciation of mercury in environmental and biological samples by analytical atomic spectrometry, Microchem. J., 103 (2012) 1-14.

[22] J. Szkoda, J. Zmudzki, A. Grzebalska, "Determination of total mercury in biological material by atomic absorption spectrometry method, J. Bull. Vet. Inst. Pulawy, 50 (2006) 363.

[23] H. Erxleben, R. Jaromir, Atomic absorption spectroscopy for mercury, automated by sequential injection and miniaturized in lab-on-valve system, Anal. Chem., 77.16 (2005) 5124-5128.

[24] W. Peng, H. Liang, Z Chengbin, H. Xiandeng, E S Ralph, Applications of chemical vapor generation in non-tetrahydroborate media to analytical atomic spectrometry, J. Anal. Atom. Spec., 25.8 (2010) 1217-1246.

[25] CF. Harrington, the speciation of mercury and organomercury compounds by using high-performance liquid chromatography, TrAC, Trends Anal. Chem., 19 (2000) 167-179.

[26] CJ, Cappon, J C Smith, Gas-chromatographic determination of inorganic mercury and organomercurials in biological materials, Anal. Chem., 49.3 (1977) 365-369.

[27] SCK. Shum, HM. Pang, RS Houk, Speciation of mercury and lead compounds by microbore column liquid chromatography-inductively coupled plasma mass spectrometry with direct injection nebulization, Anal. Chem., 64 (1992) 2444-2450.

[28] L. N. Liang, G. B. Jiang, J. F. Liu, J. T. Hu, Speciation analysis of mercury in seafood by using high-performance liquid chromatography on-line coupled with cold-vapor atomic fluorescence spectrometry via a post column microwave digestion, Anal. Chim. Acta, 477 (2003) 131-137.

[29] X Jia, Y Han, X Liu, T Duan, H Chen, Speciation of mercury in water samples by dispersive liquid–liquid microextraction combined with high performance liquid chromatography-inductively coupled plasma mass spectrometry, Spectrochim. Acta Part B: Atom. Spec., 66 (2011) 88-92.

[30] S. Mishra, R. M. Tripathi, S. Bhalke, V. K. Shukla, V. D. Puranik, Determination of methylmercury and mercury (II) in a marine ecosystem using solid-phase microextraction gas chromatography-mass spectrometry, Anal. Chim. Acta, 551 (2005) 192-198.

[31] Q. Liu, Determination of mercury and methylmercury in seafood by ion chromatography using photo-induced chemical vapor generation atomic fluorescence spectrometric detection, Microchem. J., 95 (2010) 255-258.

[32] M. Park, H. Yoon, C. Yoon, J. Y. Yu, Estimation of mercury speciation in soil standard reference materials with different extraction methods by ion chromatography coupled with ICP-MS, Environ. Geochem. health, 33 (2011) 49-56.

[33] S. Carneado, R. Peró-Gascón, C. Ibáñez-Palomino, J. F. López-Sáncheza, A. Sahuquillo, Mercury (II) and methylmercury determination in water by liquid chromatography hyphenated to cold vapour atomic fluorescence spectrometry after online short-column preconcentration, Anal. Method., 7 (2015) 2699-2706.

[34] A. Fashi, MR. Yaftian, A. Zamani, Electromembrane extraction-preconcentration followed by microvolume UV–Vis spectrophotometric determination of mercury in water and fish samples, Food chem., 221 (2017) 714-720.

[35] D. M, Sánchez, R. Martín, R. Morante, J. Marín, M.L. MunueraPreconcentration speciation method for mercury compounds in water samples using solid phase extraction followed by reversed phase high performance liquid chromatography, Talanta, 52 (2000) 671-679.

[36] M. Krawczyk, E. Stanisz, Ultrasound-assisted dispersive micro solid-phase extraction with nano-TiO2 as adsorbent for the determination of mercury species, Talanta, 161 (2016): 384-391.

[37] E. Ziaei, A. Mehdinia, A. Jabbari, A novel hierarchical nanobiocomposite of graphene oxide–magnetic chitosan grafted with mercapto as a solid phase extraction sorbent for the determination of mercury ions in environmental water samples, Anal. Chim. Acta, 850 (2014) 49-56.

[38] N. Pourreza, K. Ghanemi, Determination of mercury in water and fish samples by cold vapor atomic absorption spectrometry after solid phase extraction on agar modified with 2-mercaptobenzimidazole, J. Hazard. Mater., 161 (2009) 982-987.

[39] A Krata, K Pyrzyńska, E Bulska, Use of solid-phase extraction to eliminate interferences in the determination of mercury by flow-injection CV AAS, Anal. Bioanal. Chem., 377 (2003) 735-739.

[40] L. Adlnasab, H. Ebrahimzadeh, A. A. Asgharinezhad, M. Nasiri Aghdam, A. Dehghani, S. Esmaeilpour, preconcentration procedure for determination of ultra-trace mercury (II) in environmental samples employing continuous-flow cold vapor atomic absorption spectrometry, Food anal. Method., 7 (2014) 616-628.

[41] NH Khdary, AG Howard, New solid-phase-nanoscavenger for the analytical enrichment of mercury from water, Analyst, 136 (2011) 3004-3009.

[42] E. Zolfonoun, A. Rouhollahi, A. Semnani, Solid-phase extraction and determination of ultra-trace amounts of lead, mercury and cadmium in water samples using octadecyl silica membrane disks modified with 5, 5′-dithiobis (2-nitrobenzoic acid) and atomic absorption spectrometry, Int. J. Environ. Anal. Chem., 88 (2008) 327-336.

[43] Y. Date, et al, Trace-level mercury ion (Hg2+) analysis in aqueous sample based on solid-phase extraction followed by microfluidic immunoassay, Anal. Chem., 85 (2012) 434-440.

[44] P. Rivaro, C. Ianni, F. Soggia, R. Frache, Mercury speciation in environmental samples by cold vapour atomic absorption spectrometry with in situ preconcentration on a gold trap, Microchim. Acta, 158 (2007) 345-352.

[45] H. Shirkhanloo, A. Khaligh, H. Zavvar Mousavi, M. M. Eskandari, A. A. Miran-Beigi, Ultra-trace arsenic and mercury speciation and determination in blood samples by ionic liquid-based dispersive liquid-liquid microextraction combined with flow injection-hydride generation/cold vapor atomic absorption spectroscopy, Chem. Paper.. 69 (2015) 779-790.

[46] N. Rajesh, G. Gurulakshmanan, Solid phase extraction and spectrophotometric determination of mercury by adsorption of its diphenylthiocarbazone complex on an alumina column, Spectrochim. Acta Part A: Mol. Biomol. Spec., 69.2 (2008) 391-395.

[47] HI. Ulusoy, R Gürkan, S Ulusoy, Cloud point extraction and spectrophotometric determination of mercury species at trace levels in environmental samples, Talanta, 88 (2012) 516-523.

[48] J. C. de Wuilloud, R. G. Wuilloud, M. F. Silva, R.A. Olsina, L. D. Martinez, Sensitive determination of mercury in tap water by cloud point extraction pre-concentration and flow injection-cold vapor-inductively coupled plasma optical emission

spectrometry, Spectrochim. Acta Part B: Atom. Spec., 57 (2002) 365-374.

[49] A. Nasrollahpour, S. M. J. Moradi, S. E. Moradi. Dispersive solid phase micro-extraction of mercury (II) from environmental water and vegetable samples with ionic liquid modified graphene oxide nanoparticles, J. Serb. Chem. Soc., 82 (2017) 551-565.

[50] C. Mitani, A. Kotzamanidou, A.N. Anthemidis, Automated headspace single-drop microextraction via a lab-in-syringe platform for mercury electrothermal atomic absorption spectrometric determination after in situ vapor generation, J. Anal. Atom. Spec., 29 (2014) 1491-1498.

[51] M. Hossien-poor-Zaryabi, et al. "Application of dispersive liquid–liquid micro-extraction using mean centering of ratio spectra method for trace determination of mercury in food and environmental samples. Food Anal. Method., 7 (2014) 352-359.

[52] M. Rezaee, Y. Assadi, M. R. M. Hosseini, E. Aghaee, F. Ahmadi, S. Berijani, Determination of organic compounds in water using dispersive liquid–liquid microextraction, J. Chromatogr. A, 1116 (2006) 1-9.

[53] G. Li, K. H. Row, Utilization of deep eutectic solvents in dispersive liquid-liquid micro-extraction, TrAC, Trends Anal. Chem., 120 (2019) 115651.

[54] Li, Yanyan, et al, Magnetic effervescent tablet-assisted ionic liquid-based dispersive liquid-liquid microextraction of polybrominated diphenyl ethers in liquid matrix samples, Talanta, 195 (2019) 785-795.

Analytical Methods in Environmental Chemistry Journal Vol 2 (2019) 59-70

AMECJ

Research Article, Issue 4

Analytical Methods in Environmental Chemistry Journal

Journal home page: www.amecj.com/ir

Removal of ethylbenzene from air by graphene quantum dots and multi wall carbon nanotubes in present of UV radiation

Maling Gou[a,b] and Baharak Bahrami Yarahmadi[c,*]

[a] *State Key Laboratory of Biotherapy and Cancer Center, West China Hospital, Sichuan University and Collaborative Innovation Center for Biotherapy, Chengdu 610041, China*

[b] *Department of Thoracic Oncology, Cancer Center, West China Hospital, Medical School, Sichuan University, Chengdu 610041, China*

[C.*] *Occupational Health Engineering Department, School of Public Health, Kerman University of Medical Sciences, Kerman, Iran*

ARTICLE INFO:

Received 12 Sep 2019

Revised form 15 Nov 2019

Accepted 5 Dec 2019

Available online 28 Dec 2019

Keywords:

Graphene quantum dots,
Multi wall carbon nanotubes,
Ethylbenzene,
Air removal,
UV-radiation,
Solid gas removal

ABSTRACT

Luminescent graphene quantum dots (GQDs) and multi wall carbon nanotubes (MWCNTs) as photocatalytic sorbent based on was used for removal of toxic ethylbenzene from air in present of UV-radiation. A novel method based on solid gas removal (SGR) based on GQDs and MWCNTs as an efficient adsorbent was used for ethylbenzene removal from air in Robson quartz tubes (RGT). After synthesized and purified of GQDs and MWCNTs, a system was designed for generation of ethylbenzene in air with difference concentrations, and then the mixture was moved to quartz tubes with UV radiation in optimized conditions. The ethylbenzene in air was absorbed on the 25 mg of GQDs or MWCNTs, desorbed from sorbent at 146°C and determined by GC-FID. The main parameters such as, temperature, ethylbenzene concentration, amount of GQDs / MWCNTs and flow rate were studied and optimized. The recovery of ethylbenzene removal from air (more than 95%) and absorption capacity of adsorbent (186.4 mg g^{-1}) were achieved in present of UV radiation at room temperature by GQDs. The flow rate and temperature were obtained at 300 mL min^{-1} and less than 42 ^{0}C, respectively. Based on results, the special surface area and favorite porosity of GQDs caused to efficient removal of ethylbenzene from air in present of UV as compared to other carbon compounds such as MWCNTs, and graphene.

1. Introduction

One of the most important issues facing human beings today and even endangering their health is air pollution. Volatile organic compounds (VOCs) are one of the most important pollutants, and these compounds are listed as toxic [1, 2]. Global warming, ozone depletion, photochemical smog, and contributor of haze is the effect of this material [3, 4]. The boiling point range of volatile organic compounds is from 50 to 250 °C and because of high vapor pressure creates a notable amount of the molecules to evaporate and release in the air [5, 6]. Their health effects on humans are very important, these compounds can irritate the respiratory system and eyes, cause headaches and nausea, damage the kidneys, liver, the central nervous system and even in chronic exposure cause cancer [7-10]. Some of the major industries producing volatile organic compounds include petroleum refineries, chemical industries, automotive industries, paint industry, pharmaceuticals, cable and wire industries, printing, aerospace, textile, etc. [1, 11]. BTEX (Benzene, toluene, ethylbenzene, and xylene) are the most common VOCs and usually used in the

*Corresponding Author: Baharak Bahrami Yarahmadi
Email: baharakb72@gmail.com
DOI: https://doi.org/10.24200/amecj.v2.i04.82

petrochemical industry and as reagents for the synthesis of multiple C-based products [11-13]. Among BTEX, ethylbenzene is mainly used in the manufacture of styrene. The release of Ethylbenzene into the air could be carcinogenic, cause secondary aerosol and photochemical smog. Ethylbenzene is a colorless liquid that smells like gasoline. The odor threshold for ethylbenzene is 2.3 parts per million (ppm). The chemical formula for ethylbenzene is C_8H_{10}, and the molecular weight is 106.16 g mol^{-1}. The vapor pressure for ethylbenzene is 9.53 mm Hg at 25 °C, and its octanol/water partition coefficient is 3.13. In petrochemical factories, BTEX and mercury vapor released in air and can be absorbed in humans via the inhalation and dermal routes of exposure. So determination BTEX and mercury in air, water and human matrixes is very important [14-17]. Previous study reported the carcinogenic effects of ethylbenzene in humans. EPA has classified ethylbenzene as a Group D, not classifiable as to human carcinogenicity. ACGIH recommends a TLV-TWA of 100 ppm and STEL/C of 125 ppm for ethylbenzene based on irritation and central nervous system effects [18-20]. Acute (short-term) exposure to ethylbenzene in humans results in respiratory effects, such as throat irritation and chest constriction, irritation of the eyes, and neurological effects such as dizziness. Chronic (long-term) exposure to ethylbenzene by inhalation in humans has shown conflicting results regarding its effects on the blood. Animal studies have reported effects on the blood, liver, and kidneys from chronic inhalation exposure to ethylbenzene [21-23]. There are many successful techniques which have been developed and applied to control the VOCs emission, such as condensation, membrane, absorption, adsorption, thermal combustion, catalytic, photocatalytic oxidation, non-thermal plasma, and biofiltration [24-27]. Photocatalytic oxidation (PCO) as the most current generation of air cleaning technology has a magnificent potential to eliminate vaporous pollutants even at low concentrations [28]. Exceptional features of this method are operating at ambient temperature without notable energy supply, environmentally friendly final products (CO_2 and H_2O), and applicable for various pollutants [29]. PCO implemented using photocatalyst, ultraviolet (UV) light and oxygen to decay chemical pollutants[30]. Numerous researchers have reviewed the materials for the removal of VOCs [27, 31]. Most sources have been reviewed based on a particular kind of material, such as TiO_2 [32], graphene-based materials [33], zinc indium sulfide [34] and silica-nanosphere-based materials, etc., or concentrating on the catalytic oxidation processes in a specific condition such as low-temperature, visible light, or based on a review of the aspect of different VOCs[35].

In this study, a novel analytical method based on UV- GQDs or UV-MWCNTs was used for ethylbenzene removal from air by SGR technology. All of important parameter for photocatalytic process were optimized and the results validated by spiking standard concentration of ethylbenzene to real samples. The mixture of ethylbenzene vapor in air was generated and storage in polyethylene bags and its concentration determined by GC-MS before moved to quartz tubes. The removal efficiencies were calculated in UV- GQDs, GQDs and $MWCNT_S$ by SGR procedure.

2. Experimental

2.1. Gas Chromatography (GC-FID)

The gas chromatography with flame ionization detector (GC-FID) based on air sample loop injection was used for ethylbenzene determination in gas phase (Agilent GC, 7890A, FID, Netherland). Before injection to GC-FID, Slide the plunger carrier down and tighten. An air sample introduced into the carrier gas by sampling valves which was used to sample gases or liquids. Air sampling bags were used by valve and septum port (Tedlar, Germany). GC with a split injector (200°C), flame ionization detector (250°C), and a column with methylsiloxane was used. The oven temperature was adjusted from 25°C to 250°C which was held for 15 min. The carrier gas of hydrogen with flow rate of 1.2 mL min^{-1} were tuned. For batch system, the vials (PTFE) with air-tight cap (parker) were

prepared. TGS 2180 (China) and Dräger 3500 (Lübeck, Germany) as gas detectors was used for determination of H_2O vapor and O_2 in air. The ethylbenzene was evaporated and mixed with purified air at 135°C in chamber.

2.2. Reagents

The ultra-pure chemicals were purchased from Merck and Sigma Aldrich (Germany). The Deionized Distilled water (DDW) was prepared by (Millipore, CAS 7732-18-5). The standard of ethylbenzene ($C_6H_5C_2H_5$) was generated with ultra-pure air in chamber. The accuracy and precision of the pilot was investigated by injecting a concentration of ethylbenzene in chamber and determination of ethylbenzene in air bags by GC-MS before moved to RGT which was filled with GQDs or MWCNTs. The high purity of ethylbenzene was purchased from Merck (CAS N: 100-41-4, EC N: 202-849-4, Germany) and the calibration solutions of 0.1, 0.2, 0.5, 1.0, 1.5 and 2.0 % (v/v) were prepared. The GQDs and MWCNTs were synthesized by RIPI.

2.3. Pilot of gas generation

By pilot design, the purified air was prepared based on HEPA filter *and* activated carbon (HEPA-AC) with *electro air cleaner (EAC, Canada*). The HEPA-AC removed VOCs and the particles dust from 200 to 300 nm. The pure air passed through connection of PVC tubes and storage in 1-5 liter of bulk bag. After adjusting of H_2O, the mixture moved to GQDs or MWCNTs in optimized flow rate and temperature. All of lines and bags were covered with heating jackets capable of controlling the temperature up to 70 °C to prevent condensing.

2.4. Synthesis of LGQDs and MWCNTs

High-purity MWCNTs were synthesized by use of camphor, an environment-friendly hydrocarbon as a carbon source using chemical vapor deposition (CVD) method on Co-Mo/MgO Nano-catalysts [36]. We prepared GO from graphite adopting a modified Hummers' method [37, 38]. The GO was used for synthesizing of GQDs by Dong et al. Firstly, the amount of GO was refluxed with HNO3 (10 M) at 120°C for one day. When the reaction was completed the color of solvent darkened. Then, the suspension was centrifuged for 15 min after being cooled at 25°C. The suspension was collected after washing of product with DW and then centrifuged. Secondly, the obtained GO was dispersed in 20 mL DW, heated hydrothermally in a Teflon-lined stainless steel at 220°C for 10 hours and centrifuged (3500) for 20 min (brown color). So, GQDs were obtained in this procedure by green fluorescence under 365 nm UV light irradiation [39].

2.5 Characteristics

After hydrothermal method for synthesis nano

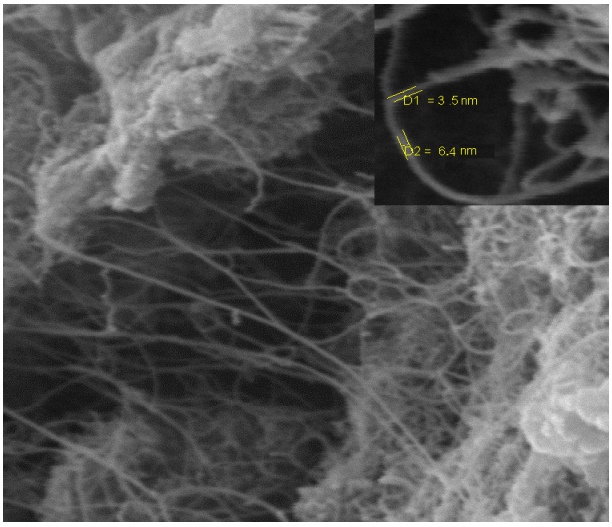

Fig. 1a. SEM of MWCNTs

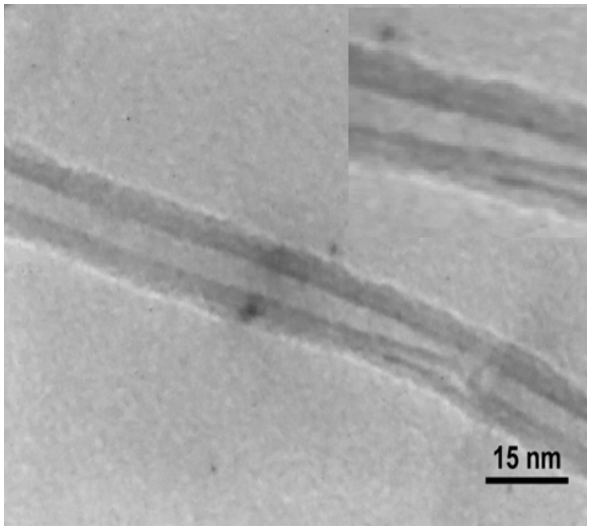

Fig. 1b. TEM of MWCNTs

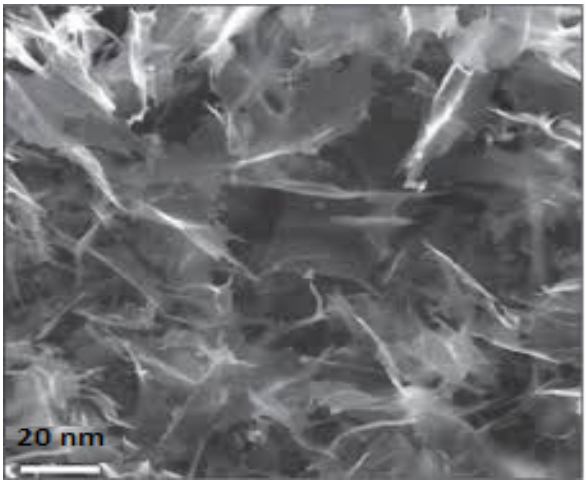

Fig. 2a. SEM of GQDs

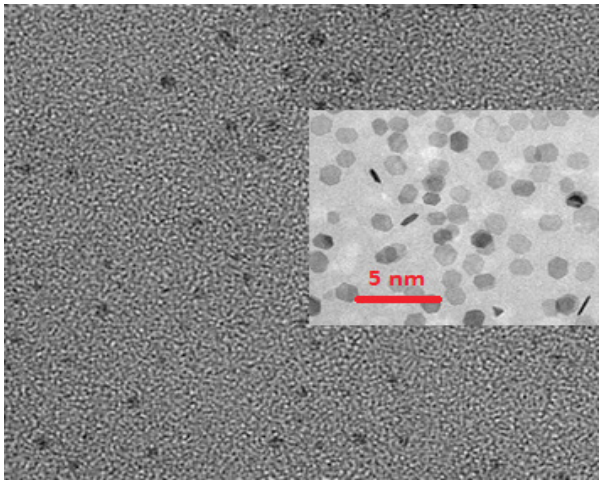

Fig. 2b. TEM of GQDs

materials, the SEM and TEM images of the MWCNTs and GQDs were shown in Figure 1 (a, b) and 2(a, b). The surface area and pore size of GQDs and MWCNTs based on nitrogen adsorption was evaluated by Brunauer-Emmett-Teller (BET) method. The surface area and porosity of the MWCNTs and GQDs, before and after heat treatment were similar values. Raman spectra of GQDs and MWCNTs show the G and D bands that are characteristic for carbon structures. Raman spectra show quality of nanostructure which was deepened on I_G/I_D (Fig. 3). The pore size, length, BET surface area and textural properties of GQDs and MWCNTs were shown in Table 1 and 2.

2.6. Removal Procedure

The 25 mg of different GQDs and MWCNTs, was used as sorbents for removal of ethylbenzene from air in optimized conditions (flow rate 300 mL min^{-1}, 42 ^{O}C). The different concentration of ethylbenzene in air (bulk bag) was passed through the GQDs and MWCNTs sorbents. After efficient adsorption in present of UV radiation, the ethylbenzene concentration in air was determined by GC-FID. Also, the removal efficiency calculated after desorption of ethylbenzene from GQDs and MWCNTs by thermal accessory at 150 ^{O}C. For sample blank, 1 mL of air in bulk bag was injected

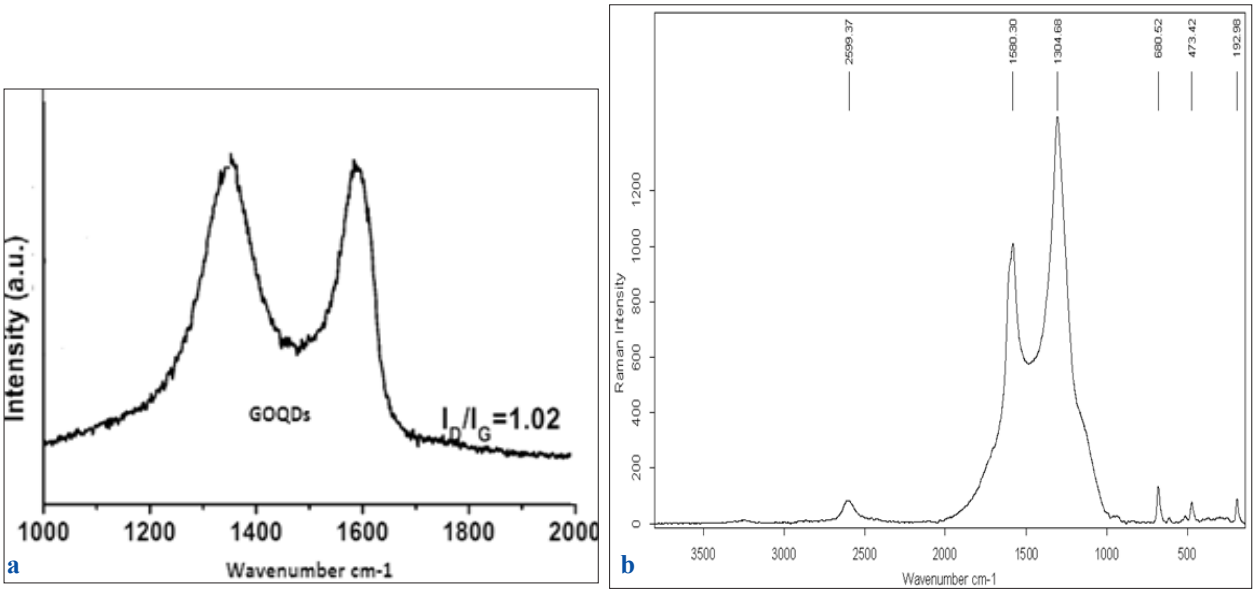

Fig. 3. Raman spectroscopy of a) GQDs and b) MWCNTs

Table 1. Textural properties of GQDs and MWCNTs

Carbon	S_{BET} [a] (m^2/g)	d_{sp} [b](nm)	d_{lp} [c] (nm)	V_{sp} [d] (cm^3/g)	V_{lp} [e](cm^3/g)	PA (A)
MWCNT	375	5.54	15.08	0.51	1.04	117.52
GQDs	343	4.65	14.17	0.53	0.89	101.18

[a]BET specific surface area, [b]diameter of small pores, [c]diameter of large pores, [d]Volume of small pores, [e]Volume of large pores, pore Diameter (PA)

Table 2. Pore size, length and BET surface area of GQDs and MWCNTs

Carbon	Diameter (nm)	Length (um)	*I_G/I_D	Surface Area (m^2/gr)
MWCNT	4-20	8-14	0.77	375
GQDs	3-15	8-12	0.68	346

*(IG/ID): LG band originates from ordered, well-graphitized carbon, D band is the disorder-activated band

to injector of GC-FID by Hamilton syringes and the concentration of ethylbenzene was determined by GC-FID and GC-MS (Agilent 7890A, USA). So, SGR procedure based on GQDs can be efficiently removed ethylbenzene from air.

2. Results and Discussion

3. 1. Optimizing of parameters

In optimized conditions, the adsorption capacity of ethylbenzene in an air is the amount of adsorbate ethylbenzene (mg) on GQDs sorbent (g). The removal efficiency of GQDs is the ratio of removed ethylbenzene to initial ethylbenzene concentration in air. The removal efficiency and adsorption capacity are depended on the important parameters such as; kind of sorbent, size of nanoparticles, temperature, flow rate, ethylbenzene concentration and humidity which were optimized. The effect of ethylbenzene concentration was investigated by SGR method from 1.0 to 100 ppm. The results showed us, high concentration of ethylbenzene, based on the GQDs was saturated early graphene dot sites. In optimized conditions, the ethylbenzene concentration for 25 mg of GQDs and MWCNTs was achieved, 4.66 ppm and 2.54 ppm, respectively in 25°C (Fig. 4). So, the absorption capacity was achieved 186.4 mg g^{-1} and 102.4 mg g^{-1}, respectively (Fig. 5). For ethylbenzene removal from air, the effects of humidity on removal efficiency of GQDs and MWCNTs were studied between 10% - 70%.

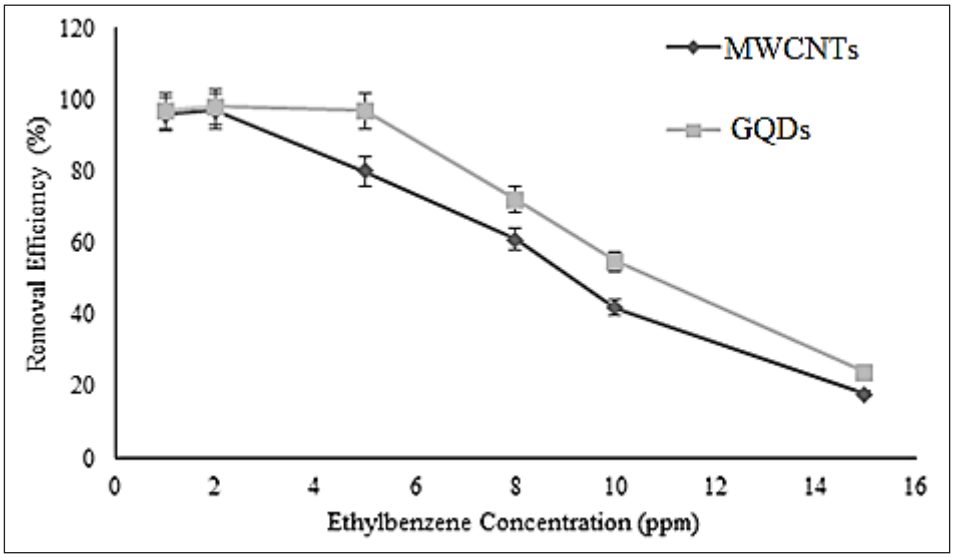

Fig. 4. The effect of ethylbenzene concentration on air removal

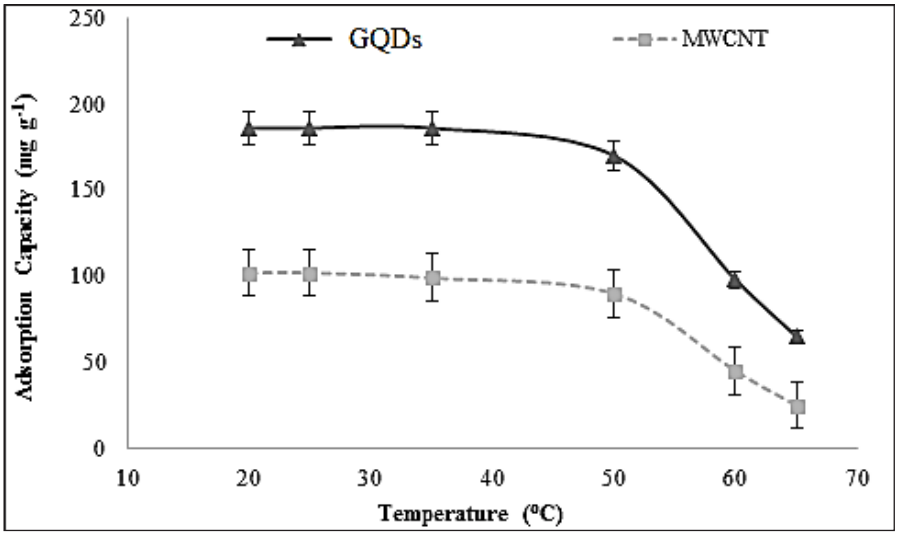

Fig. 5. The effect of temperature on absorption capacity for ethylbenzene removal from air by GQDs

The results showed, by increasing of humidity up to 10%, the removal efficiency wasn't decreased. The temperature has effected on adsorption capacity and recovery of GQDs for ethylbenzene removal from air. The effect of temperature was studied between 25─150 ^{O}C. The results showed us, the absorption efficiency of ethylbenzene by GQDs was achieved under 420 ^{o}C and desorption was obtained at 146^{o}C (Fig. 6). In optimized flow rate value, the maximum recovery was happened by GQDs by SGR procedure. So, the effect of different flow rates between 50 to 800 mL min^{-1} was evaluated based on GQDs for ethylbenzene removal from air. The results showed, the recovery of removal was decreased in more than 350 mL min^{-1}. Therefore, 300 mL min^{-1} was selected as optimum flow rate (Fig. 7). The inside of quartz tubes was filled with GQDs and MWCNTs as a sorbent for ethylbenzene removal from air. Diameter and length of quartz tubes and physical and chemical properties of GQDs and MWCNTs is important factor for adsorption efficiency of ethylbenzene which must be optimized. Based on results, 0.3 cm of diameter and 5 cm of length selected as optimum column for

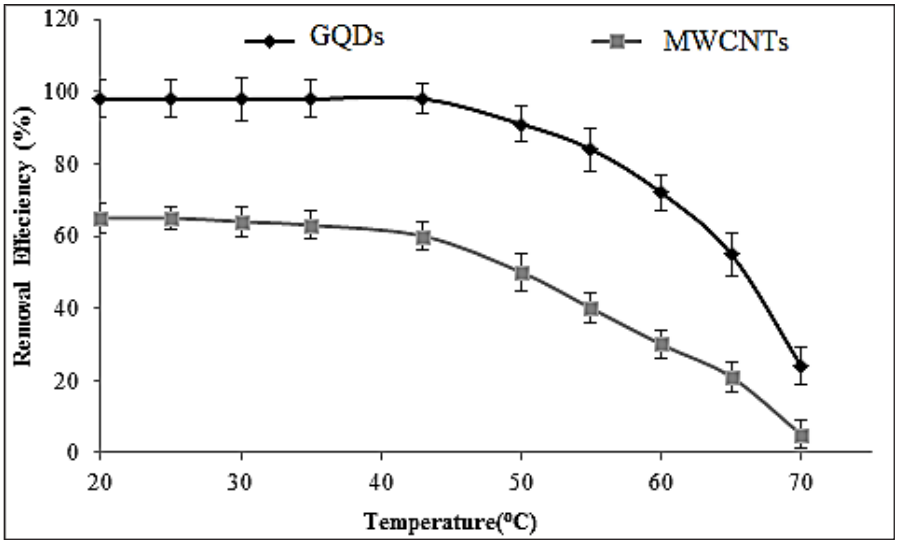

Fig. 6. The effect of temperature on ethylbenzene removal from air by GQDs

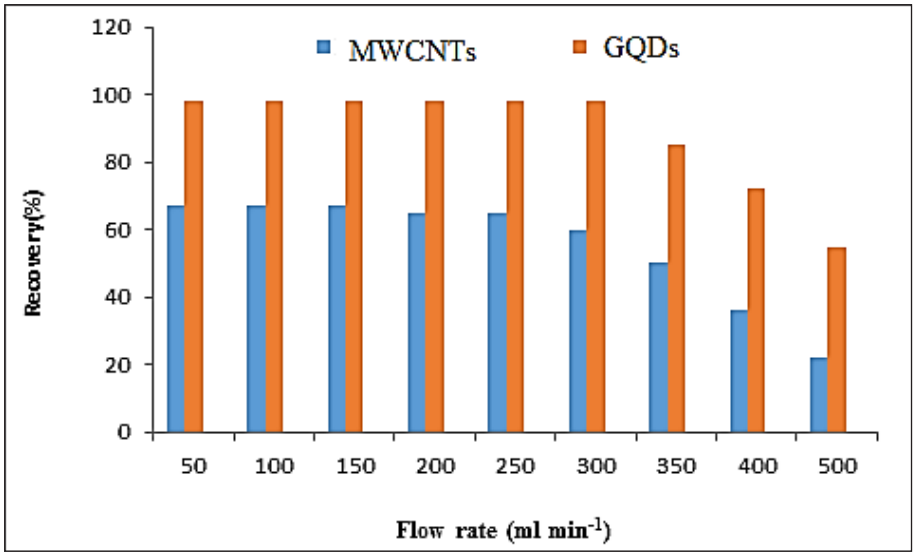

Fig.7 . The effect of flow rate on ethylbenzene removal from air by GQDs

further study.

3.2. Analyzing and Validation

The GQDs was selected as a novel sorbent for removal of ethylbenzene vapor from air in present of UV radiation by SGR method. By procedure, a mixture of 1─100 ppm of ethylbenzene in air which was generated in chamber was validated by GC-MS and then, passed through GQDs. After absorption ethylbenzene on GQDs at room temperature, the ethylbenzene desorbed from it at 146°C and determined by GC-FID. Since, the standard reference material (SRM) for ethylbenzene in air aren't available, the standard ethylbenzene concentration was generated in a bag (5 Li) by chamber and used for validation by spiking of real samples (Table 3).

3.3. Discussion

Fei Yu et al. investigated the removal of TEX from aqueous system by the functionalized magnetic nanoparticle-carbon nanotubes composites that were synthesized, characterized and applied. The APCNTs-KOH composites exhibited high adsorption capacity for TEX onto APCNTs-KOH in a decrease order of ethylbenzene > m-xylene > o-xylene > p-xylene > toluene (227.05,138.04, 63.34, 249.44, and 105.59 mg g^{-1}), which was higher than current study [40]. In another research,

Table 3. Validation of methodology with GC-FID/SGR for ethylbenzene removal from air by UV-GQDs (ppm)

* Bag GC-MS	Added Ethylbenzene	UV-GQDs [a]	Recovery (%)
1.38 ± 0.08	------	1.34 ± 0.09	97.1
	1.0	2.32 ± 0.12	98.0
5.58± 0.31	------	5.51± 0.32	98.7
	5.0	10.38 ± 0.47	97.4
10.43 ± 0.44	------	10.07 ± 0.52	96.5
	10.0	19.96 ± 0.93	98.9
20.65 ± 1.02	------	19.89 ± 1.13	96.3
	20.0	40.11 ± 2.15	101.1
80.48 ± 3.88	------	78.65 ± 4.23	97.7
	80.0	157.33 ± 7.86	98.4

[a] Mean of three determinations ± confidence interval (P = 0.95, n = 5)

* (Air bag; 1-80 ppm in 5 Li bag, 300 mL min^{-1} air flow rate, Peak Area, 25 mg, T=25°C)

Natarajan et al. used the biofiltration method for the removal of the ethylbenzene-xylene mixture while the total inlet loading rate range was 25.408 g m^{-3} per hour. The maximum removal capacities attained for ethylbenzene and toluene were 85.63 and 63.2 g m^{-3} per hour respectively, which was lower than our proposed method. The elimination capacities were evaluated at different loading rates and found to vary in a linear pattern. Based on result removal capacities was lower than this study [41]. Ye and Ariya used Fe_3O_4 nanoparticles (NPs) at different relative humidities (RH) as adsorption for removal of gaseous benzene, toluene, ethylbenzene and m-xylene (BTEX) and sulfur dioxide (SO_2). X-ray diffraction, Brunauer–Emmett–Teller, and transmission electron microscopy were deployed for nanoparticle surface characterization. Using gas chromatography equipped with flame ionization detection, Adsorption experiments of BTEX on NPs were measured, which under dry conditions indicated high removal efficiencies (up to (95 ± 2)%), which are similar to our result [42]. Bina et al. used multi-walled, single-walled, and hybrid carbon nanotubes (MWCNTs, SWCNTs, and HCNTs) for removal of ethylbenzene (EB) from aqueous solution. Ethylbenzene has a higher adsorption tendency on CNTs so that more than 98% of it adsorbed in the first 14 min, which is related to the low water solubility and the high molecular weight. Isotherm's study indicates that the BET isotherm expression provides the best fit for ethylbenzene sorption by SWCNTs [43]. Kamaei et al. used nitrogen-doped commercial TiO2 nano-catalysts for photocatalytic decomposition of ethylbenzene in the air using a packed-bed annular photoreactor. The removal efficiency of ethylbenzene under UV irradiation using N-doped catalyst was more than 90% for the initial concentrations up to 0.586 gm^{-3} (135 ppm) at 1 min residence time Moreover the removal efficiency under visible light radiation could be obtained for the initial concentrations up to 0.1 gm^{-3} (about 25 ppm) at 3 min residence time, which is lower than this article[44]. Hadi et al. used nano-magnetic particles (Fe_3O_4) as an adsorbent to eliminate ethylbenzene from aqueous solutions.

The characterization of the adsorbent was investigated by transmission electronic microscope (TEM) and X-ray diffraction (XRD) pattern. The results showed that the most amounts of ethylbenzene adsorption and distribution ratio in optimum condition were 49.9 mg g^{-1}(which was lower than our method) and, 261.9 Lg^{-1} respectively. The results explained that the removal rate of ethylbenzene was higher in batch (99.8 %) rather than continuous (97.4%) conditions [8]. Ahmed et al. used nZVI for eliminating benzene, toluene, ethylbenzene, and xylene (BTEX) contaminants from aqueous solutions. X-ray diffraction (XRD), UV spectrophotometry, and scanning electron microscopy (SEM) were used for nZVI characterization. The effects of contact time, initial BTEX mixture concentration, adsorbent dose, temperature, and pH on the amount of BTEX absorbed were studied. The highest removal efficiency of 97% for the BTEX mixture was achieved at a stirring rate of 100 rpm, the temperature of 60°C, and pH 7, which is higher than our study. The minimum effective time for efficient removal was 30 min, while the effective dose for BTEX compounds removal was 0.22 gL^{-1}[45]. Yan et al. used CuMgFe layered double hydroxide (CuMgFe-LDH), for the degradation of ethylbenzene. the degradation efficiency of 0.08 mmol L^{-1} ethylbenzene was 93.7% under the optimized conditions at 0.2 g L^{-1}, CuMgFe-LDH and 4.0 mmol L^{-1} persulfate at pH 7.6, which is lower than our result [46]. Azizi et al. used the graphene oxide grafted with polymethyl vinyl ketone and aniline (GO-MVK-ANI), for the elimination of ethylbenzene. The synthesized material was characterized via FTIR, SEM, energy-dispersive X-ray spectroscopy and Brunauer–Emmett–Teller analysis.

Based on the result with initial ethylbenzene concentration of 20 mg g^{-1} under the optimum

conditions (the contact time of 11 min, pH of 5.64 and adsorbent dose of 3.75 g L^{-1}), ethylbenzene could be adsorbed (73%), which is lower than our result [47]. Samarghandi et al. investigated Catalytic Ozonation Process (COP) to treat polluted air streams containing ethylbenzene. Respectively at 50 ppm of this pollutant, for single ozonation and single modified pumice, the best removal efficiency of ethylbenzene was 58–80%, while the maximum removal efficiency of ethylbenzene was 90% for COP (6 L min^{-1} of flow rate of inlet air, 15 g of the adsorbent, and 50 ppm of ethylbenzene), which is lower than this study[48]. Also samarghandi et al. used ozone and carbosieve in the catalytic removal of ethylbenzene from the polluted airstream. GC – FID was used for sampling and analysis. The results of this study showed that the removal effectiveness of a single ozonation process is averagely less than 25%. Also, whit the concentration increase of ethylbenzene the efficiency of absorbent decreased. The increase ratio of the efficiency in the catalytic ozonation process to the efficiency of carbosieve adsorbent was averagely 45% which is lower than the current study[49].

4. Conclusions

In this study, the GQDs and MWCNTs as nano sorbents were used for ethylbenzene removal from air in present of UV-radiation by SGR method. According to experimental procedure, the simple, reliable and sensitive method based on GQDs was demonstrated in real samples. In optimized conditions, the concentration of ethylbenzene, air flow rate, amount of GQDs and MWCNTs, temperature, and humidity were studied. The results showed, the flow rate (300 ml L^{-1}) can more effected on capacity adsorption by GQDs as physical adsorption. However, in optimized conditions, the removal efficiency and adsorption capacity of GQDs were obtained more than 95% and 186.4 mg g^{-1}, respectively as compared to MWCNTs.

5. Acknowledgments

We are thankful to Kerman University of Medical Sciences (KUMS) and Iranian Petroleum Industry Health Research Institute (IPIHRI).

6. Reference

[1] R.K. Nath, M.F.M. Zain, M. Jamil, An environment-friendly solution for indoor air purification by using renewable photocatalysts in concrete: A review, Renew. Sust. Energ. Rev., 62 (2016) 1184-1194.

[2] J. Yan, Y. Chen, W. Gao, Y. Chen, L. Qian, L. Han, M. Chen, Catalysis of hydrogen peroxide with Cu layered double hydrotalcite for the degradation of ethylbenzene, Chem., 225 (2019) 157-165.

[3] M. Li, Z. Huang, F. Kang, Progress of volatile organic compounds control technology, Chem. Ind. Eng., 32 (2015) 2-9.

[4] H. Wang, Z. Xiang, L. Wang, S. Jing, S. Lou, S. Tao, J. Liu, M. Yu, L. Li, L. Lin, Emissions of volatile organic compounds (VOCs) from cooking and their speciation: A case study for Shanghai with implications for China, Sci. Total Environ., 621 (2018) 1300-1309.

[5] M. Feiz-Arefi, F. Ghorbani-Shahna, A. Bahrami, H. Ebrahimi, A. Mahjub, Photocatalytic Removal of Methylbenzene Vapors by MnO2/Al2O3/Fe2O3 Nano composite, Iran. J. Health Safe. Environ., 6 (2019) 1158-1166.

[6] S. Zhang, J. You, C. Kennes, Z. Cheng, J. Ye, D. Chen, J. Chen, L. Wang, Current advances of VOCs degradation by bioelectrochemical systems: a review, Chem. Eng. J., 334 (2018) 2625-2637.

[7] A.N. Baghani, A. Sorooshian, M. Heydari, R. Sheikhi, S. Golbaz, Q. Ashournejad, M. Kermani, F. Golkhorshidi, A. Barkhordari, A.J. Jafari, A case study of BTEX characteristics and health effects by major point sources of pollution during winter in Iran, Environ. pollut., 247 (2019) 607-617.

[8] M. Hadei, M. Aalipour, N. Mengli Zadeh, H. Pourzamani, Ethylbenzene removal from aqueous solutions by nano magnetic particles, Arch. Hyg. Sci., 5 (2016) 22-32.

[9] A. Masih, A.S. Lall, A. Taneja, R. Singhvi, Exposure levels and health risk assessment of ambient BTX at urban and rural environments of a terai region of northern India, Environ. Pollut., 242 (2018) 1678-1683.

[10] L. Wang, C. Yang, Y. Cheng, J. Huang, H. Yang, G. Zeng, L. Lu, S. He, Enhanced removal of ethylbenzene from gas streams in biotrickling filters by Tween-20 and Zn (II), J. Environ. Sci., 26 (2014) 2500-2507.

[11] A. Carvajal, I. Akmirza, D. Navia, R. Pérez, R. Muñoz, R. Lebrero, Anoxic denitrification of BTEX: Biodegradation kinetics and pollutant interactions, J. environ. manage., 214 (2018) 125-136.

[12] M.H. El-Naas, J.A. Acio, A.E. El Telib, Aerobic biodegradation of BTEX: progresses and prospects, J. Environ. Chem. Eng., 2 (2014) 1104-1122.

[13] R. Moolla, C.J. Curtis, J. Knight, Assessment of occupational exposure to BTEX compounds at a bus diesel-refueling bay: A case study in Johannesburg, South Africa, Sci. Environ., 537 (2015) 51-57.

[14] H.Z. Mousavi, A. Asghari, H. Shirkhanloo, Determination of Hg in water and wastewater samples by CV-AAS following on-line preconcentration with silver trap, J. Anal. Chem., 65 (2010) 935-939.

[15] H. Shirkhanloo, A. Khaligh, H.Z. Mousavi, M.M. Eskandari, A.A. Miran-Beigi, Ultra-trace arsenic and mercury speciation and determination in blood samples by ionic liquid-based dispersive liquid-liquid microextraction combined with flow injection-hydride generation/cold vapor atomic absorption spectroscopy, Chem. Paper., 69 (2015) 779-790.

[16] H. Shirkhanloo, M. Osanloo, M. Ghazaghi, H. Hassani, Validation of a new and cost-effective method for mercury vapor removal based on silver nanoparticles coating on micro glassy balls, Atmos. Pollut. Res., 8 (2017) 359-365.

[17] L. Zhao, X. Qin, X. Hou, Y. Li, K. Zhang, W. Gong, J. Nie, T. Wang, Research on determination of BTEX in human whole blood using purge and trap-gas chromatography-mass spectrometry combined with isotope internal standard, Microchem. J., 145 (2019) 308-312.

[18] Ethylbenzene, International Agency for Research on Cancer (IARC), 77 (2000) 227-266.

[19] Threshold limit values for chemical substances and physical agents and biological exposure indices, in, American Conference of Governmental Industrial Hygienists(ACGIH), 1995.

[20] S. Wilbur, S. Bosch, Interaction profile for: benzene, toluene, ethylbenzene, and xylenes (BTEX), Agency for Toxic Substances & Disease Registry (ATSDR), 2004.

[21] M. Delikhoon, M. Fazlzadeh, A. Sorooshian, A.N. Baghani, M. Golaki, Q. Ashournejad, A. Barkhordari, Characteristics and health effects of formaldehyde and acetaldehyde in an urban area in Iran, Environ. pollut., 242 (2018) 938-951.

[22] F. Golkhorshidi, A. Sorooshian, A.J. Jafari, A.N. Baghani, M. Kermani, R.R. Kalantary, Q. Ashournejad, M. Delikhoon, On the nature and health impacts of BTEX in a populated middle eastern city: Tehran, Iran, Atmos. Pollut. Res., 10 (2019) 921-930.

[23] S. Hazrati, R. Rostami, M. Fazlzadeh, F. Pourfarzi, Benzene, toluene, ethylbenzene and xylene concentrations in atmospheric ambient air of gasoline and CNG refueling stations, Air Qual. Atmos. Health, 9 (2016) 403-409.

[24] M. Bahri, F. Haghighat, Plasma-based indoor air cleaning technologies: the state of the art-Review, Clean Soil Air Water, 42 (2014) 1667-1680.

[25] M. Sansotera, S.G.M. Kheyli, A. Baggioli, C.L. Bianchi, M.P. Pedeferri, M.V. Diamanti, W. Navarrini, Absorption and photocatalytic degradation of VOCs by perfluorinated ionomeric coating with TiO2 nanopowders for air purification, Chem. Eng. J., 361 (2019) 885-896.

[26] K.W. Shah, W. Li, A Review on Catalytic Nanomaterials for Volatile Organic Compounds VOC Removal and Their Applications for Healthy Buildings, Nanomaterials., 9 (2019) 910.

[27] C. Yang, G. Miao, Y. Pi, Q. Xia, J. Wu, Z. Li, J.

Xiao, Abatement of various types of VOCs by adsorption/catalytic oxidation: A review, Chem. Eng. J., 370 (2019) 1128-1153.

[28] L. Zhong, F. Haghighat, Photocatalytic air cleaners and materials technologies–Abilities and limitations, Buid. Environ., 91 (2015) 191-203.

[29] M. Malayeri, F. Haghighat, C.-S. Lee, Modeling of volatile organic compounds degradation by photocatalytic oxidation reactor in indoor air: A review, Buid. Environ., 154 (2019) 309-323.

[30] A.H. Mamaghani, F. Haghighat, C.-S. Lee, Photocatalytic oxidation technology for indoor environment air purification: the state-of-the-art, App. Catal. B: Environ., 203 (2017) 247-269.

[31] M. Hussain, P. Akhter, J. Iqbal, Z. Ali, W. Yang, N. Shehzad, K. Majeed, R. Sheikh, N. Russo, VOCs photocatalytic abatement using nanostructured titania-silica catalysts, J. Environ. Chem. Eng., 5 (2017) 3100-3107.

[32] C.H.A. Tsang, K. Li, Y. Zeng, W. Zhao, T. Zhang, Y. Zhan, R. Xie, D.Y. Leung, H. Huang, Titanium oxide based photocatalytic materials development and their role of in the air pollutants degradation: Overview and forecast, Environ. int., 125 (2019) 200-228.

[33] M. Hu, Z. Yao, X. Wang, Graphene-based nanomaterials for catalysis, Ind. Eng. Chem. Res., 56 (2017) 3477-3502.

[34] Y. Pan, X. Yuan, L. Jiang, H. Yu, J. Zhang, H. Wang, R. Guan, G. Zeng, Recent advances in synthesis, modification and photocatalytic applications of micro/nano-structured zinc indium sulfide, Chem. Eng. J., 354 (2018) 407-431.

[35] A. Truppi, F. Petronella, T. Placido, M. Striccoli, A. Agostiano, M.L. Curri, R. Comparelli, Visible-light-active TiO2-based hybrid nanocatalysts for environmental applications, Catal., 7 (2017) 100.

[36] A. Rashidi, M. Akbarnejad, A. Khodadadi, Y. Mortazavi, A. Ahmadpourd, Single-wall carbon nanotubes synthesized using organic additives to Co–Mo catalysts supported on nanoporous MgO, Nanotech., 18 (2007) 315605.

[37] Y. Xu, H. Bai, G. Lu, C. Li, G. Shi, Flexible graphene films via the filtration of water-soluble noncovalent functionalized graphene sheets, J. Am. Chem. Soc., 130 (2008) 5856-5857.

[38] N.I. Kovtyukhova, P.J. Ollivier, B.R. Martin, T.E. Mallouk, S.A. Chizhik, E.V. Buzaneva, A.D. Gorchinskiy, Layer-by-layer assembly of ultrathin composite films from micron-sized graphite oxide sheets and polycations, Chem. mater., 11 (1999) 771-778.

[39] Y. Dong, H. Pang, S. Ren, C. Chen, Y. Chi, T. Yu, Etching single-wall carbon nanotubes into green and yellow single-layer graphene quantum dots, Carbon, 64 (2013) 245-251.

[40] F. Yu, J. Ma, J. Wang, M. Zhang, J. Zheng, Magnetic iron oxide nanoparticles functionalized multi-walled carbon nanotubes for toluene, ethylbenzene and xylene removal from aqueous solution, Chemosphere, 146 (2016) 162-172.

[41] R. Natarajan, J. Al-Sinani, S. Viswanthan, R. Manivasagan, Biodegradation of ethyl benzene and xylene contaminated air in an up flow mixed culture biofilter, Int. biodet. biodeg., 119 (2017): 309-315.

[42] Z.Y. Connie, P.A. Ariya, Co-adsorption of gaseous benzene, toluene, ethylbenzene, m-xylene (BTEX) and SO2 on recyclable Fe3O4 nanoparticles at 0–101% relative humidities, J. Environ. Sci., 31 (2015) 164-174.

[43] B. Bina, H. Pourzamani, A. Rashidi, M.M. Amin, Ethylbenzene removal by carbon nanotubes from aqueous solution, J. environ. pub. health, 2012 (2012).

[44] M. Kamaei, H. Rashedi, S.M.M. Dastgheib, S. Tasharrofi, Comparing photocatalytic degradation of gaseous ethylbenzene using N-doped and pure TiO2 nano-catalysts coated on glass beads under both UV and visible light irradiation, Catal., 8 (2018) 466.

[45] A.S. Mahmoud, M.K. Mostafa, S.A. Abdel-Gawad, Artificial intelligence for the removal of benzene, toluene, ethyl benzene and xylene (BTEX) from aqueous solutions using iron nanoparticles, Water Suply., 18 (2018) 1650-1663.

[46] J. Yan, Y. Chen, L. Qian, W. Gao, D. Ouyang,

M. Chen., Heterogeneously catalyzed persulfate with a CuMgFe layered double hydroxide for the degradation of ethylbenzene. J. hazard. mater., 338 (2017) 372-380.

[47] A. Azizi, A. Torabian, E. Moniri, A.H. Hassani, H. Ahmad Panahi, Investigating the removal of ethylbenzene from aqueous solutions using modified graphene oxide: application of response surface methodology, Int. J. Environ. Sci. Tec., 15 (2018) 2669-2678.

[48] M.R. Samarghandi, Z. Daraee, G. Shekher, G. Asgari, A. Reza Rahmani, A. Poormohammadi., Catalytic ozonation of ethyl benzene using modified pumice with magnesium nitrate from polluted air. Int. J. Environ. Stutdies, 74 (2017), 486-499.

[49] M.R. Samarghandi, G. Asgari, F. Ghorbani, S.A. Babaee., The study of effect the combined use of ozone and carbosieve in the catalytic removal of ethylbenzene from the polluted airstream, J. Neyshabur UN. Medical. Sci., 5 (2017) 86-98.

Analytical Methods in Environmental Chemistry Journal Vol 2 (2019) 71-81

AMECJ

Research Article, Issue 4

Analytical Methods in Environmental Chemistry Journal

Journal home page: www.amecj.com/ir

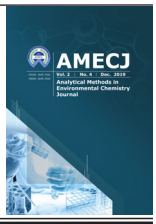

Cadmium separation in human biological samples based on captopril-ionic liquid paste on graphite rod before determination by electrothermal atomic absorption spectrometry

Kian Azami [a], Mehdi Aliomrani [b] and Mostafa Dehghani Mobarake [C,d,*]

[a] *Faculty of Pharmacy, Department of Toxicology Pharmacology, Tehran University of Medical Science, Tehran, Iran*
[b] *Department of Toxicology and Pharmacology, School of pharmacy, Isfahan University of Medical Sciences (IUMS), Isfahan, Iran*
[C] *Energy Technology Research Division, Research Institute of Petroleum Industry (RIPI), Tehran, Iran*
[d] *Department of Chemistry, University of Siegen, North Rhine Westphalia, Adolf-Reichwein-Straße 2, 57076, Siegen, Germany*

ARTICLE INFO:

Received 19 Aug 2019
Revised 24 Oct 2019
Accepted 6 Nov 2019
Available online 25 Dec 2019

Keywords:
Cadmium
Human samples
Captopril
Ionic liquid
Micro graphite rod
Micro solid phase extraction

ABSTRACT

A mixture of captopril nanoparticles (CAP-NPs) and ionic liquid (IL, [HMIM] [PF6]) paste on micro graphite rod (CAP-IL-MGR) and was used for separation cadmium in human serum and urine samples by micro solid phase extraction (μ-SPE). 0.01 g of CAP-NPs and 0.1 g of [HMIM] [PF6] mixed with 1 mL of acetone and mixture passed physically on micro graphite rod (MGR) at 55°C. Then, the graphite probe placed on 10 mL of human biological samples with 5 min of sonication, then cadmium ions complexed by thiol group of captopril (CAP-SH) at pH=5.5. The cadmium ions on micro probe were back extracted with 0.25 mL of nitric acid (0.5 M) which was diluted with DW up to 0.5 mL and finally, the cadmium concentration determined by ET-AAS. By optimizing of amount of captopril, the absorption capacity and recovery were obtained 132.4 mg g^{-1} and more than 96%, respectively. The limit of detection (LOD), linear range (LR) and enrichment factor (EF) were achieved 2 ngL^{-1}, 0.01-0.35 μg L^{-1} and 19.7, respectively (RSD %<5%). The validation was done by certified reference material (CRM, NIST) and ICP-MS analysis.

1. Introduction

Different chemical factories release toxic heavy metals such cadmium, lead and mercury in air, water, soil and also, it slowly enter to tissues of plants and animals by vary sources of erosion and abrasion of soils, forest fires and volcanic eruptions [1-3]. Cadmium with special properties such as, low melting temperature, corrosion resistance, rapid ion electrical exchange activity, high electrical and thermal conductivity can be used in battery factories [2]. Due to these properties is used to make various products including, alkaline nickel-cadmium batteries, paints, alloys, plastics, electroplating protective coatings, solders, rods, television screens, lasers, pesticides, cosmetics and barrier in nuclear process [1, 2, 4-6]. Cadmium is an important industrial and environmental pollutant because it is widely used in many industrial activities (welding, smelting, mining, refining, soldering and etc.) [1, 2, 7]. So, many employments are in Cd exposure pollution. Approximately 512,000 workers in the United States have may a cadmium exposure in each year [8]. Cadmium is one heavy metal because relatively high density and its toxic effects even at low concentration. Cadmium has

*Corresponding Author: Mostafa Dehghani Mobarake
E-mail: modeg128@yahoo.de
https://doi.org/10.24200/amecj.v2.i04.84

received considerable concern because its potential accumulation in the environment and in living organisms leading to long term toxic effects as a non-essential element [9-12]. It is classified as a human carcinogen by the north Carolina national toxicology program (NTP), international agency for research on cancer, (IARC), occupational safety and health administration (OSHA) and national institute of occupational safety and health (NIOSH) [2, 6, 10, 13, 14]. Cadmium occupational exposure to occurs primarily via respiratory tract[15] or ingestion and absorbed by the body and usually connected to metallothionein [4]. Cadmium mainly store in the liver and kidneys, but to a lesser degree rest stored throughout other organs of the body [2, 4, 16]. Toxic effects of Cd depend on enter rout, quantity, rate of exposure [4]. The values NIOSH and OSHA standard for Cd exposure ceiling limit is lowest feasible concentration and 0.005 mg m^{-3} respectively [17]. Long-term exposures to low levels of can result in renal disease but short-term Exposures to high levels of cadmium liver accumulation and hepatocellular damage. Exposures to cadmium also can produce many health effects such as lung irritation, testicular damage, pulmonary edema, renal, hepatic dysfunction, multiple sclerosis (MS) and osteomalacia and in some cases death. Various studies reported correlation between occupational Cd exposure and lung cancer and other cancers such as the prostate, renal, liver, hematopoietic system, urinary bladder, pancreatic, stomach and etc [3, 6, 10, 15, 18, 19]. In many studies, different techniques were used for cadmium analysis in water and human blood samples such as, automated anodic stripping voltammetry (ASV) technique with flow injection system, atomic absorption spectrometry (AAS), laser-induced breakdown spectrometry, hollow cathode excitation coupled to vidicon detection, atomic-fluorescence spectrophotometry, neutron activation analysis (NAA), non-flame atomic absorption spectrometry. [20-27]. Also, other methods were reported for separation and preconcentration of heavy metal in waters and blood urine of neuropsychological and multiple sclerosis patients [28-31]. Recently, the mesoporous silica nanoparticles, silver nanoparticles, nano carbon material, graphene and carbon nanotube were widely used for separation heavy metals in waters and human biological samples by different analytical technology such as ultrasound-assisted dispersive micro-solid-phase extraction (USA-DμSPE) and ultrasound assisted-Ionic liquid trap-micro solid phase extraction (USA-ILT-μSPE) [32, 33]. In this study, a new sorbent based on CAP-NPs passed on MGR with IL was used for separation of cadmium from blood and urine samples by micro solid phase extraction(μ-SPE).All samples analyzed by electro-thermal atomic absorption spectrometer (ET-AAS).

2. Experimental

2.1. Apparatus and Reagents

Cadmium was determined with electro-thermal atomic absorption spectrometer (ET-AAS Varian, USA) which was equipped with graphite furnace accessory (GFA). The current, wavelength and spectral bandwidth of multi hollow cathode lamp (MHCL) were tuned (wavelength 228.8 nm, slit 0.5 nm, lamp current 3.0 mA). All samples were analyzed by auto-sampler injector of GFA. In addition, the inductively coupled plasma mass spectrometers (Varian ICP-MS, 810-MS, 820-MS systems) with full PC control of all instrument settings and compatible accessories. Varian ICP-MS have gigahertz sensitivity (1000 Mc/s/mg/L) and low background and interferences. The Varian ICP-MS systems include a sample introduction system and solid state 27 MHz RF generators. Computer of Varian (ICP-MS) can be control of plasma positioning, triple stage vacuum system, all plasma gas flows, mass analyzer, and Discrete Dynode Electron Multiplier (DDEM) detector. To prepare the 1ppb multi-element test solution (1ppb), pipette 1mL of the 500ppb into a 500mL volumetric flask and dilute up to the mark using 1% HNO3, other concentration from 0.05-0.9 ppb prepared by dilution of DW (LOD= 2 ng L^{-1} cadmium). The pH range of samples was determined by a digital pH meter (M 744, Metrohm). The samples

were shacked by a Vortex Mixer (Thermo USA). All reagents purchased from Sigma Aldrich and Merck Company from Germany. The nitric acid, hydrochloric acid, polyoxyethylene octyl phenyl ether, acetic acid, acetone and toluene (HNO3, HCl, TX-100, CH_3COOH, AC, C_6H_5 -CH_3) were purchased from Merck, Darmstadt, Germany. The cadmium nitrate solution (500 mL, 1000 mg L^{-1}, 99.98%) as cadmium(II) nitrate stock solution (1% HNO3) was purchased from Merck(traceable to SRM from NIST $Cd(NO_3)_2$ in HNO_3 0.5 mol L^{-1}, CAS N: 119777 Germany). Standard solutions (0.05, 0.1, 0.2, 0.5, 1 µg L^{-1}) were prepared daily by dilution of DW with 1% nitric acid. The pH of the samples was adjusted with a phosphate buffer (HPO_4–$H2PO_4$) for pH 5.5. Ultrapure water (DW) was obtained from Millipore Continental Water System (Bedford, USA). The CAP-NPs (CAP, CASN: 62571-86-2, $C_9H_{15}NO_3S$) were purchased from Sigma Aldrich (Germany). CAP as an antihypertensive agent that competitively inhibits angiotensin-converting enzyme (ACE; IC_{50}= 23-35 nM) act in human body. Also, ACP acts as a reversible and competitive inhibitor of LTA_4 hydrolase (Fig. 1). Ionic liquids are made up of charged species and imidazolium-based ionic liquids have one of the nitrogen atoms in the imidazolium ring in the cationic form. These are generally synthesized by alkylation of an N-alkylimidazole and further incorporation of the desired anion by anion metathesis. 1-Butyl-3-methylimidazolium hexafluorophosphate is an imidazolium-based, hydrophobic, room temperature ionic liquid (RTIL).1-Butyl-3-methylimidazolium hexafluorophosphate{BMIM][PF6] is an ionic liquid employed in many environmentally friendly analysis (CASN: 70956, Sigma, Germany). 1-Methyl-3-(3-cyanopropyl) imidazolium bis(trifluoromethylsulfonyl)amide (CASAN: 38943 Sigma) as TSIL were purchased from Sigma, Germany. Graphite rod, L 150 mm(15 cm), diam. 3 mm, low density(CASN: 496537, 99.995% trace metals). Micro graphite rod as 5 cm was used (micro rod of graphite, MGR, Sigma Alderich)

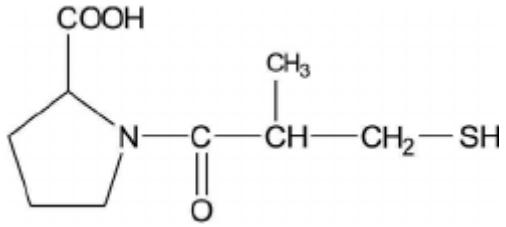

Fig. 1. The structural of captopril nanoparticles(CAP-NPs)

2.2. Preparing of solid phase

First, 50 micro gram of CAP, 100 micro liter of ionic liquid and 2 mL of acetone mixed with MGR by shaking at 5 min (50 °C). After drying in oven (120°C), washing with DW at 25°C for 10 times and then drying for 10 min at 120 °C. The CAP physically passed on MGR based on IL was used as solid phase for extraction cadmium from blood samples**.**

2.3. Extraction Procedure

By µ-SPE procedure, the CAP-IL-MGR was used for separation and determination cadmium in of blood/serum/urine samples by ET-AAS. The procedure was developed as follows: 10 mL of blood samples and standard solution containing 0.05-0.35 µg L^{-1} of cadmium was used for further analysis after the pH adjusted up to 5.5 with phosphate buffer solution. Then, the graphite rod - IL/CAP was placed in real samples which were shaken for 5 min. Cd (II) ions were extracted from samples by thiol group of CAP. Then, the rod was taking out from samples and eluted with nitric acid (0.25 mL, 0.5 M) which was diluted with DW up to 0.5 mL. Finally, the obtained solution was determined by ET-AAS. The proposed method followed by MGR without CAP or IL at room temperature. The concentration of cadmium in DW as a blank sample was determined by µ-SPE method **(**Fig. 2).

3. Results and Discussion

3.1. Characterizations of CAP-NPs

The characterization of CAP nanomaterials on MGR were achieved by X-ray diffraction spectroscopy (XRD) (Fig. 3), scanning electron microscopy (SEM) (Fig. 4), Fourier transform

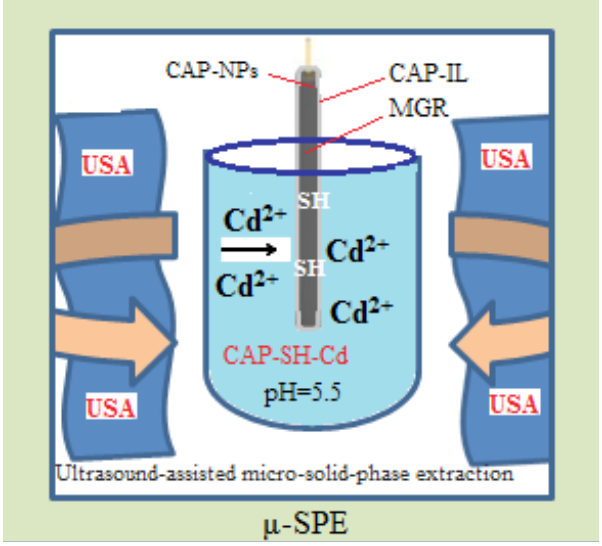

Fig. 2. The schema of cadmium extraction based on CAP-IL-MGR by µ-SPE procedure

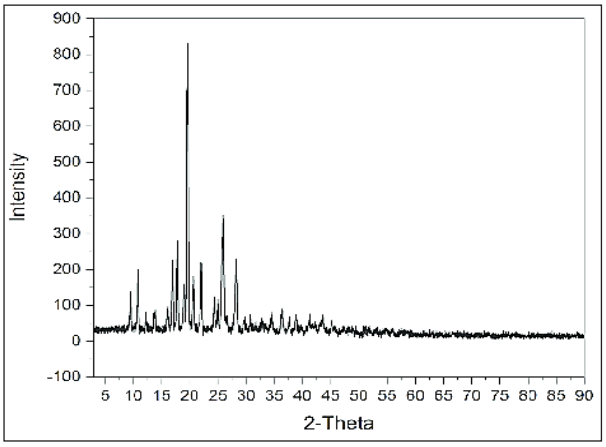

Fig. 3. The X-ray diffraction spectroscopy (XRD) of CAP nanomaterials

infrared spectroscopy (FTIR) (Fig. 5) and UV spectrum analysis (UV-Vis) with absorption in 400 nm (Fig. 6). The X-ray diffraction (XRD) was used to determine the CAP-NP structure. Due to the XRD spectra of CAP-NPs**,** no change was seen after coating on MGR (Fig. 2). In the CAP-NP, the peaks at 2979 and 2877 cm^{-1} were assigned to the asymmetric CH_3 and CH_2 stretching vibration, and the peak at 2634 cm^{-1} was due to the symmetric CH3 stretching mode. The peak at 2567 cm^{-1} corresponded to the SH stretching vibration. The peaks at 1747 and 1593 cm^{-1} were assigned to the C=O stretching vibration of carboxylic acid and amide band, respectively. The peaks at 1471 and 1385 cm^{-1} were due to the asymmetric and

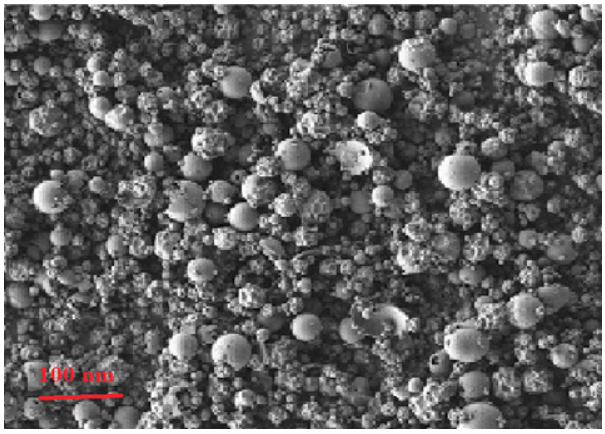

Fig. 4. The scanning electron microscopy (SEM) of CAP nanomaterials

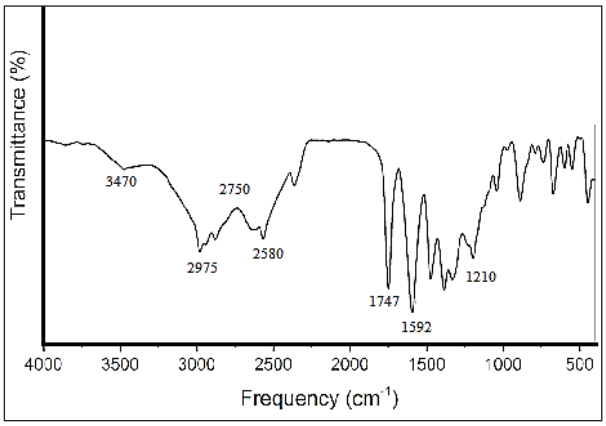

Fig. 5. The Fourier transform infrared spectroscopy (FT-IR) of CAP nanomaterials

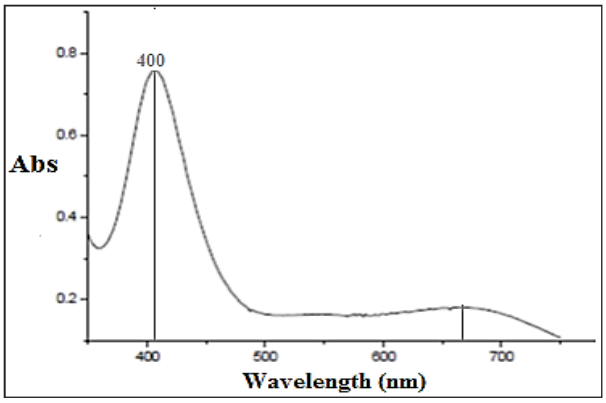

Fig. 6. The UV spectrum analysis (UV-Vis) of CAP in 400 nm

symmetric CH_3 bending vibrations, respectively. The peak at 1330 cm^{-1} was assigned to the OH bending vibration. The peaks at 1228–1200 cm^{-1} also corresponded to the C-O and/or CN stretching vibrations (Fig 4). The SEM and TEM of graphite rod were showed in Figure 7(a) and 7(b) based

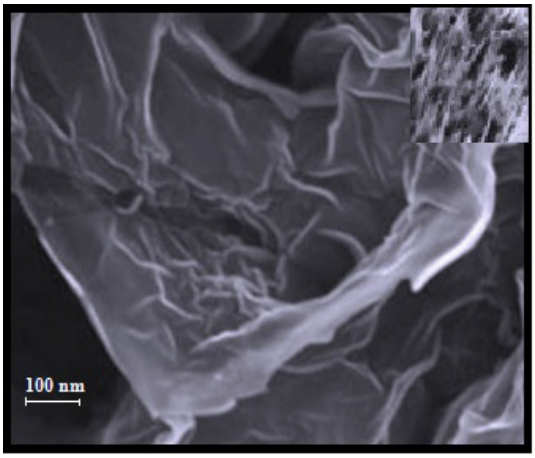

Fig. 7(a).The SEM of graphite rod - CAP/IL

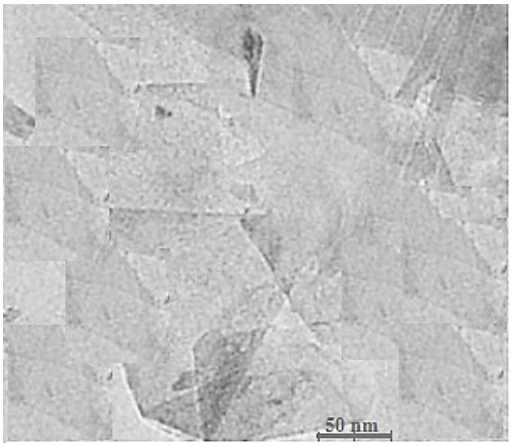

Fig. 7(b).The TEM of graphite rod - CAP/IL

on nano lawyer of graphite (≈100 nm) which was coated with CAP/IL.

3.2. Optimization of methodology

The CAP-IL-MGR as a solid phased was used for separation and determination cadmium in of blood/serum/urine samples by μ-SPE procedure. Blood samples and standard solution containing 0.05-0.3 μg L^{-1} of cadmium was used at pH 5.5. The effects of parameters were studied and optimized for 10 mL of samples by CAP/IL/MGR.

3.2.1. The effect of pH

The pH is an important factor for cadmium extraction in blood/urine sample. By proposed procedure, the formation of the cadmium–CAP as chelate agent (HS group) was evaluated for different pH range from 2 to 11 for 10 mL standard solutions containing 0.05-0.3 μg L^{-1} of Cd(II). Obviously, the efficient extraction for Cd(II) were achieved in the pH ranges of 5.0–6.0 by thiol group of CAP which was passed on MGR by butyl-3-methylimidazolium hexafluorophosphate [BMIM] [PF6]. Therefore, pH of 5.5 was selected as the optimum pH for cadmium extraction with CAP@IL in real samples (Fig. 8). The results showed, the cadmium extracted by IL@MGR up to 33% by amino acids (Cys) in serum and blood samples and lower extracted in urine up to 18%.

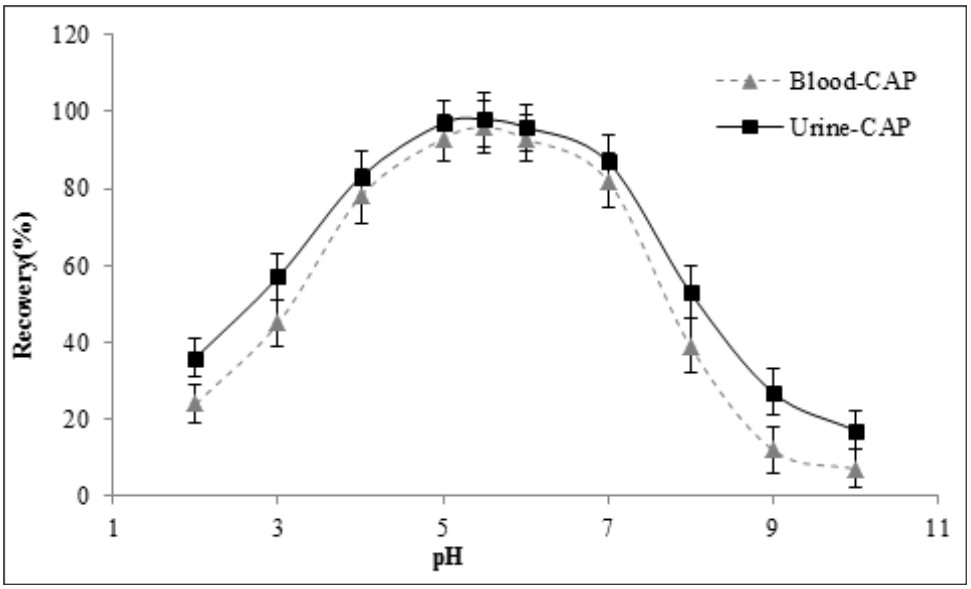

Fig. 8. The effect of pH on extraction of cadmium based on CAP by μ-SPE

3.2.2. The effect of concentration of CAP

The optimizing of CAP concentration was achieved by minimum reagent which was lead to total complex formation with highest extraction efficiency for cadmium. The effect of CAP concentration on the recoveries of cadmium was investigated using various amounts of CAP in the range of 0.1–1 μmol L^{-1} for 0.35 μg L^{-1} of Cd(II) at pH 5.5. By increasing of CAP concentration, the extraction recoveries of cadmium ions gradually increased and the total Cd(II) were extracted using 0.45 μmol L^{-1} of CAP. However, the extraction efficiencies of Cd(II) were not increased more than 0.45 μmol L^{-1} (Fig. 3). So, the 0.5 μmol L^{-1} of CAP were selected as optimum concentrations (Fig. 9).

3.2.3. The effect of sample volume

Sample volume (SV) must be optimized for preconcentration and separation of cadmium from blood/urine/standard solutions. Under optimized conditions, the effect of sample volume was studied in the range of 1–20 mL containing 0.35 μg L^{-1} of Cd(II). The results showed, the cadmium ions can be extracted quantitatively up to 14 mL of the sample. At higher volumes, the recovery values decreased. Also, in higher sample volumes (more than 14 mL), the CAP/ILs phase was partially solubilized in sample solution and lead to non-reproducible results. So, the sample volume of 10 mL was selected for further experiments (Fig. 10).

3.2.4. The effect of extraction time (CAP/Il-MGR)

For high precision and accuracy of results, the extraction time was optimized at pH=5.5. Under optimized conditions, the effects of shaking time on the recovery efficiency of cadmium were studied for 1–10 minutes. Based on obtained results, the cadmium ions were efficient extracted and separated from blood and urine samples after 5 min of sonication.

3.2.5. The effect of back extraction of MGR

After extraction process of cadmium by the proposed method, the MGR based on CAP/IL was back extracted with different acid solutions. By decreasing of pH, the cadmium–CAP complexes lead to the dissociation of complexing bond and released into the aqueous phase. In order to identify the best eluent for back-extraction of Cd(II) from the solid phase, 0.2-1.0 mL of various mineral acids (HNO_3, HCl and H_2SO_4) with different concentrations, 0.1– 1.0 mol L^{-1}, were tested. The results show that HNO3 (0.25 mL, 0.5 M) provides higher recovery efficiency compared to the other acids (Fig.11).

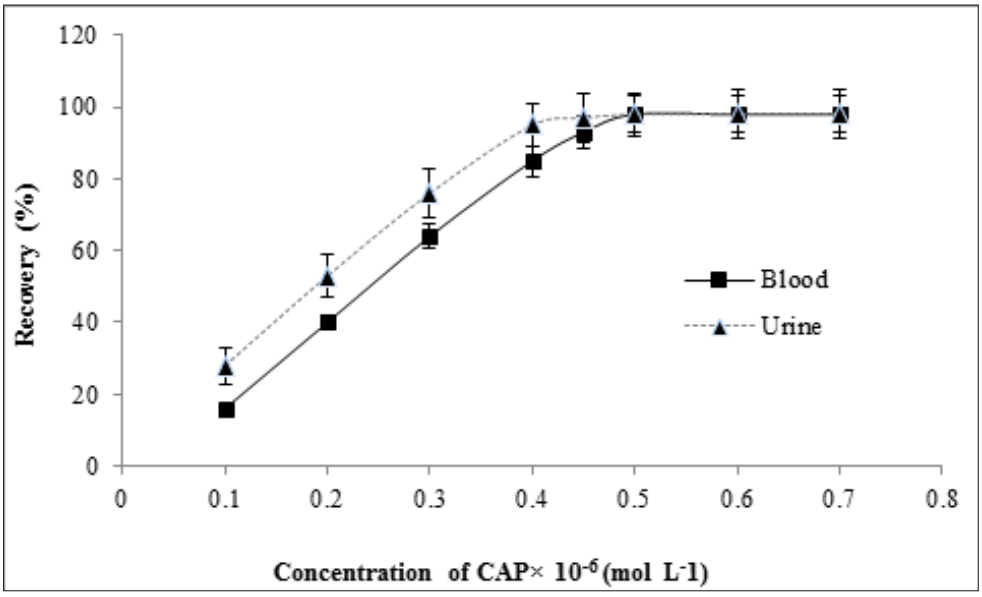

Fig. 9. The effect of concentration of CAP on extraction of cadmium based on CAP by μ-SPE

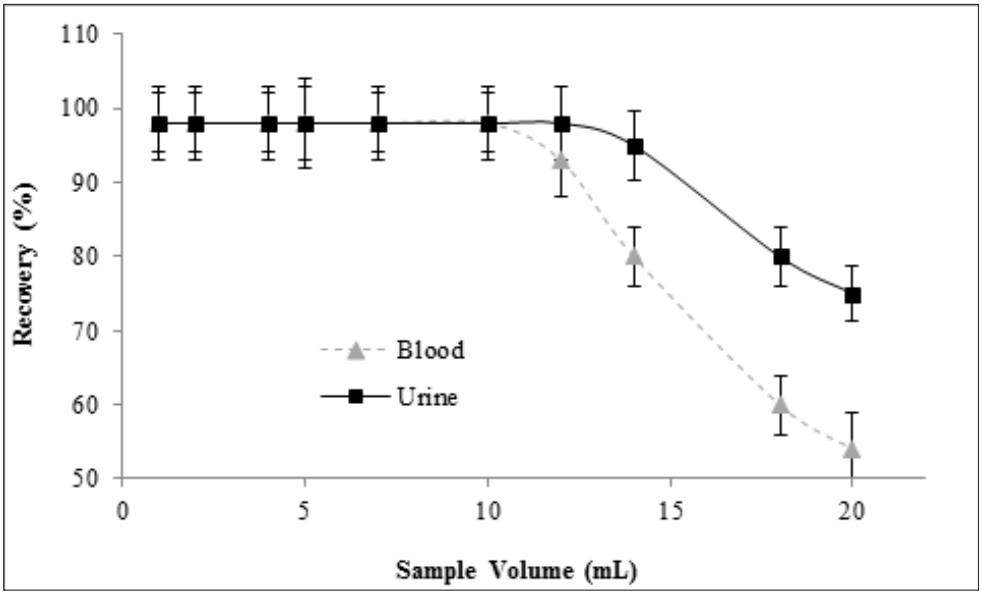

Fig. 10. The effect of sample volume on extraction of cadmium based on CAP by µ-SPE

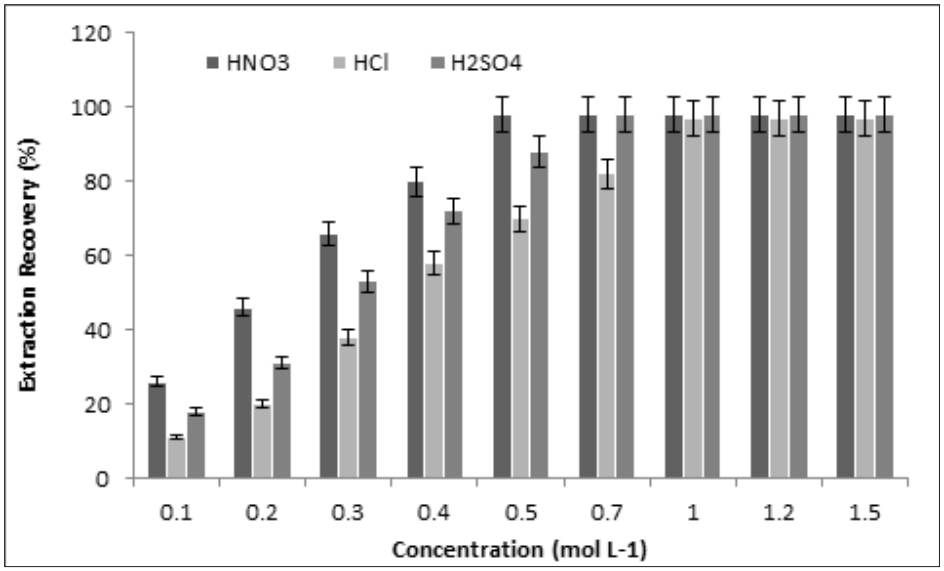

Fig. 11. The effect of inorganic acids on back extraction of cadmium from CAP/IL/MGR

3.2.6. The Interference study

Matrix effects are a very problematic factor for cadmium extraction based on CAP/IL/MGR in blood samples and must be studied by different cations and anions. Since, the thiol group in CAP acted as good chelating agent for extraction of cadmium and other transition metals, so, the different concentration of transition metals was used and examined for evaluation of µ-SPE By procedure, the recoveries of 0.35 µg L^{-1} of Cd(II) were studied in present of individual interferences ions. The deviation of the recovery by more than 5%was considered as the interference criterion. The results showed that many ions such as Co^{2+}, Cu^{2+}, $Zn^{2+}$and Pb^{2+} can be tolerated up to at least 0.6-1 mg L^{-1} when determining the Cd(II) ions based on CAP/IL/MGR by ET-AAS. For concentrations of 1 mg L^{-1} of K^{+}, Na^{+}, Mg^{2+}, $CO_3^{2-}$and PO_3^{-4} which are usually found in human blood/serum samples, any interference was seen by proposed procedure. Moreover, Ni^{2+} and Hg^{2+} can be tolerated up to at least 0.03 mg L^{-1} and 0.045 mg L^{-1} for Cd(II) extraction by CAP.

3.3. Validation

Validity of the developed method was obtained by using standard reference materials (SRM,) from the national institute of standards and technology (NIST, Gaithersburg, USA).The procedure based on CAP-NPs passed on MGR by ionic liquid was used for cadmium extraction in human blood and urine samples by µ-SPE. The results showed a good agreement with SRM (Table 1). Also, the accuracy and reliability of the results were verified by spiking of blood and urine samples (10 mL). High efficient recovery between the added and measured amounts of cadmium was obtained by CAP-NPs (Table 2). Recovery and absorption capacity for CAP-NPs were achieved more than 95 % and 136.7 mg g^{-1}, respectively. In optimized conditions, the efficiency of extraction with IL, MGR, and CAP/IL/MGR were obtained 8.5%, 7.3% and more than 95%, respectively.

3.4. Comparing to published methods

Since 2010, the different techniques for extraction and detemination cadmium in human biological fluids have been published. Different methology such as liquid–liquid microextraction (LLME), micro solid phase extraction (µ-SPE), magnetic solid phase extraction (MSPE), column solid phase extraction(CSPE) have already used for extraction and speciation cadmium in liquid phase [33-37]. The figures of merit of the µ-SPE method compared to recently published methods for cadmium determination in human samples (Table 3).

4. Conclusions

A new method for the separation and determination of ultra-trace levels of cadmium in human blood, serum, plasma and urine samples were developed by CAP/IL/MGR sorbent. Cadmium was preconcentraed based on nanoparticles of CAP pure and determined by µ-SPE coupled with ET-

Table 1. Validation of cadmium results was performed by standard reference material (SRM) by µ-SPE

SEM	ICP-MS (µg L^{-1})	Added (µg L^{-1})	Found by µ-SPE * (µg L^{-1})	Recovery (%)
SRM [a]	0.032 ± 0.005	-------	0.031 ± 0.002	96.9
		0.03	0.06 2 ± 0.003	103.3
SRM [b]	0.211 ± 0.013	-------	0.206 ± 0.013	97.6
		0.1	0.303 ± 0.018	97.0
SRM [C]	0.262 ± 0.038	-------	0.255 ± 0.012	97.3
		0.1	0.351 ± 0.019	96.0

* Mean value ± standard deviation based on three replicate measurements

[a] Concentration Values for SRM 955c Caprine Blood, Level 1(0.032 ± 0.006)

[b] Concentration Values for SRM 955c Caprine Blood, Level 2 (2.140 ± 0.240, Dilution with DW,1:10)

[C] Concentration Values for SRM 955c Caprine Blood, Level 3 (5.201 ± 0.038, Dilution with DW,1: 20)

ICP-MS: Inductively Coupled Plasma Mass Spectrometer (ICP-MS)

Table 2. Evaluation of cadmium extraction based on CAP by µ-SPE method in human biological samples by spiking of cadmium standard

Samples	Added (ng L^{-1})	Found * (ng L^{-1})	Recovery (%)
Serum		68.76 ± 3.45	-------
	50	117.53	97.5
Blood	-------	179.54± 8.32	-------
	100	280.03± 15.11	100.5
Urine	-------	234.32± 12.24	-------
	150	379.75± 18.36	96.9
Plasma	-------	148.66± 6.87	-------
	150	291.82± 14.55	95.4

* Mean value ± standard deviation based on three replicate measurements

Table 3. Comparing of proposed method based on µ-SPE with other publisher works

Techniques	preparation	Matrixes	*LOD	*EF/PF	*RSD (%)	Ref.
[a] VAM-DLLME	APDC-IL	water	0.048	76.9	4.1	33
SPE-F-AAS	[b] WMCNT-BCBATT	biological	0.2	100	3.2	34
CSPE-F-AAS	[C] sorbent of Am 15	water	0.23	20.0	3.0	35
[D]FIA-TS-FF-AAS	[E] IIP	Hair	0.024	165	5.0	36
SPE-F-AAS	M-MWCNT	Blood	0.04	120	1.2	37
[F] DLLME-ET-AAs	[G] TOMAS-X100	Blood, Urine	0.005	10.4	2.3	38
µ-SPE-ET-AAS	[H] CAP-IL-MGR	Blood, Urine	0.002	19.7	2.4	This work

* Linear rang (LR, µg L^{-1}); Detection limit (DL, µg L^{-1}), the *relative standard deviation* (RSD%)

[a] Vortex-assisted modified dispersive liquid-liquid microextraction (VAM-DLLME)

[b] Multi wall carbon nanotube- benzyl-4-[-chlororbenzylidene amine]-4H-1,2,4-triazole-3-thiol (BCBATT) [C] Amberlyst 15 as sorbent

[D] Thermospray flame furnace atomic absorption spectrometry (FIA-TS-FF-AAS)

[E] Ion imprinted polymer (IIP)

[F] Dispersive liquid–liquid microextraction coupled by elecrothermal atomic absorption spectrometer

[G] Trioctylmethyl ammonium thiosalicylate(TOMAS, TSIL)

[H] Captopril nanoparticles - ionic liquid ([HMIM] [PF6]) paste on micro graphite rod

AAS. The developed method provides relatively lower LOD, LOQ and RSD (< 2%, n=10) with favorite enrichment factor (19.7) and recoveries (more than 95 %). .As low cadmium concentration in blood and serum samples (< 0.2 µg L^{-1}), a good linear range from 0.01 µg L^{-1} to 0.35 µg L^{-1} was used for a 10 mL sample by µ-SPE . In optimized conditions, the accurate / precise results with simple sample treatment and high efficient extraction were obtained with CAP/IL/MGR sorbent before cadmium concentration determined by ET-AAS.

5. Acknowledgements

The authors wish to thank the Petroleum Industry Health Organization (PIHO), The Ethical Committee of Iranian Petroleum Industry Health Research Institute approved the human sample analysis by IPIHRI Lab (R.IPIHRI.PN.1397. 010)

6. References

[1] K. Rao, M. Mohapatra, S. Anand, P. Venkateswarlu, Review on cadmium removal from aqueous solutions. Int. j. Eng. Sci. Technol., 2 (2010) 81-103.

[2] A. Sarkar, G. Ravindran, V. Krishnamurthy, A brief review on the effect of cadmium toxicity: from cellular to organ level, Int. J. Biotechnol. Res., 3 (2013) 17-36.

[3] V. Arroyo, Liver and cadmium toxicity, J. Drug Metab. Toxicol., S5 (2012)1-7.

[4] R.A. Bernhoft, Cadmium toxicity and treatment, The Sci. World J., 2013(2013) 394652.

[5] D. Bagchi, S.S. Joshi, M. Bagchi, J. Balmoori, E.J.Benner, C.A. Kuszynski, S.J. Stohs, Cadmium□and chromium□induced oxidative stress, DNA damage, and apoptotic cell death in cultured human chronic myelogenous leukemic K562 cells, promyelocytic leukemic HL□60 cells, and normal human peripheral blood mononuclear cells. J. Biochem. Mol. Toxicol., 14 (2000) 33-41.

[6] H.S. Ashby, Welding fume in the workplace, Profession. Safe., 47 (2002) 55-63.

[7] F. Gil , A.F. Hernández, C. Márquez , P. Femia, P. Olmedo , O. López-Guarnido, A. Pla, Biomonitorization of cadmium, chromium, manganese, nickel and lead in whole blood, urine, axillary hair and saliva in an occupationally exposed population, Sci. Total Environ., 409 (2011) 1172-1180.

[8] R. Wittman, H. Hu, Cadmium exposure and nephropathy in a 28-year-old female metals worker, Environ. health persp., 110 (2002) 1261-1266.

[9] J.O. Duruibe, M. Ogwuegbu, J. Egwurugwu, Heavy metal pollution and human biotoxic effects. Int. J. phys. sci., 2 (2007) 112-118.

[10] B. Wang, Y. Du, Cadmium and its neurotoxic effects, Oxidative medicine and cellular longevity, 2013 (2013) 898034.

[11] O. Akinloye et al., Cadmium toxicity: a possible cause of male infertility in Nigeria, Reprod. Biol.,

6 (2006) 17-30.

[12] M.P. Benavides, S.M. Gallego, M.L. Tomaro, Cadmium toxicity in plants. Brazil. j. plant physiol., 17 (2005) 21-34.

[13] T. Fatur et al., DNA damage and metallothionein synthesis in human hepatoma cells (HepG2) exposed to cadmium, Food chem. Toxicol., 40 (2002) 1069-1076.

[14] G. Jiang et al., Effects of long-term low-dose cadmium exposure on genomic DNA methylation in human embryo lung fibroblast cells, Toxicol., 244 (2008) 49-55.

[15] L. Järup, Cadmium overload and toxicity, Nephrol. Dial. Transpl., 17 (2002) 35-39.

[16] S. Satarug et al., A global perspective on cadmium pollution and toxicity in non-occupationally exposed population, Toxicol. letter., 137 (2003) 65-83.

[17] NIOSH. Manual of analytical methods. 5th ed. U.S. department of health and human services, 2015.

[18] W. L. Zhang et al., Cadmium exposure and its health effects: a 19-year follow-up study of a polluted area in China, Sci. Total Environ., 470 (2014) 224-228.

[19] G. F. Nordberg, Cadmium and health in the 21st century–historical remarks and trends for the future, Biometal., 17 (2004) 485-489.

[20] K. P.Ang et al., The determination of cadmium, copper and lead in ambient air particulates in Singapore, Int. J. Environ. Studies, 32 (1988) 49-58.

[21] M. Blanuša et al., Assessment of exposure to lead and cadmium through air and food in inhabitants of Zagreb, Arh. Hig. Rada Toksiko., 42 (1991) 257-266.

[22] J. W. Robinson et al., The determination of cadmium by atomic absorption in air, water, sea water and urine with a rf carbon bed atomizer, Anal. Chim. Acta, 66 (1973) 13-21.

[23] M. Essien, L. J. Radziemski, J. Sneddon, Detection of cadmium, lead and zinc in aerosols by laser-induced breakdown spectrometry, J. Anal. Atom. Spect., 3 (1988) 985-988.

[24] J. A. C. Broekaert, Application of hollow cathode excitation coupled to vidicon detection to the simultaneous multielement determination of toxic elements in airborne dust. A Unique sampling analysis procedure for lead and cadmium, Bull. Soc. Chim. Belg., 85 (1976) 755-761.

[25] R. M. Dagnall, T. S. West, P. Young, Determination of cadmium by atomic-fluorescence and atomic-absorption spectrophotometry, Talanta, 13 (1966) 803-808.

[26] S. Landsberger, D. Wu, Improvement of analytical sensitivities for the determination of antimony, arsenic, cadmium, indium, iodine, molybdenum, silicon and uranium in airborne particulate matter by epithermal neutron activation analysis, J. Radioanal. Nucl. Chem., 167 (1993) 219-225.

[27] K. G. Brodie, J. P. Matoušek, Determination of cadmium in air by non-flame atomic absorption spectrometry, Anal. Chim. Acta, 69 (1974) 200-202.

[28] M Aliomrani, MA Sahraian, H Shirkhanloo, M Sharifzadeh, Correlation between heavy metal exposure and GSTM1 polymorphism in Iranian multiple sclerosis patients, Neurol. Sci., 38 (2017) 1271-1278.

[29] H. Shirkhanloo, A. Khaligh, HZ. Mousavi, MM. Eskandari, AA. Miran-Beigi, Ultra-trace arsenic and mercury speciation and determination in blood samples by ionic liquid-based dispersive liquid-liquid microextraction combined with flow injection, Chem. Paper., 69 (2015) 779-790.

[30] H. Hassani, F. Golbabaei, H. Shirkhanloo, M. Tehrani-Doust, Relations of biomarkers of manganese exposure and neuropsychological effects among welders and ferroalloy smelters, Ind. Health, 54 (2016), 79-86.

[31] H. Shirkhanloo, ZH. Mousavi, A. Rouhollahi, Preconcentration and determination of heavy metals in water, sediment and biological samples, J. Serb. Chem. Soc., 76 (2011) 1583-1595.

[33] H. Shirkhanloo, M. Falahnejad, HZ. Mousavi, On-line ultrasound-assisted dispersive micro-solid-phase extraction based on amino bimodal mesoporous silica nanoparticles for the preconcentration and determination of cadmium, Biol. Trace Elem. Res., 171 (2016) 472-481.

[32] H. Shirkhanloo, SD. Ahranjani, A lead analysis based on amine functionalized bimodal mesoporous silica nanoparticles in human biological samples by ultrasound assisted-ionic liquid trap-micro solid phase, J. Pharm. Biomed. Anal., 157 (2018) 1-9.

[33] S. Nizamani , TG. Kazi, HI. Afridi, S. Talpur, A. Lashari, J. Ali , Vortex-assisted modified dispersive liquid-liquid microextraction of trace levels of

cadmium in surface water and groundwater samples of Tharparkar, Pakistan, optimized by multivariate technique, J. AOAC Int., 101(2018) 858-866.

[34] A. A. Gouda, W. A. Zordok, Solid-phase extraction method for preconcentration of cadmium and lead in environmental samples using multiwalled carbon nanotubes, Turk. J. Chem., 42 (2018) 1018 – 1031.

[35] A. Tunçeli, A. Ulaş , O. Acar, AR. Türker , Solid phase extraction of cadmium and lead from water by amberlyst 15 and determination by flame atomic absorption spectrometry, Bull. Environ. Contam. Toxicol., 102 (2019) 297-302.

[36] A. Campos do Lago, C. Marchioni, T. Venga Mendes, C. Wisniewski, C. Wisniewski, P. Sergio Fadini, P. Orival Luccas, Ion imprinted polymer for preconcentration and determination of ultra-trace cadmium, employing flow injection analysis with thermo spray furnace atomic absorption spectrometry, Appl. Spect., 70 (2016) 1842-1850.

[37] S.Z. Mohammadi, D. Afzalib, D. Pourtalebi, Flame atomic absorption spectrometric determination of trace amounts of lead, cadmium and nickel in different matrixes after solid phase extraction on modified multiwalled carbon nanotubes, Cent. Eur. J. Chem., 8(2010) 662–668.

[38] H. Shirkhanloo, M. Ghazaghi b, H. ZavvarMousavi, Cadmium determination in human biological samples based on trioctylmethyl ammonium thiosalicylate as a task-specific ionic liquid by dispersive liquid–liquid microextraction method, J. Mol. Liq., 218 (2016) 478–483.